

THE UNIVERSITY OF CALGARY

A High Speed Variable Rate Transmission System
for an Indoor Wireless LAN

by

Sheelo Lilene M^cGuire

A THESIS

SUBMITTED TO THE FACULTY OF GRADUATE STUDIES
IN PARTIAL FULFILLMENT OF THE REQUIREMENTS FOR THE
DEGREE OF MASTER OF SCIENCE

DEPARTMENT OF ELECTRICAL AND COMPUTER ENGINEERING

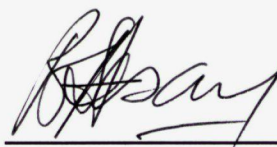
CALGARY, ALBERTA

NOVEMBER, 1995

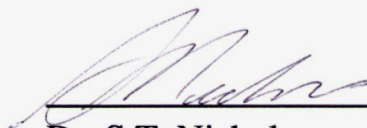
© Sheelo Lilene M^cGuire 1995

THE UNIVERSITY OF CALGARY
FACULTY OF GRADUATE STUDIES

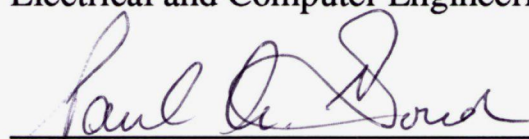
The undersigned certify that they have read, and recommend to the Faculty of Graduate Studies for acceptance, a thesis entitled "A High Speed Variable Rate Transmission System for an Indoor Wireless LAN" submitted by Sheelo Lilene M^cGuire in partial fulfillment of the requirements for the degree of Master of Science.



Supervisor, Dr. A. Sesay
Electrical and Computer Engineering



Dr. S.T. Nichols
Electrical and Computer Engineering



Dr. P.A. Goud
Electrical and Computer Engineering
University of Alberta

Dec. 3/1995

Date

Abstract

This thesis investigates a new multiple access scheme termed code-frequency-time division multiple access (CFTDMA) for high variable rate data systems operating in indoor wireless channels, for future multimedia applications.

High rate systems present difficulties because the symbol duration is comparable to the amount of time dispersion introduced by an indoor wireless channel. This difficulty may be overcome by converting the high rate source into an equivalent number of low rate sources. The low rate sources are then multiplexed using CFTDMA for transmission.

A CFTDMA system was investigated to determine conditions under which an adequate level of performance may be attained without the complexities of synchronization, coding, equalization, and diversity techniques. The resulting system was modular in design facilitating an ease in implementation.

Analysis and simulation results are presented. The CFTDMA system performance degrades as the system rate is increased. Potential measures for achieving improved performance are discussed.

Acknowledgments

I would like to thank Dr. A. Sesay for his supervision as well as TRILabs and the University of Calgary for their financial support. TRILabs provided the opportunity to complete my degree in an informal setting where one is surrounded by experts from both academia and industry, a situation which I enjoyed and greatly appreciated. I would also like to thank the staff and students at TRILabs for their guidance and friendship.

I offer especially warm thanks to those old and new friends who have provided never-ending encouragement. I extend special thanks to Sisay Yirga who helped me tremendously at the onset of this project.

Finally, I express my deepest gratitude to my family who have always provided me with encouragement and support in all my undertakings.

Dedication

I would like to dedicate this thesis to those I love, may it not associate you with the grief it gave me; if it does I revoke my dedication and devote it to those I despise.

Table of Contents

Abstract	iii
Acknowledgements	iv
Dedication	v
Table of Contents	vi
List of Tables	ix
List of Figures	x
List of Symbols & Abbreviations	xvi
Chapter 1 Introduction	1
Chapter 2 The Indoor Wireless Channel	8
Chapter Overview	8
2.1 Multipath Fading	9
2.2 Characterization of the Wireless Channel	12
2.2.1 Multipath Delay Spread.....	13
2.2.2 Power Gradient	13
2.2.3 Doppler Spread	14
2.3 Wireless System Design	15
Chapter 3 Multiple Access Techniques	16
Chapter Overview	16
3.1 Frequency Division Multiple Access	17
3.2 Time Division Multiple Access	18
3.3 Code Division Multiple Access	19
3.4 Comparison of Multiple Access Techniques	20
3.5 Hybrid Multiple Access Techniques	21
3.5.1 CFDMA	21
3.5.2 CTDMA.....	22
Chapter 4 Direct Sequence Spread Spectrum	23
Chapter Overview	23
4.1 Spectrum Spreading	24
4.2 Spectrum Despreading	25
4.3 Spreading Codes	27
4.3.1 PN Sequences	28

4.3.1.1	m-Sequences	28
4.4	Synchronization	31
4.4.1	Code Acquisition	33
4.4.2	Code Tracking	37
Chapter 5	Proposed System	38
Chapter Overview	38
5.1	System Description	39
5.1.1	CFDMA	42
5.1.2	CTDMA	44
5.1.3	CFTDMA	45
5.2	System Expansion	47
5.3	Summary	48
Chapter 6	Implementation Dependency on Despreader Circuits	50
Chapter Overview	50
6.1	Matched Filter Despreader	51
6.2	Limitation of Spreading Technique Due to CFDMA	54
6.2.1	Limitation of Adjacent Channel Interference Due to Harmonics	55
6.2.2	Band Limitation of Narrowband Spectra	57
6.3	Summary	57
Chapter 7	Transmitter	59
Chapter Overview	59
7.1	Transmitter Implementation	60
7.1.1	Bit sources	62
7.1.2	DQPSK Modulation	62
7.1.3	Symbol Timing	62
7.1.4	Spreading Process	65
7.1.4.1	Selection of PN Code Length, M, and Time Offset, Δ	65
7.1.5	Spectrum Limiting	71
7.1.5.1	Pulse Shaping	72
7.1.6	Frequency Upshifting	76
7.2	Determination of CFTDMA Bandwidth	79
Chapter 8	Receiver	80
Chapter Overview	80
8.1	Chip Synchronization	81
8.2	Data Demodulation	81
8.2.1	Frequency Downshifting	83
8.2.2	Despreading	84

8.3	Data Recovery	86
Chapter 9	Simulation Results and Analysis	87
Chapter Overview	87
9.1	Desired System Performance	88
9.2	Simulation Parameters	89
9.3	Performance in a Gaussian Channel	90
9.3.1	Performance Dependence on Code Time Offset, Δ	90
9.3.2	Performance Dependence on Number of Source Pairs, N	92
9.4	System Errors Due to SRN Pulse Shaping	94
9.5	Alternate Method of Pulse Shaping	96
9.5.1	Performance Dependence on Code Time Offset, Δ	98
9.5.2	Performance Dependence on Number of Source Pairs, N	100
9.6	Analysis of System Dependence on Number of Source Pairs	103
9.6.1	CFTDMA System with $T_m = 0$	103
9.6.2	CFTDMA System with $T_m = \Delta$	105
9.6.3	Analysis Results	106
9.7	Performance in a Two-Ray Channel.....	108
9.8	Performance in a Four-Ray Channel	113
9.9	Summary	114
Chapter 10	Conclusions	116
Chapter Overview	116
10.1	System Overview	117
10.2	Simulation Results	118
10.3	Recommendations for Future Work.....	120
References	122
Appendix 1	Analysis of Pulse Shaping via matching SRN Filters in the Transmitter and Receiver for a CFDMA System	128
Appendix 2	Analysis of Pulse Shaping via a RCF for a CFDMA System	137
Appendix 3	Theoretical Analysis of a CFTDMA System with $T_m = 0$ Over a Direct Connection	145
Appendix 4	Theoretical Analysis of a CFTDMA System with $T_m = \Delta$ Over a Direct Connection	151

List of Tables

Table A.1.1	Error values introduced by SRN pulse shaping.....	136
Table A.3.1	Interference due to adjacent source pairs' B data when demodulating stream A data for $T_m = 0$	150
Table A.4.1	Interference due to adjacent source pairs' B data when demodulating stream A data for $T_m = \Delta$	154

List of Figures

Figure 2.1	Indoor multipath environment.	9
Figure 2.2	Spreading of a pulse by a multipath channel.	9
Figure 2.3	Time-variant indoor multipath environment.	10
Figure 2.4	Frequency selective and frequency nonselective fading in a radio channel.	12
Figure 2.5	ISI of multiple symbols passing through a multipath channel.	15
Figure 3.1	Frequency-power-time domain for a simple FDMA system.	17
Figure 3.2	TDMA system (a) Frequency-power-time diagram. (b) Timing diagram.	19
Figure 4.1	Simple DS-SS system.	24
Figure 4.2	Despreading of DS-SS signal via correlation in a perfectly synchronized noiseless system.	26
Figure 4.3	Illustration of processing gain in a DS-SS system with (a) multiple users (CDMA), (b) narrowband interference, and (c) AWGN.	27
Figure 4.4	Linear feedback shift-register used to generate PN sequences.	29
Figure 4.5	(a) Normalized autocorrelation of m-sequence with period M. (b) Autocorrelation of a white noise signal.	30
Figure 4.6	DS-SS system with perfect and imperfect chip synchronization of $\frac{1}{5}T_c$	32
Figure 4.7	Block diagram of sliding correlator code acquisition circuit.	34

Figure 4.8	Block diagram for parallel search code acquisition using correlators.	35
Figure 4.9	Output of filter matched to PN code present in incoming signal.	36
Figure 4.10	Block diagram for basic parallel search code acquisition using a matched filter.	36
Figure 4.11	Block diagram for early-late tracking circuit.	37
Figure 5.1	Conversion of a high speed source to an equivalent set of low rate sources.	40
Figure 5.2	Mixed rate sources that generate data at a multiple of the base rate are assigned of a subset of the number of low rate sources.	41
Figure 5.3	(a) 3 source FDMA system. (b) Frequency spectra for the 3 branches of the FDMA system. (c) Spectrum for FDMA waveform. (d) 3 source single code CFDMA system. (e) Frequency spectra for the 3 branches of the CFDMA system. (f) Spectrum for CFDMA waveform.	43
Figure 5.4	Multiple code CFDMA transmitter.	44
Figure 5.5	A 3 source CTDMA transmitter.	45
Figure 5.6	Block diagram for a $N_f N_t$ source CFTDMA transmitter.	46
Figure 5.7	Block diagram of proposed CFTDMA transmitter.	46
Figure 5.8	CFTDMA high rate system. A single high rate source is converted into a number of low rate sources which are divided into two equal groups. CFDMA is used to multiplex sources within a group and CTDMA is used to multiplex the two groups.	47

Figure 5.9	Variable rate CFTDMA system.....	48
Figure 6.1	Equivalence of a MF despreader to a correlator despreader.....	51
Figure 6.2	Output of a filter matched to the PN code used to spread the incoming signal.	52
Figure 6.3	A simple MF despreader system. The signal is illustrated at various points during the spreading, despreading and data recovery process.	53
Figure 6.4	Use of harmonics to eliminate ACI in FDMA data. (a) FDMA transmitter and receiver for source 1 data. (b) Signals at various points in the system.....	56
Figure 6.5	Narrowband source spectra prior to spreading in CFDMA systems.	57
Figure 7.1	CFTDMA transmitter with $2N$ sources.	60
Figure 7.2	Transmitter block diagram for variable high data rate CFTDMA system.	61
Figure 7.3	Intersymbol interference due to multipath channel. (a) Dispersion of single symbol transmitted over a multipath channel. (b) ISI due to multipath spread. (c) Illustration of method to combat ISI by leaving dead time between symbols.....	63
Figure 7.4	Insertion of a time gap between symbols.	64
Figure 7.5	(a) Source of interference between $N_t = 2$ CTDMA system streams in a gaussian channel. (b) Level of interference between $N_t = 2$ CTDMA system streams in a gaussian channel for various m-sequence lengths.....	67

Figure 7.6	The timing diagram for a source pair.	68
Figure 7.7	a) Region of interference between $N_t=2$ CTDMA streams in a multipath channel. (b) Level of interference between $N_t=2$ CTDMA streams in a multipath channel for various m-sequence lengths where $T_m=\Delta$	69
Figure 7.8	Time domain response of a nyquist pulse.	72
Figure 7.9	Consecutive nyquist pulses. (a) Overlay of time offset nyquist pulses. (b) Superposition of time shifted nyquist pulses showing ideal sampling time to recover information.	73
Figure 7.10	Frequency response of a nyquist pulse.	73
Figure 7.11	Frequency spectra at various points of the transmitter rails.	75
Figure 7.12	Example of CFDMA combining for setup with 15 source pairs.	78
Figure 8.1	Simplicity of receiver implementation for a single source pair using a MF for despreading versus a correlator.	82
Figure 8.2	Block diagram of a CFTDMA receiver to recover the entire transmitted signal.	83
Figure 8.3	Output of the MF despreader for the CFTDMA system where $\Delta=T_m$ in a Gaussian channel.	85
Figure 9.1	BER Performance in a Gaussian channel for CFTDMA system with $T_m=0$, 10 source pairs, and variable Δ	91
Figure 9.2	BER performance in a Gaussian channel with $\Delta = 19$ chips, $T_m = 0$, and variable number of source pairs.	93

Figure 9.3	Loss of data due to SRN filtering at the receiver for 3 source pair CFTDMA system when recovering source pair 1 data.	95
Figure 9.4	Removal of double frequency components through the use of a LPF after frequency downshifting to recover source pair 1 data for a 3 source pair CFTDMA system.	98
Figure 9.5	Comparison of performance results using 2 cascaded SRN filters to pulse shape versus one single raised-cosine filter (RCF) for a 10 source pair CFTDMA system.	99
Figure 9.6	Performance in a Gaussian channel using a RCF for band limitation for a variable number of source pairs where $\Delta = 19$ chips.	100
Figure 9.7	Performance in a Gaussian channel using a RCF for band limitation for a variable number of source pairs where $\Delta = 20$ chips.	101
Figure 9.8	Performance in a Gaussian channel using a RCF for band limitation for a variable number of source pairs where $\Delta = 21$ chips.	101
Figure 9.9	Symbol timing for CFTDMA system with $\Delta = T_m = M$	107
Figure 9.10	Performance in a Gaussian channel for a CFTDMA system with $\Delta = T_{mc} = M$	108
Figure 9.11	Performance over a 2 equal ray channel for CFTDMA system with $\Delta = T_{mc} = M$	109
Figure 9.12	Performance over a 2 ray channel where the magnitude of the second ray is 75% of the magnitude of the first ray for a CFTDMA system with $\Delta = T_{mc} = M$	110

Figure 9.13	Performance over a 2 ray channel where the magnitude of the second ray is 50% of the magnitude of the first ray for a CFTDMA system with $\Delta = T_{mc} = M$	111
Figure 9.14	(a) Two equal ray channel impulse response. (b) Two ray channel creates delayed versions of the stream A and stream B data.	112
Figure 9.15	CFTDMA system performance in a 2 ray and 4 ray channel for 20 source pairs where magnitude of LOS is greater than or equal to twice the NLOS rays.	113
Figure A.1.1	CFDMA system employing matching SRN filters for pulse shaping with a direct connection between transmitter and receiver.	129
Figure A.1.2	Symbol stream for one source.	128
Figure A.1.3	Use of correlation to determine the MF output at the ideal sampling time.	132
Figure A.2.2	Symbol stream for one source.	137
Figure A.2.1	CFDMA system employing raised-cosine filters for pulse shaping.	138
Figure A.2.3	Use of correlation to determine the MF output at the ideal sampling time.	141
Figure A.3.1	CFTDMA system to be analyzed.	146
Figure A.3.2	Interference due to B data when demodulating A data for a $T_m=0$ CFTDMA system.	147
Figure A.4.1	Interference due to B data when demodulating A data for a $T_m = \Delta$ CFTDMA system.	152

List of Symbols and Abbreviations

Φ	chip fraction to which initial alignment is required
$\delta(t)$	delta dirac function
θ_k	phase of k^{th} multipath component
β	SRN or raised-cosine filter rolloff factor
α_k	strength of k^{th} multipath component
τ_{DS}	delay spread
τ_k	delay of k^{th} multipath component
τ_{rms}	rms delay spread
BER	bit error rate
B_{LPF}	low pass filter bandwidth
B_{RCF}	raised-cosine filter bandwidth
B_s	null to null source bandwidth
B_{SRN}	square-root nyquist filter bandwidth
B_T	CFTDMA system bandwidth
CDMA	Code Division Multiple Access
CFDMA	Code Frequency Division Multiple Access
CFTDMA	Code Frequency Time Division Multiple Access
CTDMA	Code Time Division Multiple Access
DQPSK	Differential Quadrature Phase Shift Keying

f_B	offset frequency for adjacent source pairs
FDMA	Frequency Division Multiple Access
f_o	initial upshift intermediate frequency
f_{sam}	sample frequency
FSK	Frequency Shift Keying
IF	intermediate frequency
ISI	intersymbol interference
L	processing gain
LAN	local area network
LPF	low pass filter
M	m-sequence code length
m	m-sequence order
MF	matched filter
N_c	number of codes used by a CFDMA system
N_f	number of sources multiplexed by a CFDMA system
N_t	number of sources multiplexed by a CTDMA system
P	zero extended PN-sequence period in chips: $P=M+T_{mc}$
pg	power gradient
PN	pseudo noise
QAM	Quadrature Amplitude Modulation
QPSK	Quadrature Phase Shift Keying

R_b	bit rate
R_c	chip rate
R_s	symbol rate
R_T	transmission rate for a CFTDMA system
SAW	Surface Acoustic Wave
SNR	signal to noise ratio
SRN	Square-Root Nyquist
T_b	bit period
T_c	chip period
TDMA	Time Division Multiple Access
T_m	time gap between symbols in seconds
T_{mc}	time gap between symbols in chips
T_s	symbol period
T_{sam}	sample period
T_{sym}	symbol duration
$u(t)$	unit step function
WLAN	Wireless LAN
W_s	null to null spread source bandwidth
Δ	time offset of CTDMA spreading codes

Chapter 1

Introduction

Wireless technology seems to be the passion of the decade. Portable stereos, televisions, telephones and computers inundate our lives as we seek release from confinement. The quest for wireless technology has especially affected today's telecommunications engineer. The wireless voice industry has made significant progress since Marconi's radio transmission from a land-based station to a tugboat in 1897 [1] to today's cellular phone technology. The evolution of wireless communications is now being developed for data communications due to an increased dependence on data communications in today's business transactions. Cellular phone users want to transmit data via their cellular phone, computer operators want computers that do not have a physical connection to the local area network; in general, today's office worker wants portable tools that perform the same tasks as their wired equivalents. Wireless data communications is divided into two categories: mobile data which concerns low-speed wide-area data communications, and wireless LAN's which concern local high-speed data communications [2]. This thesis will discuss a possible transmission technology for a high speed variable rate wireless LAN for future multimedia applications.

A local area network (LAN) provides a means of communication between several computers within a small area. This provides many benefits, such as allowing workers to share licensed software and output devices. A wireless local area network (WLAN) would provide the same

services but without the need for physical connections. WLAN's may provide a financial savings over typical wired LAN's due to their ease of installation, extension, alteration and maintenance, [3], in addition to providing portability. Due to these characteristics, the wireless LAN is being marketed for applications in manufacturing facilities, offices with wiring difficulties, and branch and temporary offices [2].

There are few WLAN's in operation currently but the research and development into new improved WLAN's is developing rapidly. One of the reasons for so few WLAN's is the necessity of a high data rate ($>1\text{MB/s}$) for a LAN. The announcement in May 1985 by the FCC permitting the use of the unlicensed Industrial, Scientific, and Medical (ISM) bands for commercial spread spectrum products has aided in the development of WLAN's as these bands can accommodate high-speed communications [2], [4]. Existing WLAN systems consist of unlicensed spread spectrum systems operating in ISM bands, licensed cellular systems operating at 18-19 GHz, and infrared (IR) systems [2]. Two examples of unlicensed WLAN's operating in the ISM bands are FreePortTM and WaveLAN[®] [5], [6]. FreePort provides an Ethernet hub using direct-sequence spread spectrum while WaveLAN provides peer-to-peer communications using direct-sequence spread spectrum with CSMA/CA protocol. An operational WLAN that operates in the licensed spectrum is Altair [5], [6].

Standards are being developed for WLANs in order that the LANs being developed by different manufacturers are compatible. In the United

States, standards are being developed under IEEE 802.11 which is focused on medium rate unlicensed spread spectrum technologies for the ISM band [4]. In Europe, standards are being developed for a high performance radio LAN (HIPERLAN) [3]. The HIPERLAN has a target rate of 20 Mbits/sec and will operate in the licensed 5 or 17 GHz band. The transmission scheme is that of single carrier modulation and will make use of an equalizer to compensate for intersymbol interference. In Japan, standards have been developed for two types of WLANs: a medium rate WLAN using spread spectrum in the ISM band and a high rate using QAM, QPSK, or 4-level FSK at approximately 18 GHz [5].

This thesis investigates a transmission scheme to achieve variable rate transmission up to 150 Mbits/sec and above. The high speeds and variable rate are necessary for multimedia applications. Because of the excessive bandwidth requirement in multimedia applications, the technique will be suitable for the frequency bands above 30 GHz. The characterization of the indoor propagation channel in these high frequency bands can be found in [7], [8], [9], [10]. There is no standard available to date for these frequency bands.

Wireless data communications poses a far greater problem than wireless voice communications. The human brain has an innate error-correction capability for voice, thus errors in transmission of voice data must be significant for a listener to not be able to understand what the speaker is saying. For data communications a single bit error may result in drastic consequences and thus the performance must be far superior to that of

existing wireless voice communications. In fact, bit error rates on the order of 10^{-2} can be tolerated for packetized voice whereas bit error rates on the order of 10^{-5} are tolerated for packetized data in addition to zero tolerance for packet loss [2]. The requirements of speed and bandwidth imposed by data communications are also far greater than that for voice applications.

The lack of a direct physical link in wireless communications between the transmitter and the receiver results in significant difficulties over systems where a direct connection is present. The propagation of radio signals in free space, rather than baseband signals via a wire cable, results in signal distortion as the signal will encounter objects that may scatter, reflect, and dissipate it before it arrives at the receiver [1]. This results in several signal paths arriving at the receiver at different times with different energies, a phenomenon known as multipath propagation. The impulse response of the channel is modeled to reflect multiple paths as

$$c(\tau; t) = \sum_{k=1}^L \alpha_k e^{j\theta_k} \delta(t - \tau_k) \quad (1.1)$$

where α_k , τ_k , and θ_k represent the strength, excess delay, and phase of the arriving paths, respectively. The radio propagation used to transmit the signals can be characterized by three parameters: rms multipath delay, distance-power gradient, and Doppler spread [2]. As a WLAN typically operates in an indoor environment, these parameters can be estimated based on the indoor channel.

The multipath channel is constantly changing due to transmitter and receiver motion. Furthermore, the objects reflecting the signal may also be in motion. The nature of the time varying environment affects the quality of

reception and limits the methods to overcome the multipath fading. A transmission scheme known as spread spectrum has been found to be an effective means of overcoming multipath [11]. Spread spectrum modulates a low data rate information signal with a high data rate pseudo-noise code. Spread spectrum systems have been found to be able to resolve the multipath components arriving at the receiver if the time between paths is greater than the pseudo-noise bit [12], [13], [14]. This enables the receiver to lock onto the strongest multipath component and to treat the remaining multipath arrivals as interference [15]. Alternatively, the receiver may lock onto several paths and combine the energy from these paths to achieve a form of diversity [14].

The availability of spectrum is limited in the lower frequency bands (< 20 GHz) and thus bandwidth must be used efficiently to provide a system that allows a number of users access while keeping interference between users at a minimum. This is accomplished through multiple access techniques that permit multiple users access to a system through separation in time, frequency or other forms. In the higher frequency bands (> 30 GHz) for which this system is proposed bandwidth limitation is not an issue.

In multipath channels intersymbol interference (ISI) can cause large bit error rates. In order for ISI to be negligible, the time required to transmit a single symbol must be much greater than the spreading of the symbol due to multipath. This cannot be achieved via one high rate source, as very narrow symbol pulses are required. This is because, in an indoor channel, the width of these pulses can be comparable to or greater than the amount of

multipath spread. This limitation can be overcome by multiplexing several low rate sources to achieve a high data rate system. This provides improvement in a multipath channel because the symbol duration will be longer than the multipath spread. A suitable multiple access technique must be found that enables the multiple sources to transmit simultaneously.

This thesis proposes a multiple access technique to implement a high speed variable rate spread spectrum system transmission technology for a wireless LAN operating in the 30 GHz band. The proposed multiple access scheme, termed code-frequency-time division multiple access (CFTDMA), makes use of a combination of the known spread spectrum multiple access techniques: code-frequency division multiple access (CFDMA), [16], and code-time division multiple access (CTDMA), [17]. These multiple access techniques will be discussed followed by a detailed discussion of direct-sequence spread spectrum.

A portable receiver unit for a wireless system must be kept simple in order to reduce hardware and power requirements. The modular structure of the proposed scheme partially addresses these issues. The need for accurate synchronization in spread spectrum systems increases the receiver complexity. The synchronization required by spread spectrum can be overcome by using a matched filter to reverse the effects of spreading at the receiver. The use of CFDMA by the system poses complications for a matched filter (MF) implementation of the receiver. A means of overcoming these difficulties is introduced. The theory behind the proposed system will be presented followed by one possible implementation of the theory based

on using a MF at the receiver to reverse the effects of spectrum spreading.

The goal of this thesis is to determine the CFTDMA system performance without the complexities of equalization, coding, and diversity. Furthermore, it is required to determine the conditions under which adequate performance is achievable and recommend some parameters for implementation.

Chapter 2

The Indoor Wireless Channel

Chapter Overview

Wireless communications transmits information via radio propagation. The lack of a direct link in wireless communications results in significant difficulties over a system where a direct connect is present. These difficulties are due to the transmitted signal taking multiple paths to the receiver in a time varying channel. Severe signal fading can occur resulting in loss of data.

This chapter discusses the multipath channel for an indoor environment. A model of the multipath channel is given and used to discuss the fading that results from the presence of multipath transmission. Characterization of the indoor wireless channel based on radio propagation parameters will also be discussed.

2.1 Multipath Fading

A transmitted radio signal will encounter objects termed scatterers enroute to the receiver that may dissipate, reflect, and/or diffract the signal [1]. The end result of this distortion is the arrival of several versions of the transmitted signal at the receiver varying in strength, phase, and time of arrival. This phenomenon is known as multipath fading and is depicted in Fig. 2.1.

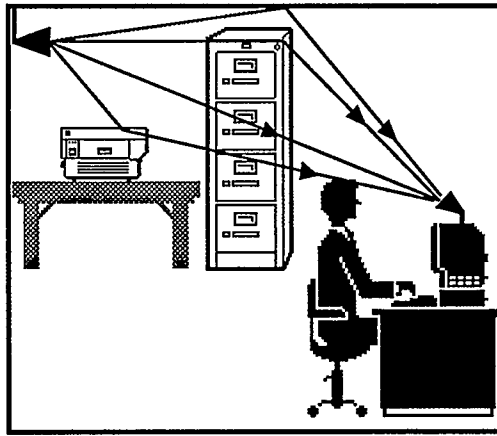


Figure 2.1 *Indoor multipath environment.*

The presence of multiple paths from the transmitter to the receiver results in the spreading of a transmitted pulse as shown in Fig. 2.2. The spreading in time observed in the received signal is termed delay spread, denoted τ_{DS} .

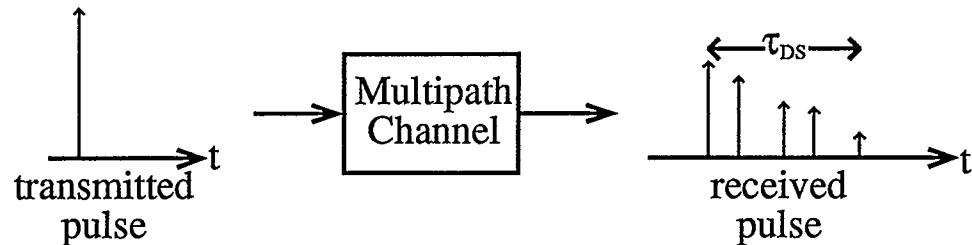


Figure 2.2 *Spreading of a pulse by a multipath channel.*

Due to the portability of the wireless communication system and the

unpredictable motion of scatterers, the multipath channel is time varying as shown in Fig. 2.3.

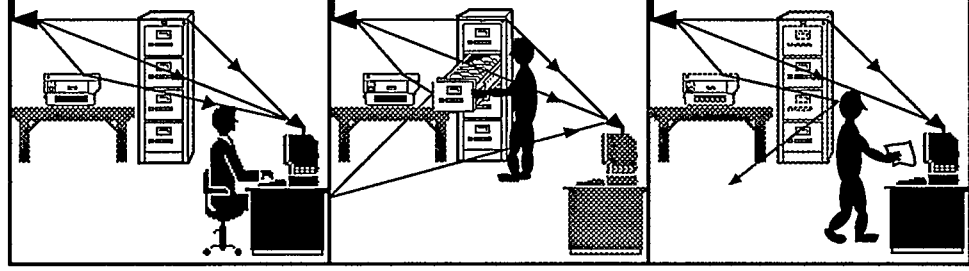


Figure 2.3 *Time-variant indoor multipath environment.*

Statistical means are used to characterize the time variant multipath channel. Following the discussion of multipath channels in [18], we can arrive at a model of the multipath channel as follows. The transmitted bandpass signal is written as

$$s_{BP}(t) = \text{Re}[s_{LP}(t)e^{-j2\pi f_c t}] \quad (2.1)$$

where $s_{LP}(t)$ is the lowpass equivalent response of the signal and f_c is the carrier frequency. If this signal is transmitted over a multipath channel, then multiple signals arrive at the receiver at different times with different attenuations. The channel is time variant and thus the propagation delays and attenuation factors are also functions of time. The received bandpass signal can be written as

$$r_{BP}(t) = \sum_{n=1}^N \alpha_n(t) s_{BP}(t - \tau_n(t)) \quad (2.2)$$

where the n^{th} path is characterized by $\alpha_n(t)$ and $\tau_n(t)$, the time-varying attenuation factor and propagation delay, respectively. By substituting (2.1) into (2.2) and taking the lowpass equivalent form of the received signal we arrive at

$$r_{LP}(t) = \sum_{n=1}^N \alpha_n(t) e^{-j2\pi f_c \tau_n(t)} s_{LP}(t - \tau_n(t)). \quad (2.3)$$

The equivalent lowpass channel response for a N path channel can then be written as the discrete time-variant impulse response

$$c(\tau; t) = \sum_{n=1}^N \alpha_n(t) e^{-j\theta_n(t)} \delta(t - \tau_n(t)) \quad (2.4)$$

where $\theta_n(t) = 2\pi f_c \tau_n(t)$.

The fading due to the arrivals of multiple paths at the receiver is most easily described by rewriting (2.3) as

$$r_{LP}(t) = \sum_{n=1}^N \alpha_n(t) e^{-j\theta_n(t)} s_{LP}(t - \tau_n(t)). \quad (2.5)$$

Thus the received signal is the sum of time-variant versions of the lowpass transmitted signal with amplitudes $\alpha_n(t)$ and phases $\theta_n(t)$. The phases may not be aligned, thus these components may add destructively or constructively, resulting in virtually no received signal or large amplitude received signals, respectively; hence, signal fading. The time-varying variables $\alpha_n(t)$, $\theta_n(t)$, and $\tau_n(t)$ change in an unpredictable manner and thus $c(\tau; t)$ is modeled as a random process. The central limit theorem is applied if there is a large number of paths resulting in $c(\tau; t)$ being a complex-valued Gaussian random variable. This results in the channel envelope $|c(\tau; t)|$ being modeled as a Raleigh-distributed random variable for a non-line of sight (NLOS) channel and as a Ricean-distributed random variable for a line of sight (LOS) channel [2].

The span of frequencies that experience nearly the same local fading is called the coherence bandwidth, B_C [19]. The coherence bandwidth is approximately the inverse of the delay spread of the channel.

$$B_C = \frac{1}{\tau_{DS}} \quad (2.6)$$

Frequency diversity is present in a system if the signal bandwidth is greater than the coherence bandwidth. A wideband signal will experience fades only on selected regions of the spectrum and thus experiences frequency selective fading as shown in Fig. 2.4. When the signal bandwidth is less than the coherence bandwidth, the signal's entire spectrum experiences approximately the same fade; thus, frequency nonselective fading is present. The narrowband signal may be wiped out by a deep fade due to frequency nonselective fading. In selective fading the entire signal is never lost because of the implicit frequency diversity.

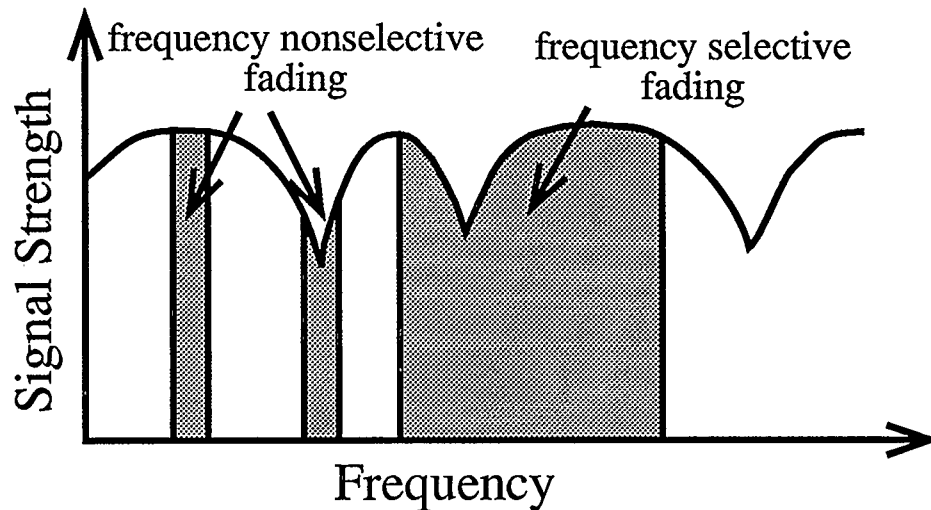


Figure 2.4 *Frequency selective and frequency nonselective fading in a radio channel.*

2.2 Characterization of the Wireless Channel

In addition to modeling the wireless channel through statistical means it can also be characterized in terms of propagation properties. Radio propagation can be characterized by three parameters: rms multipath delay, distance-power gradient, and Doppler spread [2].

2.2.1 Multipath Delay Spread

The amount of time dispersion of a signal acquired after passing through a multipath channel is usually quantified by the rms delay spread. The rms multipath delay spread, τ_{rms} , is determined from the delay power spectrum which is the normalized average received power as a function of delay. The 2nd central moment of the delay power spectrum is the square of the rms multipath delay spread and is given by

$$\tau_{\text{rms}}^2 = \frac{\sum_{k=1}^L \left(\tau_k - \frac{\sum_{j=1}^L \tau_j \alpha_j^2}{\sum_{j=1}^L \alpha_j^2} \right)^2 \alpha_k^2}{\sum_{k=1}^L \alpha_k^2} \quad (2.7)$$

for a L path channel. The mean rms multipath delay spread is typically between 20 ns and 100 ns for transmissions over distances less than 100 m in most indoor radio environments [2], [20]. The exact values of delay spread for a system may depend on various factors: the size and construction of the room in which the system is operating, transmitter-receiver antenna separation, and the carrier frequency used [20].

2.2.2 Power Gradient

In free space, the power density at a given distance from the transmitter is inversely proportional to the square of the distance from the transmitter. In an indoor environment the power is observed to decay faster than in free space due the effects of scatterers and the destructive interference of multipaths [3]. To account for this increased decay in power

density, the inverse square characteristic is replaced with one of a higher order. An exponent, typically ranging from 2 for corridors and large open indoor areas to 6 for metal buildings, replaces the free space exponent of 2 [2]. This exponent is termed the distance-power gradient and thus the loss in power over distance can be written as

$$P_r \propto r^{-pg} \quad (2.8)$$

where pg is the power gradient [2].

2.2.3 Doppler Spread

The wireless scenario is further complicated as, due to the absence of connections, the receiver and transmitter may be in motion. Doppler spread as described in [2] results from the portability of wireless communications. The received carrier frequency differs from the transmitted carrier frequency when the receiver and/or transmitter are in motion relative to one another. This shift in frequency, termed "Doppler shift", is given by the equation:

$$f_d = \frac{v_m}{c} f_c \quad (2.9)$$

where v_m is velocity of the relative motion between transmitter and receiver and c is the velocity of radio wave propagation. Doppler shift may also occur due to motion in the channel other than that of the transmitter and receiver such as a person or object moving within the propagation path.

Due to the multipath nature of the wireless environment, several Doppler shifts occur during transmission. Thus the transmitted sinusoid is received as a spectrum due to the many shifts and this spreading of the transmitted signal in frequency is called Doppler spread.

2.3 Wireless System Design

Knowledge of radio propagation characteristics for an indoor channel affects the design of the wireless system. Doppler spread is typically not a major factor in indoor communications due to the limited speed of motion in an indoor environment [20], [21]. The rms delay spread limits the data rates that can be used for a particular channel without channel protection [11], [12]. The delay spread causes energy transmitted in one symbol slot to spread to adjacent slots as shown in Fig. 2.5 resulting in intersymbol interference (ISI) [19]. If the amount of spread is of the same magnitude as the symbol period then irreducible errors will occur. Thus the data rate must be slowed down to lengthen the symbol period so that it is far greater than the delay spread.



Figure 2.5 *ISI of multiple symbols passing through a multipath channel.*

The power gradient affects the wireless communication system by limiting the range of the system. The path loss characteristic, calculated from the distance-power gradient and the maximum transmitter power, determines the acceptable range of an indoor wireless system.

The proposed system design deals mainly with the problems introduced by time dispersion of the channel. Issues due to power are important but are beyond the scope of this thesis.

Chapter 3

Multiple Access Techniques

Chapter Overview

Multiple access is necessary for systems where more than one user is transmitting and receiving information on a common channel. There are three main multiple access schemes: FDMA, TDMA, and CDMA. The schemes distinguish between users by separation in frequency, by separation in time, and by uniquely separable codes, respectively.

This chapter discusses the three multiple access techniques, outlining their advantages and disadvantages in comparison to one another. Hybrid multiple access techniques, a combination of two or more of the above schemes, will also be discussed.

3.1 Frequency Division Multiple Access

Frequency division multiple access (FDMA) allows for multiple users in a system through frequency separation, as shown in Fig. 3.1. Each user is assigned a disjoint narrow frequency band within the channel bandwidth, permitting the users to transmit and receive at any time.

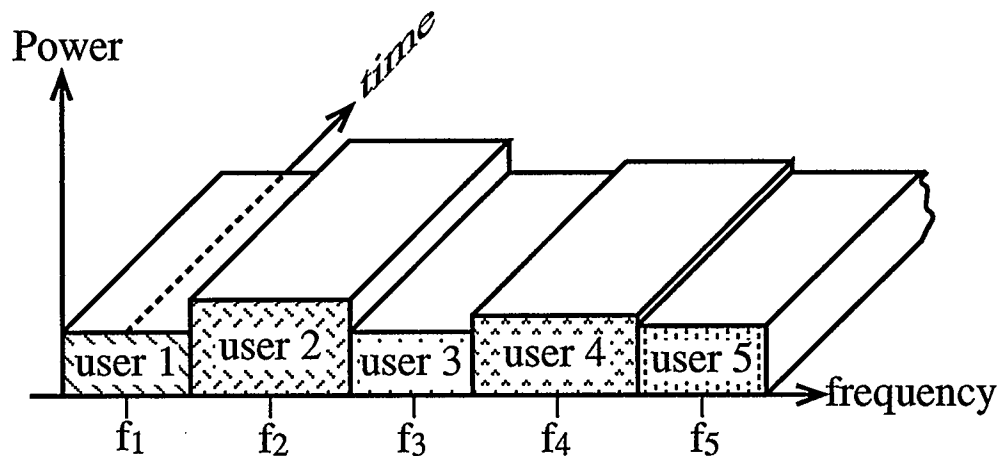


Figure 3.1 *Frequency-power-time domain for a simple FDMA system.*

Ideally, the assigned frequency bands for different users do not overlap and hence the transmissions are orthogonal. Orthogonality of the transmissions indicates that there is no cross-talk between users. Crosstalk will occur in FDMA when individual carrier spectra are not sufficiently separated from one another in the frequency domain [22]. This crosstalk may be eliminated by inserting guard bands between the adjacent frequency bands at the cost of reducing the number of users in the system.

All users may transmit simultaneously in FDMA, resulting in the presence of multiple carriers at any given time. This can result in the

intermodulation of individual carrier frequencies and division of the base station power among all the carriers during downlink when the RF power amplifier is not sufficiently linear [22]. The division of the power among the carriers can cause weaker carriers to be suppressed by stronger ones [22].

3.2 Time Division Multiple Access

Time division multiple access (TDMA) differentiates between multiple users by the assignment of disjoint time slots within a time frame, as shown in Fig. 3.2 [22]. Each user uses the entire channel bandwidth but only during an allotted time interval, thus only one user is active at any given time, as shown in Fig. 3.2(a). The users' transmissions are completely orthogonal in TDMA due to total separation in the time domain and therefore do not interfere with one other. In a time dispersive channel, guard times will be needed to maintain orthogonality between the users.

The timing diagram for a simple TDMA system is shown in Fig. 3.2(b). The time domain is divided into successive time frames composed of smaller time slots each assigned to a particular user. Users transmit information in bursts. Time slots must be short so that a significant delay is not introduced in the transmission of information.

The main disadvantage of TDMA is the requirement for accurate timing synchronization [22]. This is crucial so that users can transmit and receive only during their assigned time slot. Receivers must be resynchronized at the start of each new time frame due to possible changes in the medium.

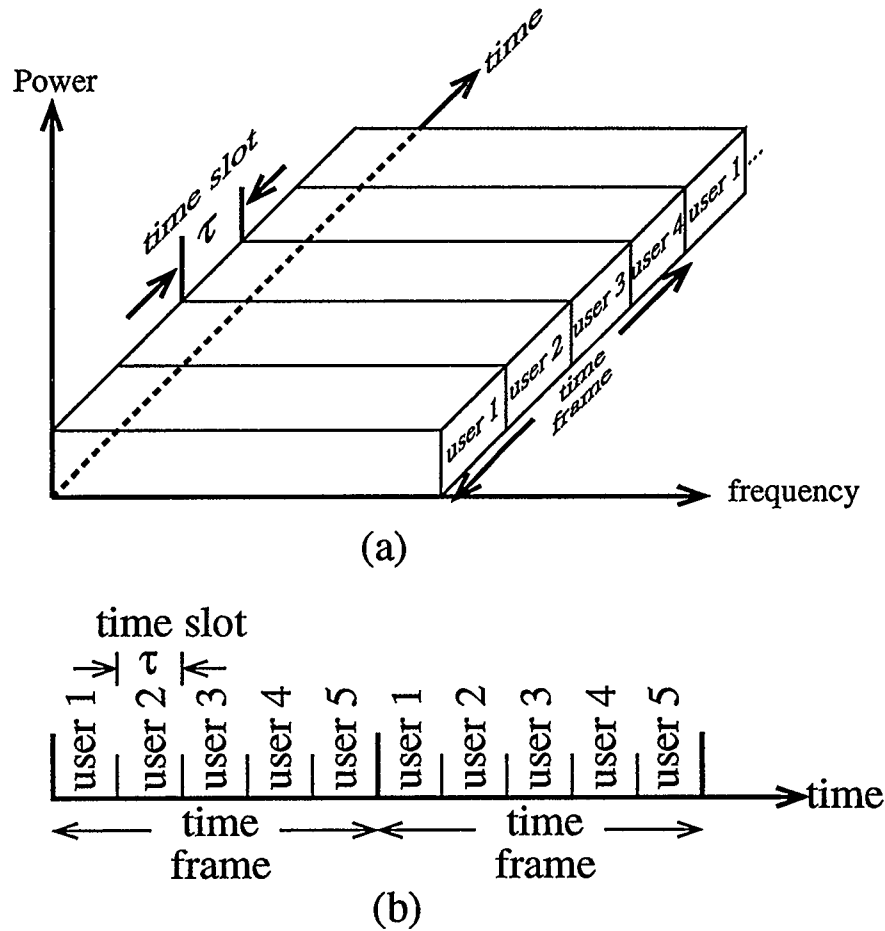


Figure 3.2 TDMA system (a) Frequency-power-time diagram. (b) Timing diagram.

Because only one user transmits at any given time in TDMA, intermodulation distortion and carrier suppression are not present when nonlinear amplification is used. The need for accurate synchronization results in more complicated receivers in TDMA systems.

3.3 Code Division Multiple Access

Code division multiple access (CDMA) differentiates between users by assigning a unique code to each user [22]. Each user can transmit at any

time and the transmission may occupy the entire channel bandwidth. There are two main variations of CDMA: direct sequence CDMA, whereby the user's information signal is directly modulated onto a user's assigned code and frequency hopping CDMA where the code is used to select the carrier frequency for a multiple FSK modulation system. This causes the transmission to hop from one spectral region to the other. Both methods result in spectral spreading beyond what is required for transmission, hence the term spread spectrum. Direct sequence CDMA is important to the system to be proposed in this thesis and will be discussed in detail in Chapter 4. Frequency hopping CDMA is not relevant to the system to be proposed and will not be discussed further.

The number of users in a CDMA system is limited by the inability to correlate out other user's codes, necessitating the use of codes with low cross-correlation. CDMA crosstalk occurs when other users codes are inadequately correlated out while synchronizing to the correct code at the receiver.

Intermodulation of frequencies will not be present as all users are transmitting in the same frequency interval. Synchronization of the codes used to spread and despread the data is necessary.

3.4 Comparison of Multiple Access Techniques

FDMA is much simpler than both TDMA and CDMA and this is reflected in the complexity of the system hardware. TDMA requires that

time intervals be short and accurately synchronized. To accommodate stations transmitting with widely varied bit rates in a common frame requires station buffering and storage and by assigning multiple time slots for higher rates [22]. Variable bit rates impose no difficulties for FDMA and CDMA systems. FDMA is subject to intermodulation of carrier frequencies and weak carrier suppression due to the presence of multiple carriers. This is not so for TDMA, as only one user is active at any given time. CDMA experiences no frequency intermodulation as all carriers are at the same frequency. The ability to recognize codes becomes difficult for CDMA if the system is large.

3.5 Hybrid Multiple Access Techniques

Hybrid multiple access techniques make use of two or more of the aforementioned schemes. This allows a combination of the advantages of the multiple access schemes being used. This section will describe code frequency division multiple access (CFDMA) and code time division multiple access (CTDMA) as outlined in [16] and [17], respectively. These hybrid multiple access techniques are used in the proposed system.

3.5.1 CFDMA

In [16] the application of CFDMA is described for a mobile communication system. This scheme uses FDMA to distinguish users within a cell and CDMA is used to distinguish users between cells. Within each cell the users' signals are upshifted to intermediate frequencies such

that they occupy nonoverlapping bands. A common code is used to spread the resulting signal for each user within a given cell. The frequency bands for individual users are nonoverlapping only prior to spreading. Strong frequency overlap is present during transmission. After the transmissions are despread they return to their disjoint narrowbands thereby allowing their separation at the receivers.

3.5.2 CTDMA

In [17] a CTDMA system for an indoor wireless cellular system is described. In this system, users share a common frequency band and their data are spread by time offset versions of the same code. The time offset is an integer number of chip lengths and all time offsets can be no greater than the length of the spreading code divided by the total number of users. At the receiver the superposition of all users' signals is passed through an aperiodic inverse filter which is very complex. The aperiodic filter ideally achieves perfect separation of the users in a TDMA fashion.

Chapter 4

Direct Sequence Spread Spectrum

Chapter Overview

Spread spectrum is a transmission technology that makes use of more channel bandwidth than is necessary to transmit information. DS-SS employs direct sequence spread spectrum (DS-SS) to allow multiple users to access a system. Accurate synchronization is crucial in order to correctly recover DS-SS data at the receiver.

This chapter discusses DS-SS systems. The process of how DS-SS systems spread the source data spectrum, how to reverse the spectrum spreading at the receiver, and the basic code synchronization methods are presented. The ability of DS-SS systems to combat multipath is introduced.

4.1 Spectrum Spreading

In a DS-SS system a low rate data sequence is modulated onto a high rate periodic code sequence, as shown in Fig. 4.1 [23]. This modulation results in the spreading of the signal spectrum.

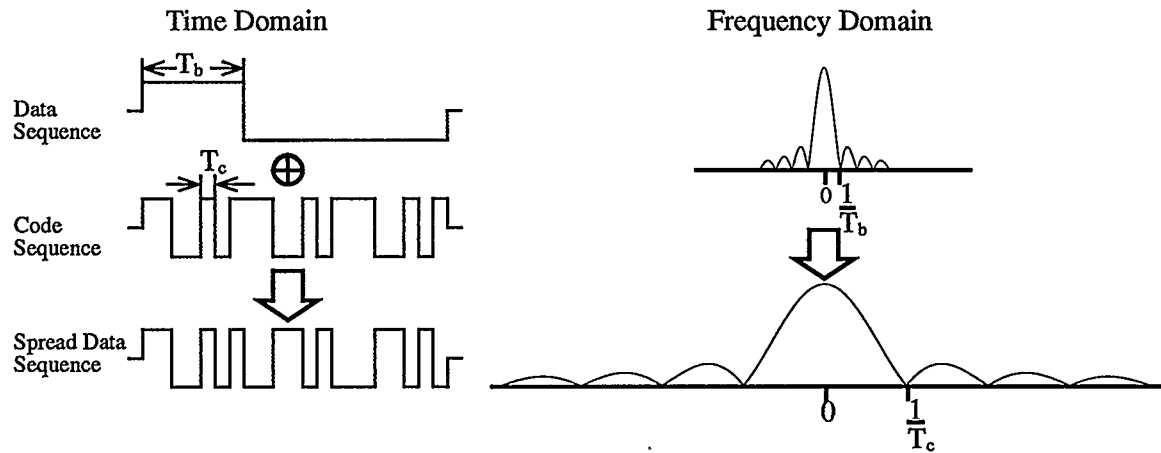


Figure 4.1 *Simple DS-SS system.*

It is common to use the term chip to refer to a code sequence bit in a spread spectrum system in order to differentiate it from a data sequence bit. The term chip will be used when referring to a code sequence bit. The bit duration, T_b , is often an integer multiple of the chip duration, T_c , so as to reduce complexity in the system and will be assumed so throughout the rest of the thesis.

In a DS-CDMA system each user's data will be modulated onto a unique code sequence. The unique code sequences must exhibit low cross-correlation in order for the signals to be successfully recovered at the receiver.

The DS-SS system increases the signal bandwidth by a factor L where

$$L = \frac{T_b}{T_c}. \quad (4.1)$$

The amount of spreading, L , is called the processing gain of the system and it determines the spread spectrum system's interference rejection capability. The interference may be due to multipath, other CDMA users, and narrowband interference [15]. No improvement in performance is provided by the processing gain in AWGN [23]. This rejection capability is discussed further in the next section in terms of despreading at the receiver. In most spread spectrum systems one period of the code sequence is equivalent to one data bit duration. Hence the processing gain is equal to the code sequence period M . A processing gain of $L = M$ will be assumed for the spread spectrum systems discussed throughout this thesis.

The spreading of the bandwidth may provide implicit frequency diversity to the system depending on the amount of processing gain. As discussed in section 2.1, frequency diversity is provided in systems with signal bandwidths greater than the coherence bandwidth, a scenario more likely to occur for wideband systems like spread spectrum.

4.2 Spectrum Despreading

Despreading of the spectrum occurs at the receiver when the received signal is correlated with a locally generated reference code. If the reference code is identical and synchronized in time to that used to spread the information signal at the transmitter, then the effect of spreading is reversed as illustrated in Fig. 4.2.

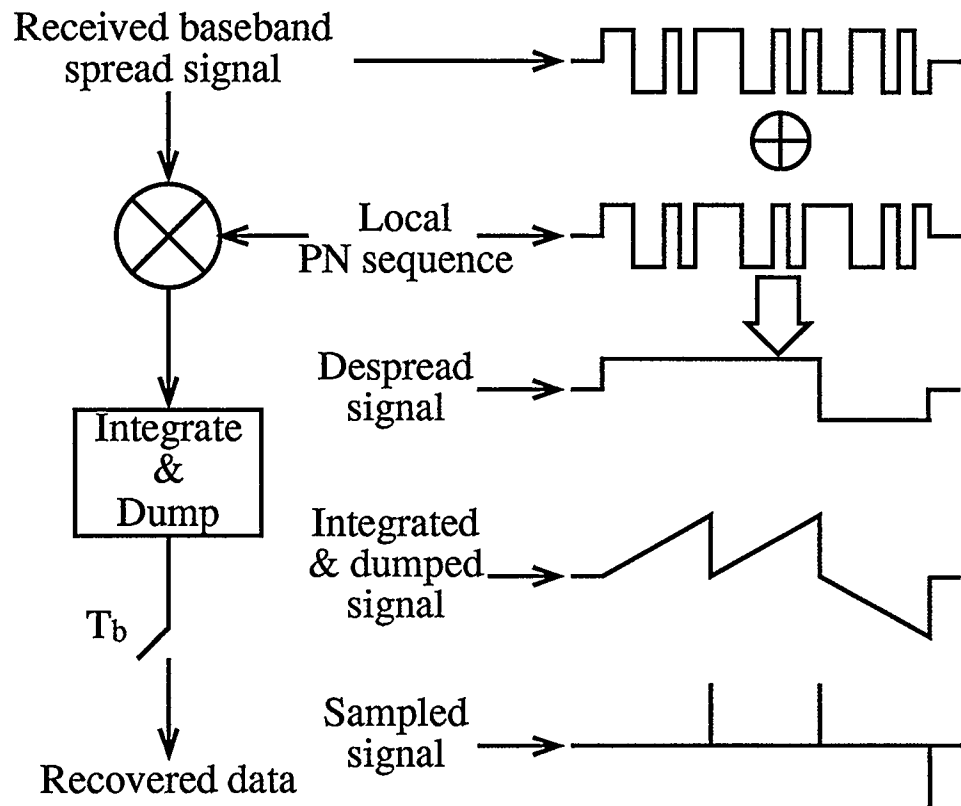


Figure 4.2 Despreding of DS-SS signal via correlation in a perfectly synchronized noiseless system.

Despreding collapses the data sequence's spread bandwidth to the original narrowband data bandwidth B . For a DS-CDMA system, the desired user's signal power density over the despread bandwidth will be L times greater than that of the other users in the system whose signals were spread by different codes at the transmitter as shown in Fig. 4.3(a). As the despreding process involves a further modulation of the received signal with a high rate code, any narrowband interference present in the received signal will be spread out as shown in Fig. 4.3(b). Narrowband filtering can therefore be used at the receiver to reduce the level of interference due to co-users and narrowband interference. The power density of an AWGN signal is unaffected by the despreding process, as shown in Fig. 4.3(c).

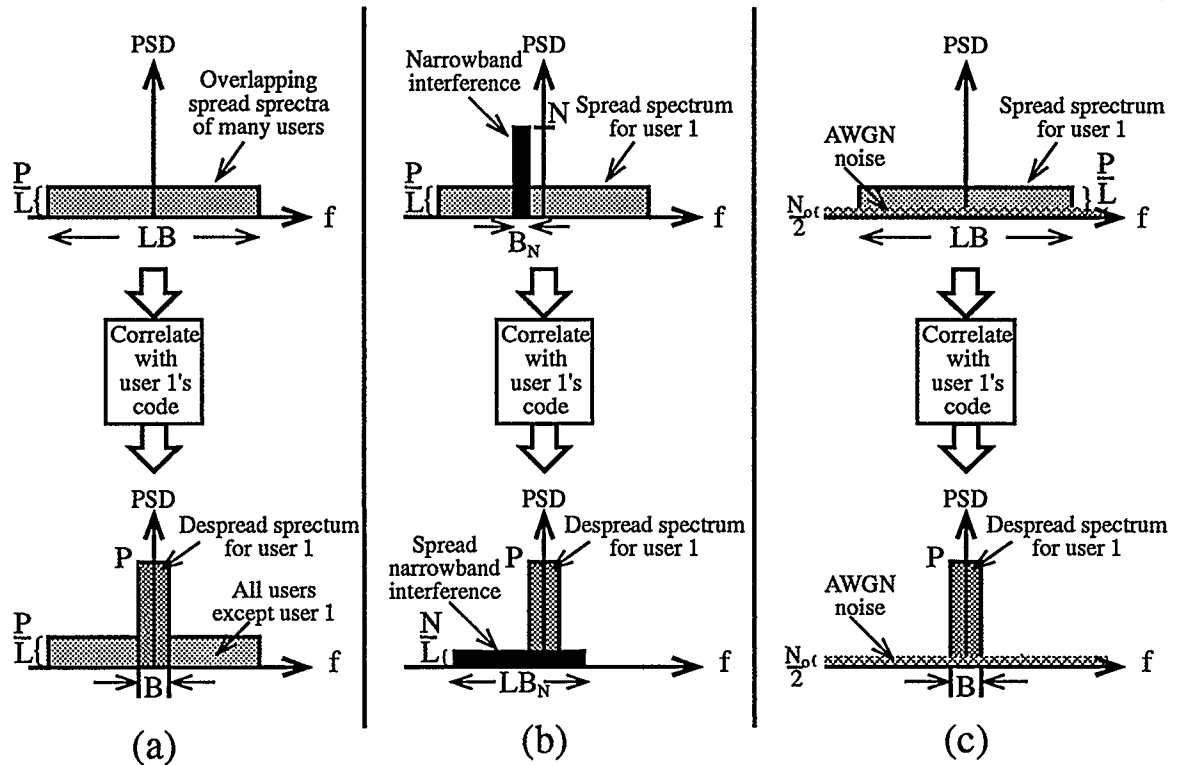


Figure 4.3 Illustration of processing gain in a DS-SS system with (a) multiple users (CDMA), (b) narrowband interference, and (c) AWGN.

In a multipath channel, delayed versions of the desired user's signal will arrive at the receiver. The despreading process will only synchronize to one multipath arrival, usually the strongest, thus the remaining paths will be treated as interference and correlated out [24]. Alternatively, the multipaths with ray separations greater than one chip can be resolved and the signal energy collected from several signal arrivals to provide a form of diversity [1], [12], [14].

4.3 Spreading Codes

DS-SS allows multiple access to a system by the assignment of unique codes to the different users. Thus each user's data is spread by modulation

with a different code sequence. In order for a large number of users to effectively use the system, the code sequences must be nearly orthogonal or in effect have low cross-correlation. Spread spectrum systems achieve this by using pseudo-random or pseudo-noise (PN) codes.

4.3.1 PN Sequences

Pseudo-noise (PN) codes are deterministic codes that behave similar to white noise. A PN sequence consists of repetitions of a PN code resulting in a sequence with a period equal to the PN code length. The seeming randomness of PN sequences allows DS-SS transmissions to have low detectability as they appear totally random to a casual observer. Low cross-correlation also allows multiple users on the system with little interference. A signal made up only of white noise would have zero cross-correlation.

There are many types of PN sequences available: m-sequences, Gold sequences, and Kasami sequences to name a few [18]. m-sequences are discussed in detail in the following section.

4.3.1.1 m-Sequences

The proposed system will use a class of PN sequences known as m-sequences. These sequences are formally known as binary maximal length shift-register sequences.

Binary shift-register sequences are generated using a linear feedback shift-register and exclusive-OR gates, as shown in Fig. 4.4 [23]. Shift-register sequences are periodic and have different periods depending on the switch settings. The maximum period of a binary shift-register sequence is $M = 2^m - 1$ where m is the number of shift registers and will also be referred to as the sequence order in this thesis. The shift-register sequences that exhibit this maximum period are termed m -sequences. The combinations of the feedback switches which produce m -sequences can be found in tables such as in [23].

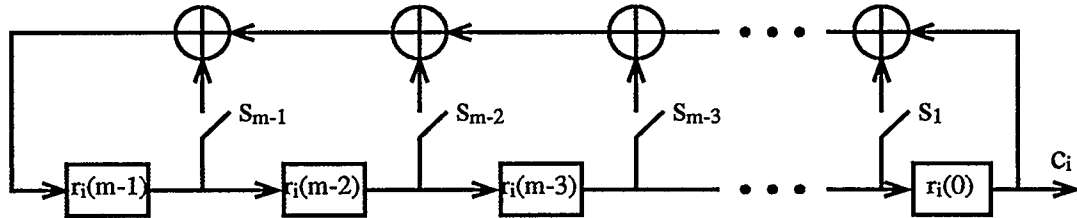


Figure 4.4 *Linear feedback shift-register used to generate PN sequences.*

A disadvantage of using m -sequences for spreading is the low number of codes available for a given order, thus limiting the number of users for a CDMA system. The number of codes can be increased by increasing the order of the m -sequence. This results in an increase in hardware and bandwidth and is often not a realistic compromise. Further problems using m -sequences for CDMA arise due to poor correlation properties. The autocorrelation of an m -sequence $c(t)$ with period M is shown in Fig. 4.5.

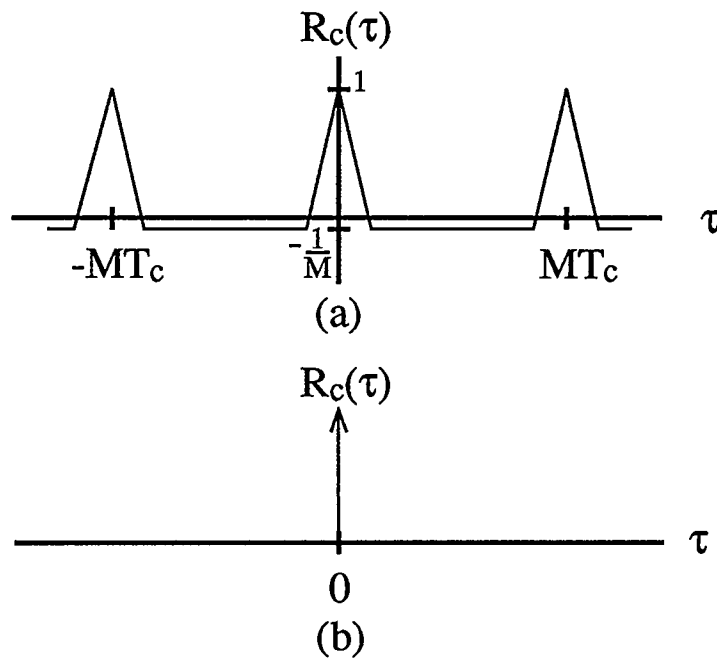


Figure 4.5 (a) *Normalized autocorrelation of m-sequence with period M .* (b) *Autocorrelation of a white noise signal.*

The cross-correlation values between two m-sequences are a large percentage of the peak value of the autocorrelation of a m-sequence; they thus are unacceptable for CDMA; however, it is possible to select a small subset of m-sequences with lower cross-correlation peak values [18]. The number of such sequences is usually too small for CDMA applications.

The proposed system will use m-sequences to spread data. Several PN sequences are not necessary for the system as will be discussed in Chapter 5. m-sequences were chosen due simply to their ease of generation. Future work should look at the use of other types of sequences.

4.4 Synchronization

Despreading is attained by correlating the received spread signal with a locally generated reference sequence identical to the spreading sequence. The receiver has apriori knowledge of the spreading code, but it does not know the code phase when it arrives at the receiver. The steps in the recovery of the original message signal are illustrated in Fig. 4.6 for perfect and imperfect chip synchronization.

To correctly demodulate and decode the received data the despreading code must be correctly synchronized to the phase of the incoming spread data. If synchronization is not attained, then multiplying by the PN sequence at the receiver will not result in despreading. The two branches in Fig. 4.6 illustrate the waveforms when data is properly despread and when it is not.

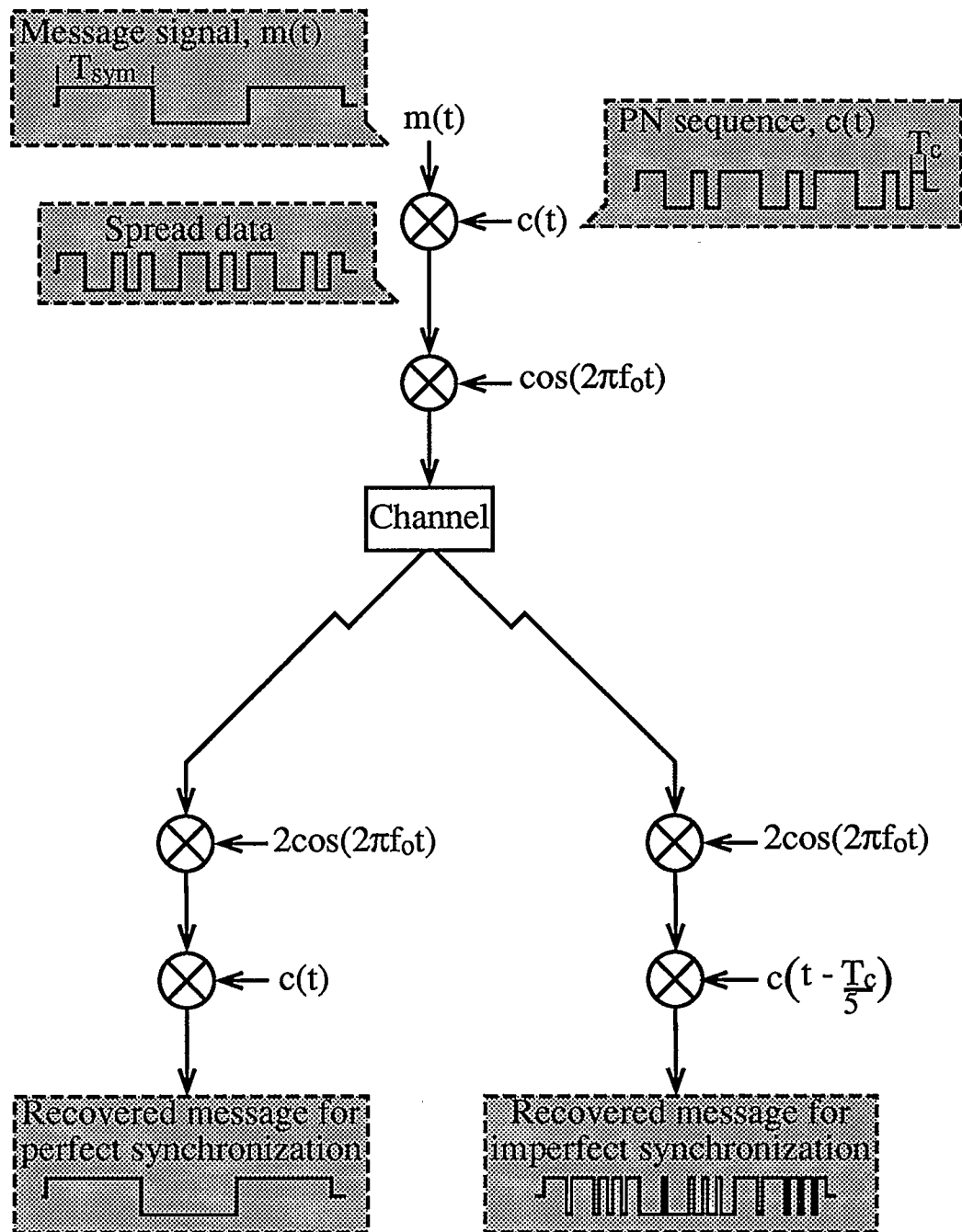


Figure 4.6 DS-SS system with perfect and imperfect chip synchronization of $\frac{1}{5}T_c$.

Synchronization consists of two steps: code acquisition and code tracking [23], [25], [26]. Code acquisition refers to the initial synchronization of the receiver. Code acquisition is usually coarse in that

the locally generated reference code's phase is only aligned to within a fraction of a chip period, $\pm\Phi T_c$, to the received code's phase. Code tracking refers to the ongoing synchronization process performed at the receiver. Tracking performs fine synchronization, aligning the reference code phase exactly with the received code phase.

4.4.1 Code Acquisition

Code acquisition is a search through all possible phases of a local PN signal for one which aligns with the incoming PN signal [23], [25]. To facilitate this initial synchronization of the receiver spreading code, a preamble is transmitted before the transmission of real data. The preamble consists of several repetitions of a PN code of smaller order than the PN code used to spread the information signal. No data modulation is performed on this training sequence. The search for the correct phase can be performed using two possible search strategies: serial and parallel. A serial search inspects one phase at a time to check alignment whereas a parallel search would inspect all possible phases simultaneously and select the most probable. These search strategies can be implemented in several ways.

One possible implementation of the serial search strategy is a sliding correlator as shown in Fig. 4.7.

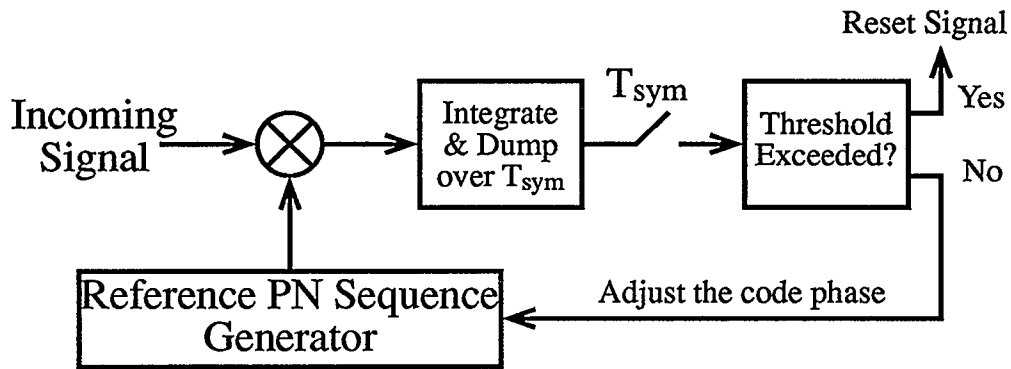


Figure 4.7 Block diagram of sliding correlator code acquisition circuit.

The sliding correlator synchronizer works by multiplying the incoming signal by a reference code at an arbitrary phase and integrating over a time period. The output of the integrator is sampled and compared to a threshold. If the threshold is exceeded then the reference spreading code and the incoming PN code are synchronized. A reset signal is then sent to the PN generator that produces the higher order PN code for despreading real data. If the threshold is not exceeded then the reference spreading code is adjusted by a fraction of a chip length and the process repeated. The time to acquire synchronization can be lengthy and is dependent on the code length and the specified accuracy for acquisition. If a code of length M is used in the synchronization preamble data then there are up to

$$K = \frac{M}{2\Phi} \quad (4.2)$$

phases to check for alignment where Φ is the fraction of a chip to which initial alignment is required.

A parallel search can be implemented by a bank of K correlators each multiplying the incoming signal with a reference code at a different phase as shown in Fig. 4.8 [23]. The phase corresponding to the correlator producing

the largest output is selected as the code phase.

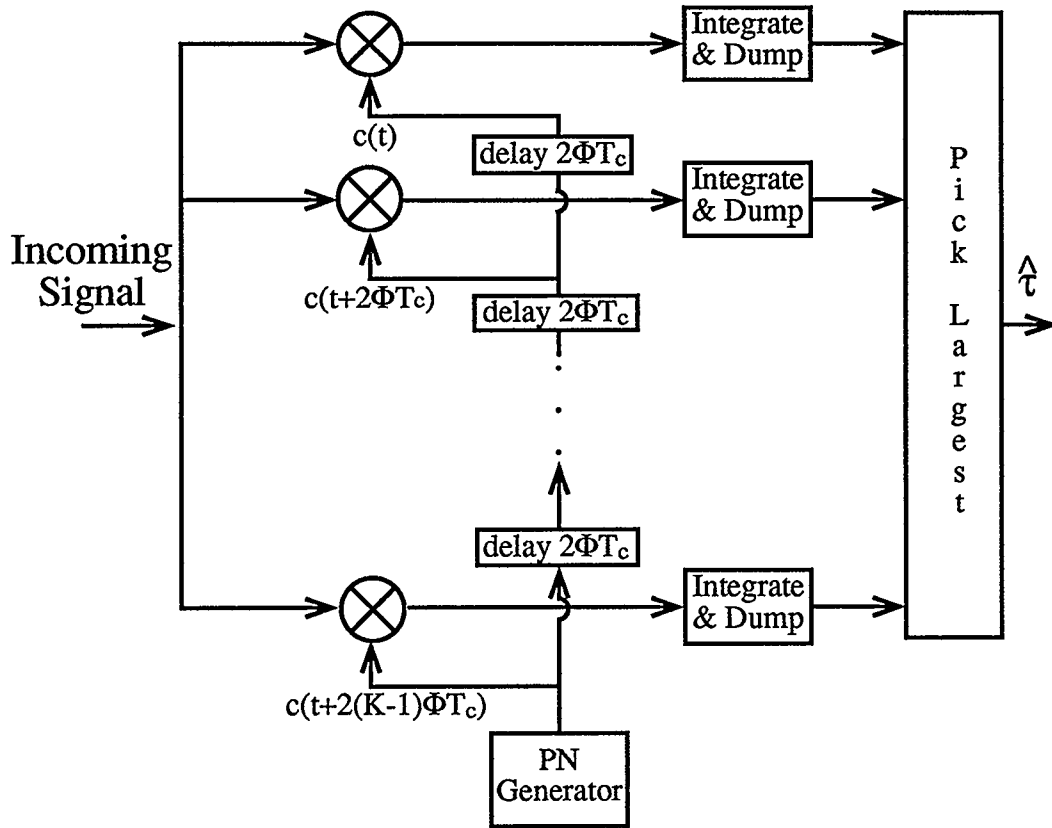


Figure 4.8 Block diagram for parallel search code acquisition using correlators.

The time to synchronize for a parallel search is independent of the code length, but the amount of hardware required is excessive for long codes. The circuit for a serial search is much simpler than the parallel search circuit but requires more time to acquire synchronization. The search strategy should be chosen based upon limitations imposed by the system.

A method of simplifying the circuit for the parallel search algorithm is to implement the parallel correlators using a single matched filter [25], [27]. The filter is matched to the coefficients of one period of the PN code used in the preamble data. A large spike is produced at the output of the matched

filter when the incoming signal is aligned with the taps of the matched filter as shown in Fig. 4.9.

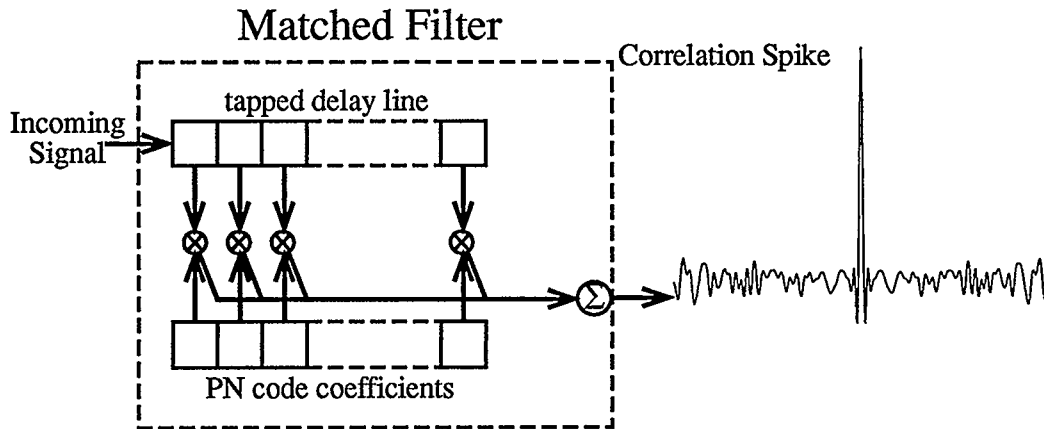


Figure 4.9 Output of filter matched to PN code present in incoming signal.

The block diagram for an acquisition circuit using a matched filter is shown in Fig. 4.10. A threshold detector checks the matched filter output for the presence of the large correlation spike. A reset signal is sent to the local PN sequence generator if the spike is detected.



Figure 4.10 Block diagram for basic parallel search code acquisition using a matched filter.

It is important to note that very basic synchronization circuits have been presented here. Variations of these circuits are used in practice and issues like verification of acquisition must also be considered.

4.4.2 Code Tracking

Code tracking is an ongoing process that attains and maintains perfect synchronization once initial synchronization has occurred [23], [25]. An example of a tracking circuit is shown in Fig. 4.11.

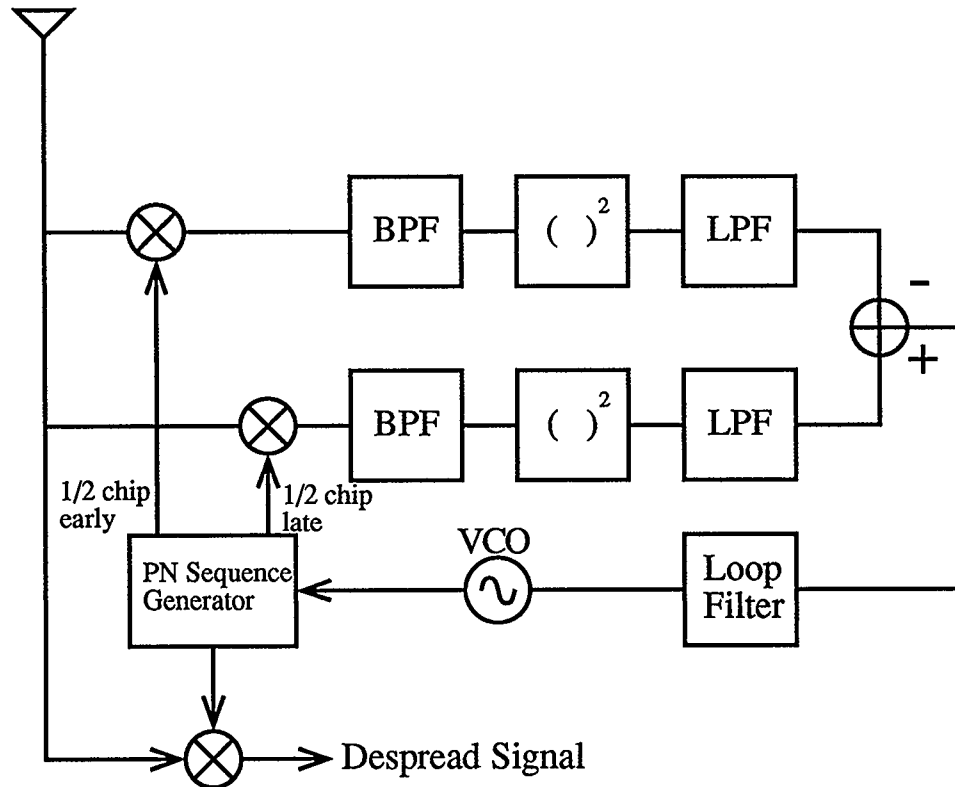


Figure 4.11 Block diagram for early-late tracking circuit.

The circuit of Fig. 4.11 tracks the incoming code sequence by comparing the energy of two signals, one that is correlated half a chip early and one that is correlated half a chip late. The clock of the PN sequence generator is adjusted depending on which signal has more energy.

Chapter 5

Proposed System

Chapter Overview

Two main requirements in multimedia applications over an indoor wireless local area network are high speed and variable rate. Variable rate requires an adaptable system that can adjust to different rates with ease without degradation of performance. High speed and variable rate are crucial to multimedia applications in that speech, data, text and video all require different rates. The proposed system can be used to either transmit data from a single high speed source or from a number of mixed rate sources.

The transmission technique proposed is a hybrid of spread spectrum and other multiple access techniques. The system multiplexes low rate sources using a combination of the hybrid multiple access techniques CFDMA and CTDMA, discussed in Chapter 2, to achieve high speed and variable rate. Multiple access is utilized so that several low rate sources are used rather than a single high rate source in order to reduce the effects of intersymbol interference (ISI). ISI due to multipath becomes significant in systems where the duration of the transmitted symbols is comparable to the delay spread, a scenario which occurs in high rate RF systems. Spread spectrum is used to combat multipath fading. The chosen multiple access techniques will also satisfy the variable rate requirement. This chapter presents the theory for the chosen form of multiplexing in terms of its relevance to the proposed system.

5.1 System Description

In multipath channels intersymbol interference (ISI) can cause large bit error rates. Channel equalization would be required to reduce the bit error rates for a system where ISI is not negligible [28]. In order for ISI to be negligible the time to transmit a single symbol must be much greater than the multipath spread, typically on the order of 10 times the rms delay spread. This cannot be achieved via one high rate source in an indoor channel as typical rms delay spreads are on the order of 50 ns which restricts data rates to be no greater than 2 Mbits/sec. This limitation can be overcome through conversion of a single high speed source to an equivalent set of low rate sources. The low rate sources are then multiplexed and transmitted simultaneously. This provides improvement in a multipath channel over a single high rate source as the bit duration is longer and thus better able to withstand multipath spread.

For example, consider the system shown in Fig. 5.1 where data from a high rate 20 Mbits/sec system is converted to ten 2 Mbits/sec low rate sources. The bit duration is increased from 50 ns to 500 ns greatly reducing the effects of delay spread. A rms delay spread of 50 ns would introduce severe ISI in a system with bit durations of 50 ns whereas the ISI for a 500 ns bit duration is negligible.

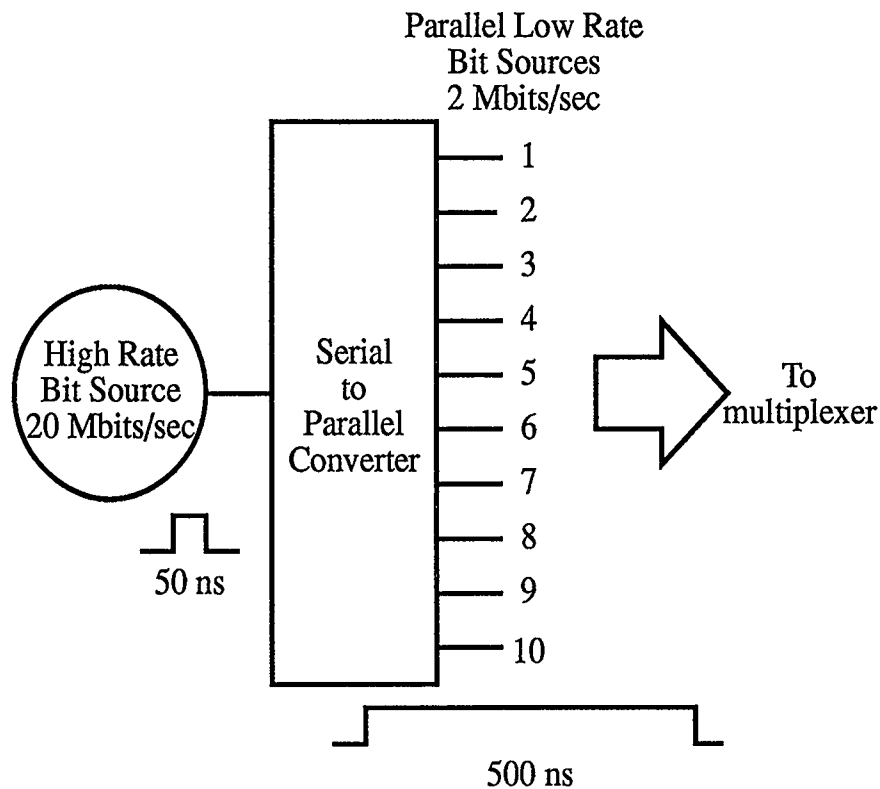


Figure 5.1 *Conversion of a high speed source to an equivalent set of low rate sources.*

Alternatively, a number of sources that generate data at multiples of a base rate can be multiplexed and transmitted simultaneously. Fig. 5.2 illustrates a mixed rate system with a base rate of 2 Mbits/sec that provides multimedia service. Each portable receiver for the mixed rate system will receive only at the rate it is designed for. Thus the portable interested in the data portion of the system shown in Fig. 5.2 will operate only at 6 Mbits/sec while the portable for the video portion of the signal will operate only at 10 Mbits/sec.

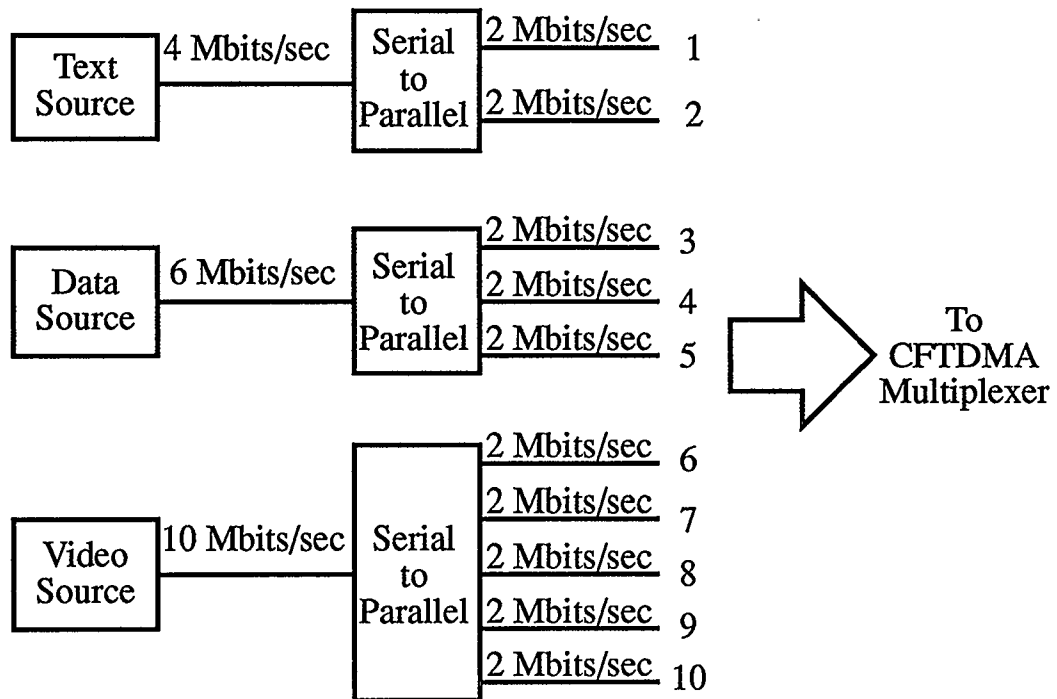


Figure 5.2 *Mixed rate sources that generate data at a multiple of the base rate are assigned to a subset of the number of low rate sources.*

The basic requirement to implement a high variable rate system utilizing several parallel low rate sources is to find a suitable method of multiplexing the data from the different sources so as to reduce the inter-source interference. The CFTDMA system is a proposed solution to this problem. A CFTDMA system uses a combination of CFDMA and CTDMA to efficiently combine low rate sources to gain both high speed and variable rate. Each technique will be described separately, somewhat reiterating the discussion of Section 3.4, and then the combination of the two techniques will be outlined.

5.1.1 CFDMA

CFDMA describes the multiple access technique whereby the spectra of several sources multiplexed using FDMA are spread using DS-SS as outlined in Section 3.5.1. Spreading is a desirable feature in a wireless system to provide anti-multipath capability.

For illustration purposes, consider the multiplexing of 3 low rate sources with bandwidth B . A 3 source FDMA system is shown in Fig. 5.3(a). The data spectrum for each FDMA source occupies an orthogonal narrow frequency band, as shown in Fig. 5.3(b) and Fig. 5.3(c). A comparable 3 source CFDMA system is shown in Fig. 5.3(d). The CFDMA system spreads each source's spectrum with an identical code in addition to offsetting the sources' data in the frequency spectrum. The spreading process increases the bandwidth for each source by the processing gain L as shown in Fig. 5.3(e). Strong frequency overlap is introduced by spreading as the amount of frequency offset between the sources is much smaller than the increase in bandwidth, and is at least equal to the narrowband bandwidth, B , of each source. The wideband signals are combined resulting in the CFDMA spectrum illustrated in Fig. 5.3(f).

The bandwidth of a CFDMA system is $LB + (N-1)B$, a significant increase from the FDMA system bandwidth of NB , where N is the number of sources to be multiplexed.

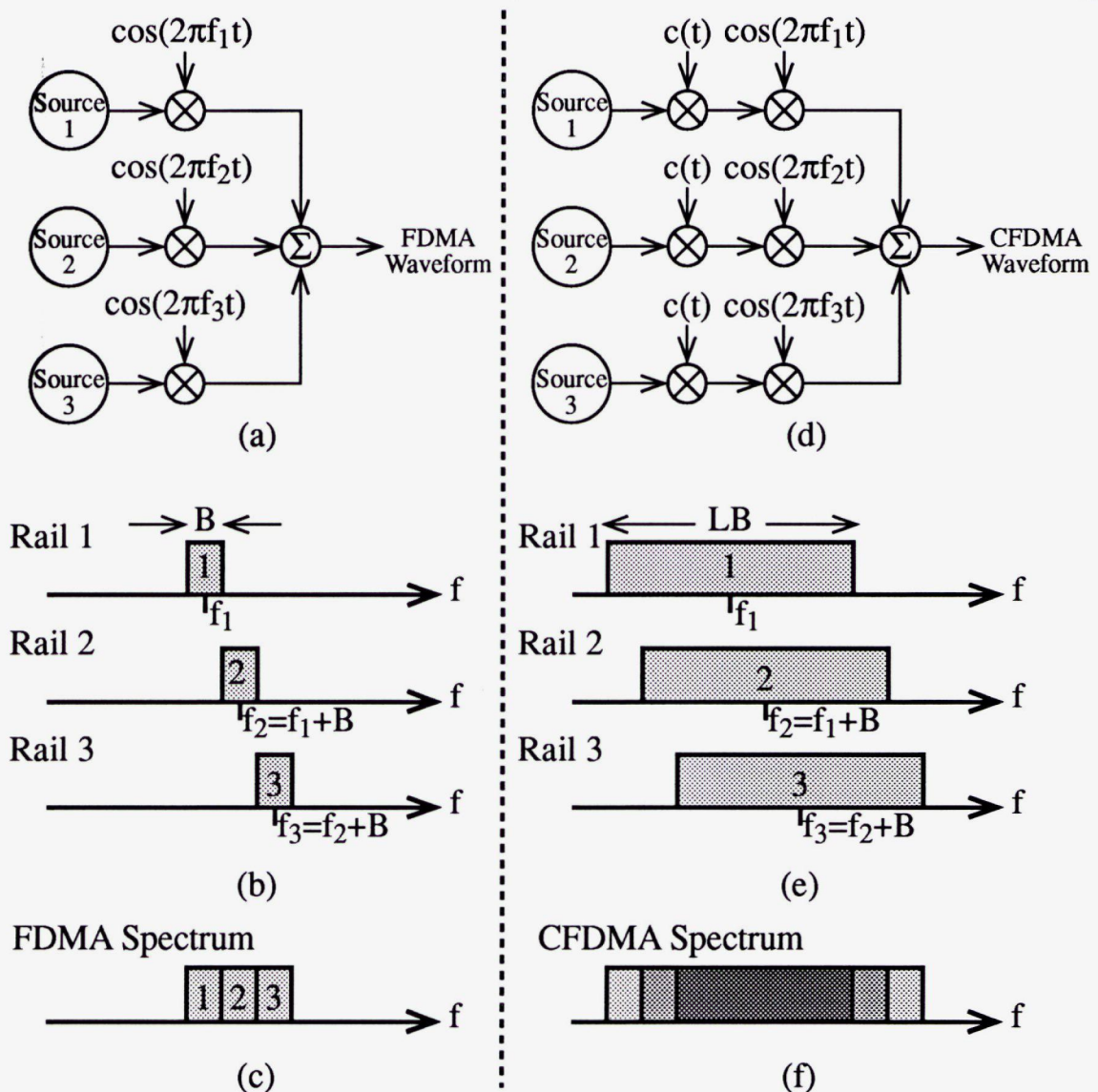


Figure 5.3 (a) 3 source FDMA system. (b) Frequency spectra for the 3 branches of the FDMA system. (c) Spectrum for FDMA waveform. (d) 3 source single code CFDMA system. (e) Frequency spectra for the 3 branches of the CFDMA system. (f) Spectrum for CFDMA waveform.

The strong frequency overlap present in the CFDMA spectrum will be reversed at the receiver by modulation of the CFDMA signal with a reference code. Thus the original N nonoverlapping narrow bands are restored. The data from the different sources can then be recovered via a

series of bandpass filters with different center frequencies so that the only source of interference is AWGN.

The use of additional codes will increase the data rate of the CFDMA system without requiring extra bandwidth. The block diagram for a multiple code CFDMA transmitter is shown in Fig. 5.4. The number of codes, N_c , is limited by the amount of cross-correlation between the codes.

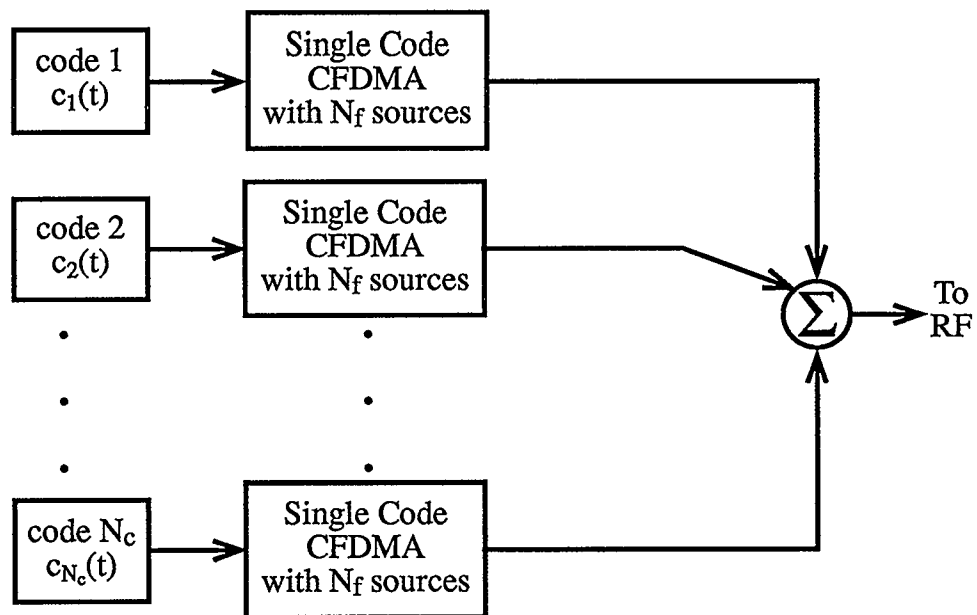


Figure 5.4 *Multiple code CFDMA transmitter.*

5.1.2 CTDMA

CTDMA describes the multiple access technique whereby spread source data occupying a common frequency band is multiplexed using a form of TDMA as outlined in Section 3.5.2. Fig. 5.5 illustrates a 3 source CTDMA transmitter.

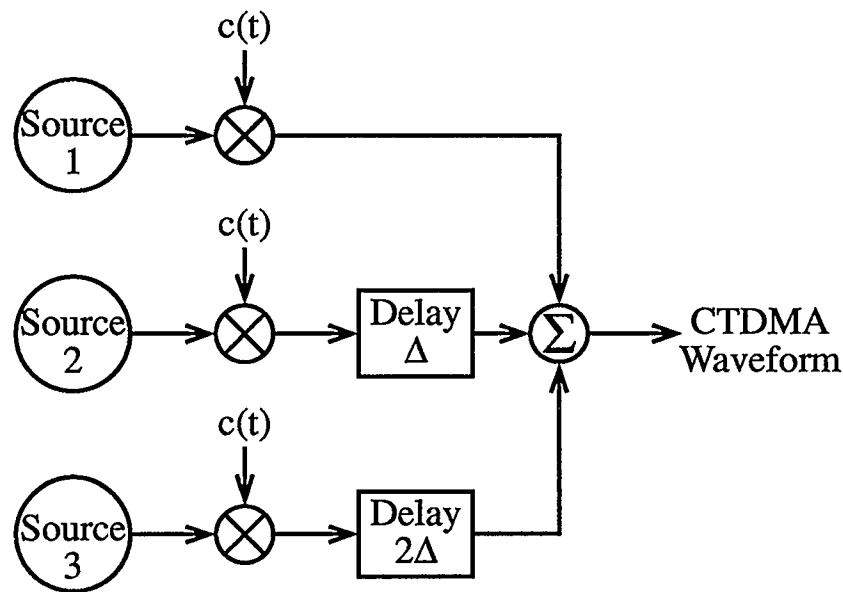


Figure 5.5 A 3 source CTDMA transmitter.

The data from the 3 sources is spread by the same code but the transmissions are offset in time by Δ thus achieving a type of TDMA. The offset Δ is an integer number of chip lengths. The delay Δ between source transmissions is chosen so that a low cross-correlation results between the spreading code and its time offset version.

5.1.3 CFTDMA

A combination of the two hybrid multiple access techniques described in the preceding two sections leads to an increase in data rate over the two schemes independently without requiring additional bandwidth. This technique will be termed CFTDMA and will be described in this section.

A general CFTDMA system is the superposition of N_t time offset single code N_f source CFDMA systems as illustrated in Fig. 5.6. The single

code CFDMA systems all use the same code thus only the time offset differentiates the CFDMA waveforms, hence a type of TDMA is achieved.

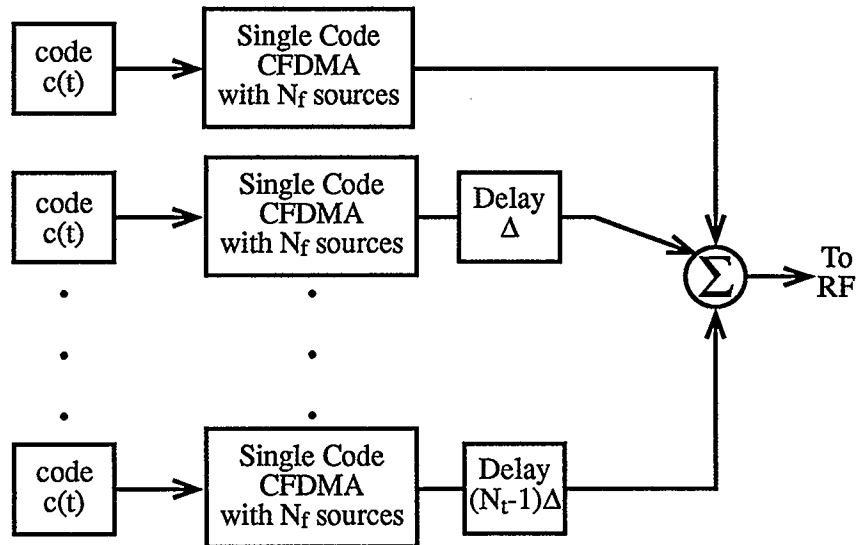


Figure 5.6 Block diagram for a $N_f N_t$ source CFTDMA transmitter.

The CFTDMA system has $N_t N_f$ sources each transmitting at R_b giving a maximum rate of

$$R_T = N_t N_f R_b. \quad (5.1)$$

The CFTDMA system to be implemented in this paper looks at a simplified system where $N_t = 2$, thus only two CFDMA waveforms are multiplexed by offsetting the waveforms in the time domain. The block diagram for the transmitter for this basic system is shown in Fig. 5.7.

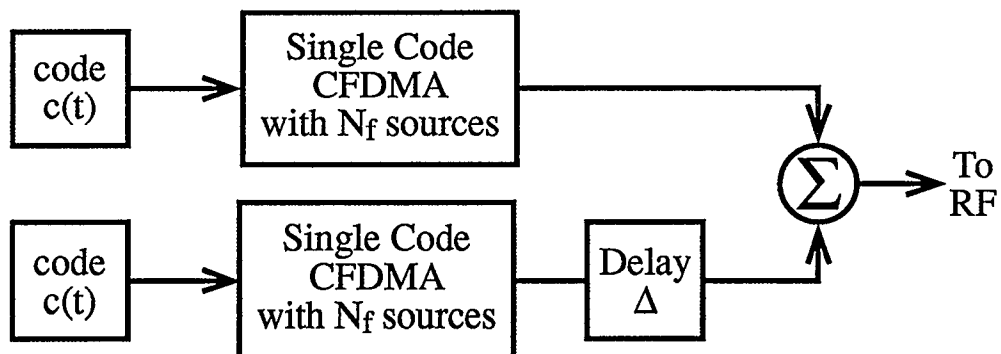


Figure 5.7 Block diagram of proposed CFTDMA transmitter.

The CFTDMA system is shown in Fig. 5.8 with the $2N_f$ source data originating from a single high rate source. The transmission rate for the CFTDMA system is

$$R_T = 2N_f R_b. \quad (5.2)$$

The low rate sources could also originate from mixed rate sources as was shown in Fig. 5.2.

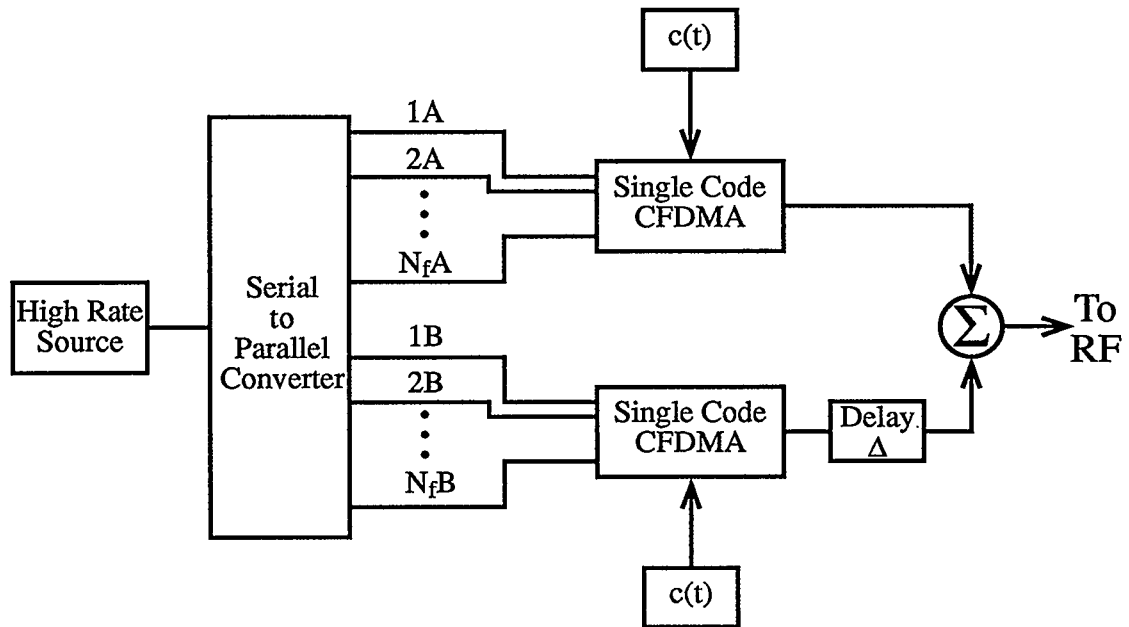


Figure 5.8 CFTDMA high rate system. A single high rate source is converted into a number of low rate sources which are divided into two equal groups. CFDMA is used to multiplex sources within a group and CTDMA is used to multiplex the two groups.

5.2 System Expansion

Variable rate is necessary to accommodate a variety of bit rates that a wireless LAN would potentially use. The CFTDMA system produces an overall rate of $2N_f R_b$ bits/sec. Variable rate can be achieved by assigning only a subset of the $2N_f$ sources, thus rates from R_b bits/sec to $2N_f R_b$ bits/sec

are possible.

The CFTDMA system can be expanded by using multiple codes if data rates larger than $2N_f R_b$ bits/sec are required. The CFTDMA system described in Section 5.1.3 used only one PN code for the entire system. If this CFTDMA system is considered as one transmitter unit with overall rate R_T , then we can combine N_c of these units each using an entirely different PN code to get a subset of rates of nR_T where $n = 1, 2, \dots, N_c$. Thus a variable rate system that can achieve even higher rates is obtained by combining a variable number of these units as desired as shown in Fig. 5.9.

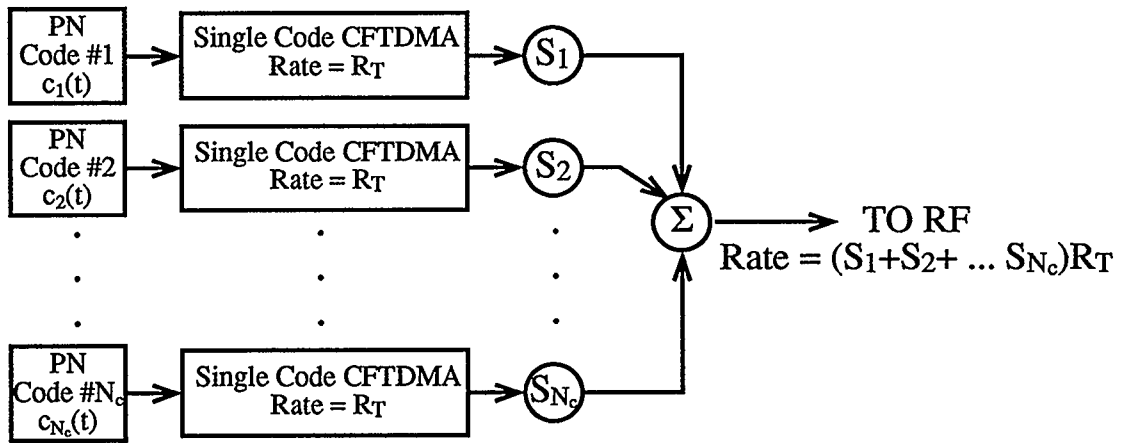


Figure 5.9 Variable rate CFTDMA system.

The multiplier variables S_n of Fig. 5.9 are either 1 or 0 thus allowing the appropriate rate to be selected by the system.

5.3 Summary

A high speed variable rate system is theoretically achieved via the use of CFTDMA to multiplex several low rate sources. The actual performance

will be limited by the available bandwidth, ISI, multipath fading, noise, interuser interference and other interferences. The purpose of this thesis is to investigate the performance of the CFTDMA system in an indoor multipath channel without the complexities of coding, equalization, and diversity techniques.

Chapter 6

Implementation Dependency on Despreader Circuits

Chapter Overview

The CFTDMA system uses DS-SS to overcome multipath fading. The performance of systems that employ DS-SS is limited by their ability to synchronize to the spreading code. The use of matched filters (MF) to despread direct-sequence spread spectra has become popular in spread spectrum receivers [27], [29], [30], [31]. MF despreader enable a simple circuit to be used for despreading and require only symbol synchronization whereas a correlator requires both chip and symbol synchronization. Surface acoustic wave (SAW) technology has made the use of matched filters simple and affordable [30]. The receiver unit for a wireless portable unit should be kept as simple as possible in order to keep size and cost to a minimum and save battery life, thus a MF despreader is desirable.

This chapter will discuss the use of matched filters to despread direct-sequence spread spectrum data. The system design should try to incorporate despreading via a MF to accommodate the requirement for a simple receiver. The strong frequency overlap present in CFDMA systems poses a problem for MF despreader. This problem will be explained along with a solution for CFDMA systems. The solution will affect both the transmitter and receiver design for the proposed CFTDMA system.

6.1 Matched Filter Despreader

A direct-sequence spread spectrum waveform is despread via correlation. Correlation is a form of matched filtering, thus a matched filter (MF) despreader can be implemented. A MF despreader consists of a filter matched to the coefficients of one period of the PN code used to spread the data at the transmitter and a sampler operating at the symbol rate. If the output of the MF is sampled at the end of a symbol interval the narrowband data is recovered.

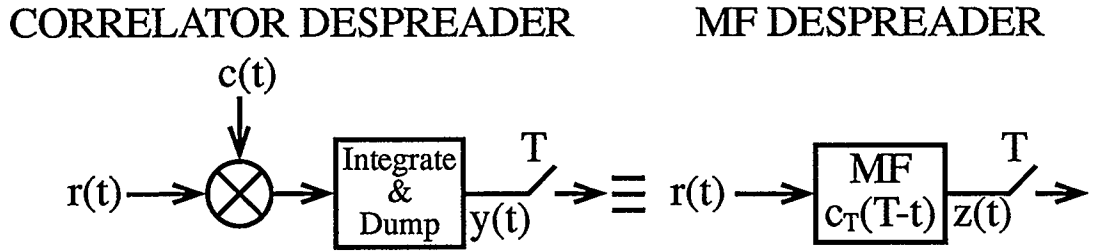


Figure 6.1 *Equivalence of a MF despreader to a correlator despreader.*

The output of a correlator and a MF are only equivalent at the symbol sampling instances. This is shown by considering the two circuits illustrated in Fig. 6.1. Assume the input $r(t)$ consists of only one spread symbol for simplicity. The output of the correlator $y(t)$ can be written as

$$y(t) = \int_0^t c(\tau)r(\tau)d\tau. \quad (6.1)$$

If the output of the integrate and dump filter is sampled at the end of the symbol interval, the output of the sampler can be written

$$y(T) = \int_0^T c(\tau)r(\tau)d\tau \quad (6.2)$$

where T is the symbol period. Similarly the output of the MF, $z(t)$, can be

written as

$$\begin{aligned}
 z(t) &= c_T(T-t) * r(t) \\
 &= \int_{-\infty}^{\infty} c_T(T-\tau) r(t-\tau) d\tau \\
 &= \int_0^T c_T(T-\tau) r(t-\tau) d\tau
 \end{aligned} \tag{6.3}$$

where $c_T(t)$ represents one period of the reference PN code. The output of the MF circuit is the same as the correlator circuit only if the output is also sampled at the end of the symbol interval. Thus we can write the output of the sampler as

$$z(T) = \int_0^T c_T(T-\tau) r(T-\tau) d\tau. \tag{6.4}$$

By inspection of equations (6.2) and (6.4) it can be seen that $y(T) = z(T)$ and thus the output of a MF sampled at the correct time instant gives the despread symbol value. A stream of K symbols can be despread by sampling the output of the MF at kT where $k = 1, 2, \dots, K$. This can be seen easily by looking at the output of the MF prior to sampling. Fig. 6.2 shows a block diagram implementation of a matched filter. A large correlation spike is produced at the output of the MF when the incoming signal is aligned with the taps of the matched filter.

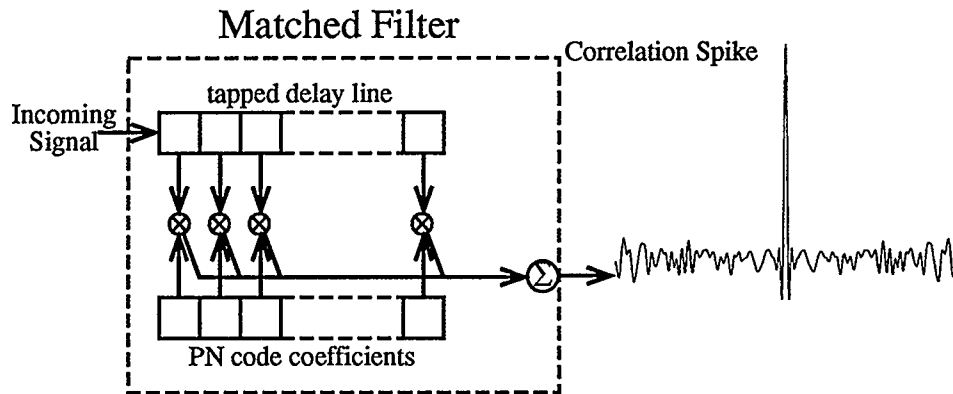


Figure 6.2 Output of a filter matched to the PN code used to spread the incoming signal.

One period of the PN code was modulated onto each symbol at the transmitter, thus an alignment of the signal with the filter taps will occur for each symbol producing correlation spikes at the symbol rate. A simple system is shown in Fig. 6.3 to illustrate the use of a matched filter for despreading.

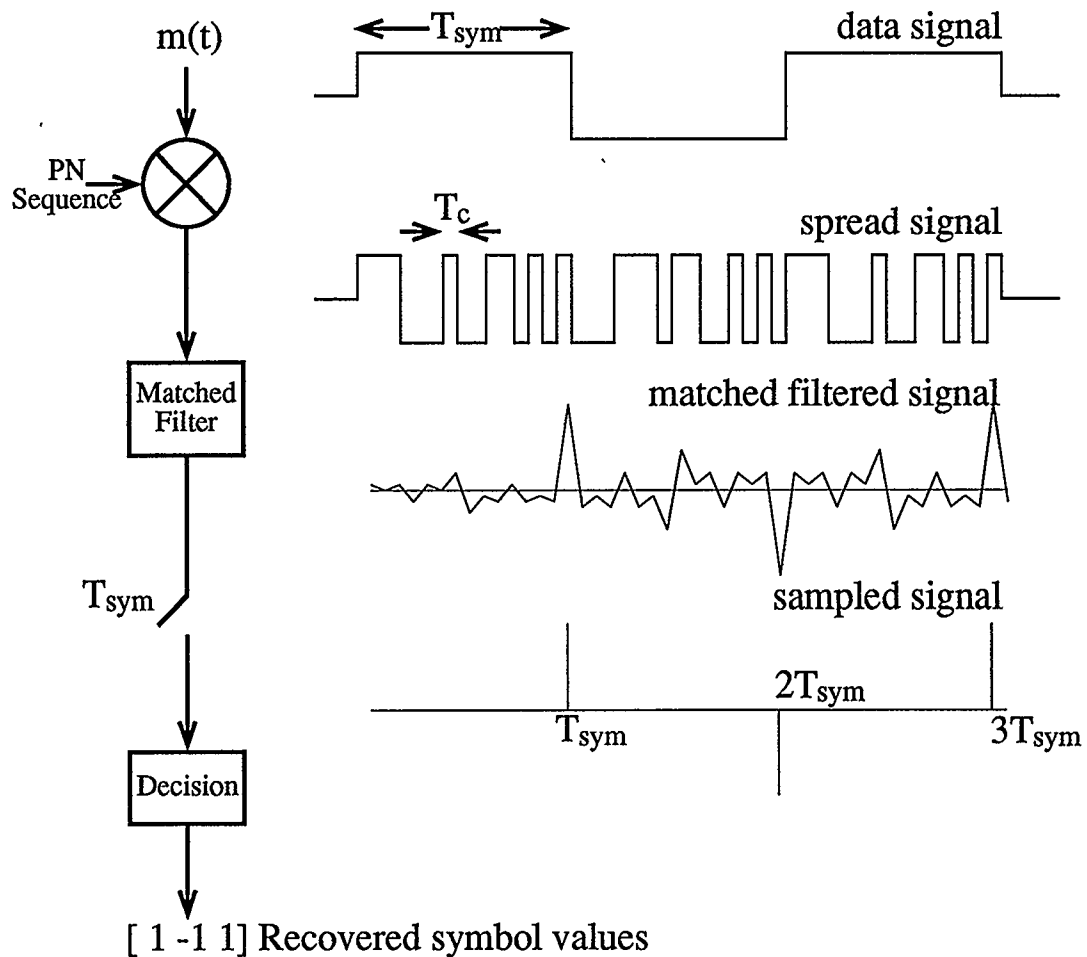


Figure 6.3 A simple MF despreader system. The signal is illustrated at various points during the spreading, despreading and data recovery process.

In Fig. 6.3 a message signal $m(t)$ is spread by a PN sequence. To recover the data, the spread signal is passed through a filter matched to the spreading code resulting in a signal which exhibits correlation peaks at the

symbol rate. The matched filter output between the correlation spikes is due to partial correlations of the incoming signal with the filter taps. The system in Fig. 6.3 used only a 15 chip length PN code so the partial correlation spikes can be quite high in comparison to the full correlation spikes. If a longer PN code were used, the partial correlation spikes would be much smaller than the full correlation spikes and the output would appear more like that shown in Fig. 6.2. In a coherent system the polarity of the full correlation spikes indicates that of the respective symbol.

The advantage of using a matched filter for despreading is that chip synchronization is not needed in order to correctly despread the received signal although symbol synchronization is still crucial. Tracking can be easily done by taking additional samples on either side of the symbol sample time to represent the early-late correlation results. A decision can be made based on these samples and the symbol clock adjusted accordingly throughout the receiver processing to ensure that correct symbol synchronization is maintained.

6.2 Limitation of Spreading Technique Due to CFDMA

The CFDMA system of [16] assumes that adjacent channels are nonoverlapping prior to spreading. The spreading process introduces strong frequency overlap, as was shown in Fig. 5.3(f), that is removed at the receiver. Modulation of the CFDMA waveform with a reference code collapses the spread bandwidth, resulting in a series of nonoverlapping narrowband spectra. A narrow band LPF is used to eliminate the

narrowband orthogonal spectra due to other source pairs prior to integration over the symbol interval. This method cannot be implemented using a MF despreaders. The correlator despreaders that was shown in Fig. 6.1, consists of two steps only: modulation of the received signal with a reference code and integration over the symbol interval. If a narrowband LPF were to be inserted between these two steps then there would be no way to implement the circuit using a MF. Due to the strong frequency overlap of adjacent source pair spectra present in the CFDMA waveform the source data cannot be isolated prior to despreading, seeming to suggest that CFDMA data cannot be recovered using a MF despreaders. This is not true, however, as the inherent integration of the MF over the symbol interval can be used to eliminate the data from other sources. This method is described in the following section.

6.2.1 Limitation of Adjacent Channel Interference Due to Harmonics

In order to use a MF as a despreaders for a CFDMA system, the inter-source pair interference must be limited without the need for lowpass filtering once the spread spectra are collapsed to the narrowband spectra. Only the integration process of the MF can be used to eliminate the interference. Integration over the symbol interval can be used to remove signals at different frequencies if the signals occur at harmonics of the symbol frequency and the desired signal is at baseband. This method of cancellation of adjacent channel data is easiest shown considering a simple FDMA system, as shown in Fig. 6.4. Source 1 data is recovered as the baseband signal integrates to a nonzero value with a polarity that indicates

that of the corresponding transmitted symbol. The signals due to the remaining sources integrate to zero as they occur at harmonic frequencies of the symbol rate.

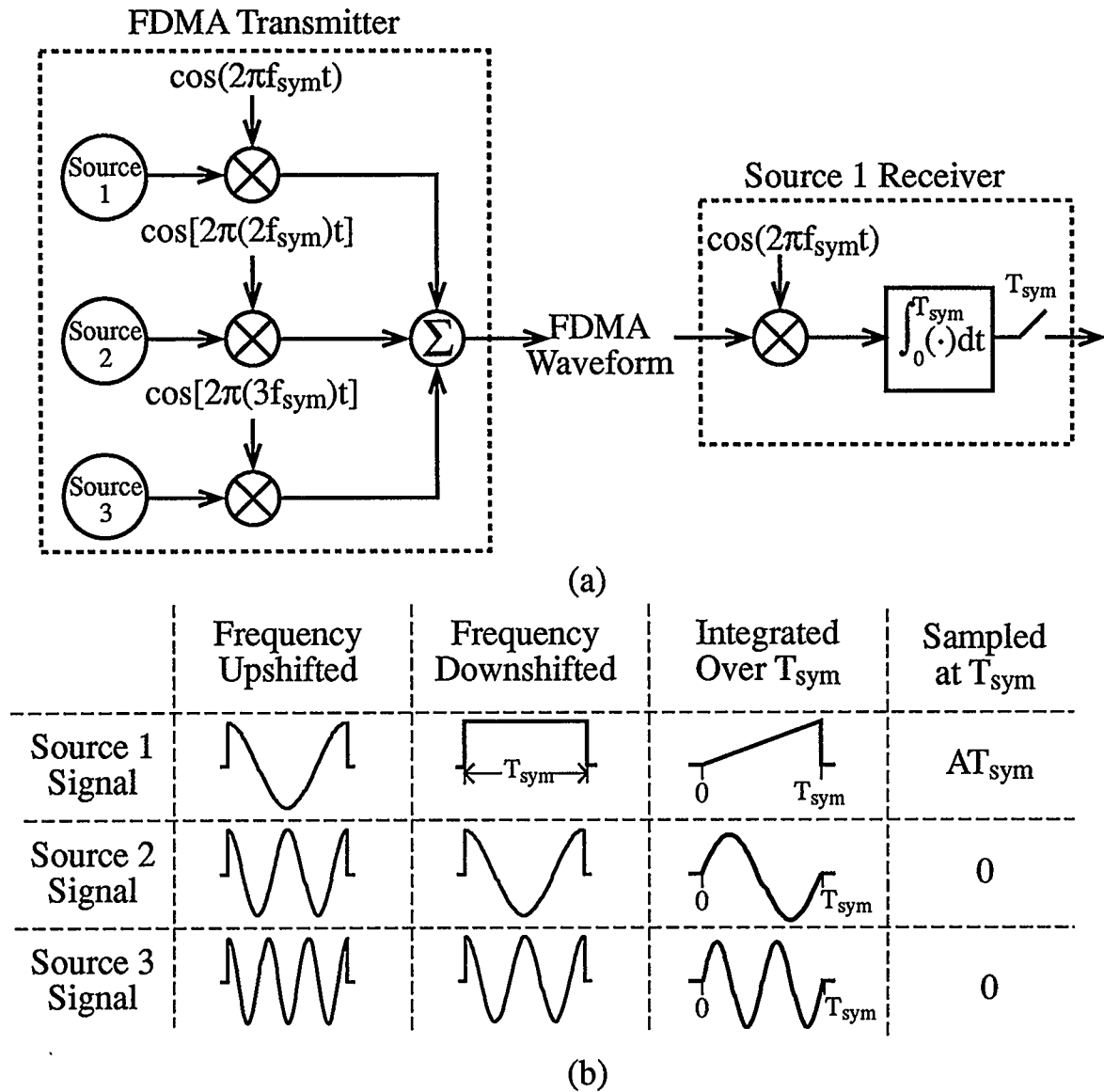


Figure 6.4 Use of harmonics to eliminate ACI in FDMA data. (a) FDMA transmitter and receiver for source 1 data. (b) Signals at various points in the system.

6.2.2 Band Limitation of Narrowband Spectra

The CFDMA system described in [16] requires band limitation of the narrowband source data prior to spreading so that despreading results in narrowband orthogonal spectra that can be isolated through filtering. If the undesired source data is to be removed through integration, the narrowband data need not be band limited. The CFDMA transmitter design is simplified as filtering is no longer required prior to spreading. The spectra for the narrowband sources prior to spreading in a CFDMA system are shown in Fig. 6.5 for the original CFDMA system outlined in [16] and the modified CFDMA system proposed in Section 6.2.1.

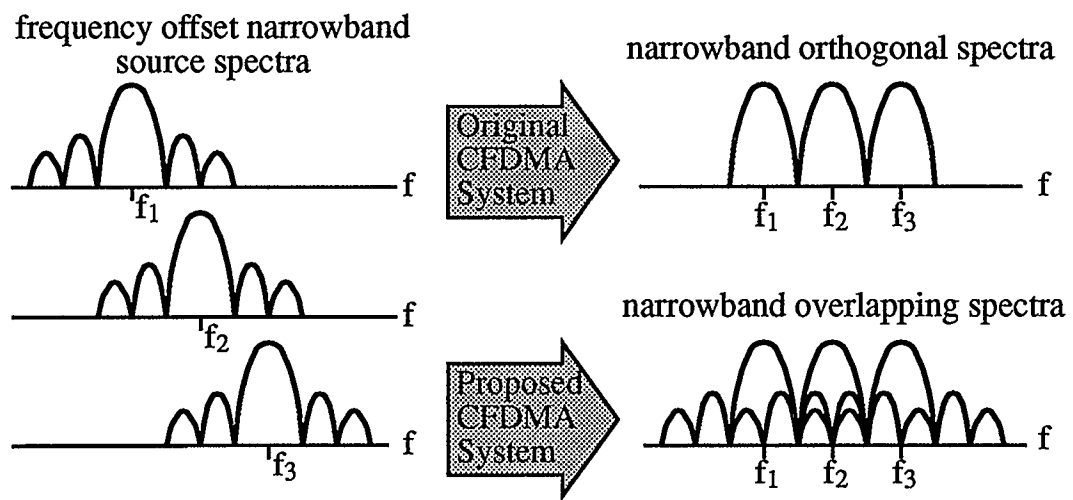


Figure 6.5 *Narrowband source spectra prior to spreading in CFDMA systems.*

6.3 Summary

The use of a MF despreader in a CFDMA system affects both the transmitter and receiver design. Band limitation of the narrowband data is

no longer necessary at the transmitter. The source spectra must be offset from one another by an integer multiple of the symbol rate. Chip synchronization circuits are not necessary at the receiver simplifying the receiver design. These factors will be taken into consideration in the implementation of the transmitter and receiver for the proposed CFTDMA system.

Chapter 7

Transmitter

Chapter Overview

This chapter outlines the implementation of a transmitter for the CFTDMA system presented in Chapter 5 taking into consideration the limitations imposed by a MF despreaders as discussed in Chapter 6. In order to realize this system, several factors must be taken into consideration. The amount of spectrum spreading introduced by PN code modulation must be determined. A suitable time offset must be found such that the cross-correlation between the spreading code and its time offset version is minimum. Bandwidth limitation must be taken into account prior to transmission over a channel. Intersymbol interference (ISI) introduced by a multipath channel must be controlled. All these issues will be dealt with in this chapter as the design for the transmitter is explained.

7.1 Transmitter Implementation

The block diagram of the CFTDMA transmitter of Fig. 5.7 is redrawn in Fig. 7.1. The N_f bit sources used by the upper and lower branch CFDMA systems are respectively labeled nA , where $n = 1, 2, \dots, N$ and mB , where $m = 1, 2, \dots, N$ to differentiate them from one another. Due to the underlying FDMA, A and B sources with $n = m$ will be shifted to the same intermediate frequency (IF) band during transmission. The implementation of the transmitter is simplified by grouping these sources into N subsequent source pairs so that the frequency upshift need only be implemented N times versus $2N$ times.

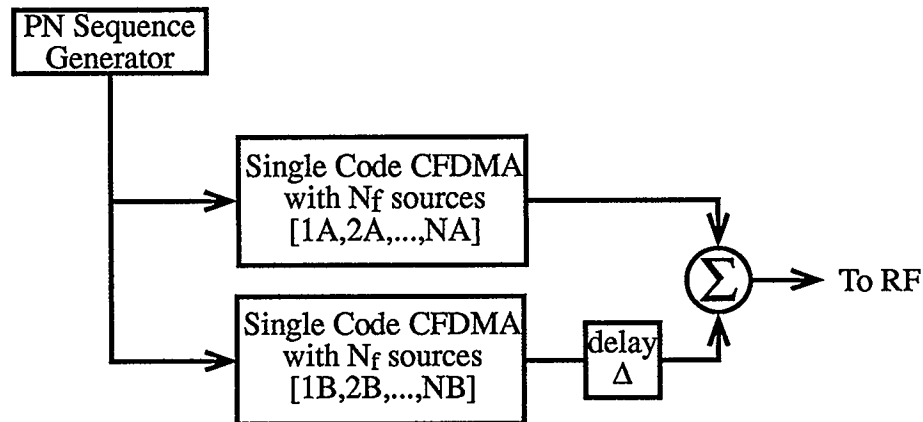


Figure 7.1 CFTDMA transmitter with $2N$ sources.

A detailed block diagram of the transmitter unit for the CFTDMA is shown in Fig. 7.2. By inspection of Fig. 7.2, it can be seen that the source data is multiplexed using CTDMA within a source pair and CFDMA between the N different source pairs, resulting in the CFTDMA system discussed in Chapter 5. The use of source pairs results in modular design for the transmitter. Rectangular symbol pulses are modulated with a PN code and offset in time within a source pair. The chips are pulse shaped to band

limit the signal. The resulting spread spectra from each source pair is offset in frequency by the source symbol bandwidth from its adjacent source pairs. The details of the individual blocks will be discussed in subsequent sections.

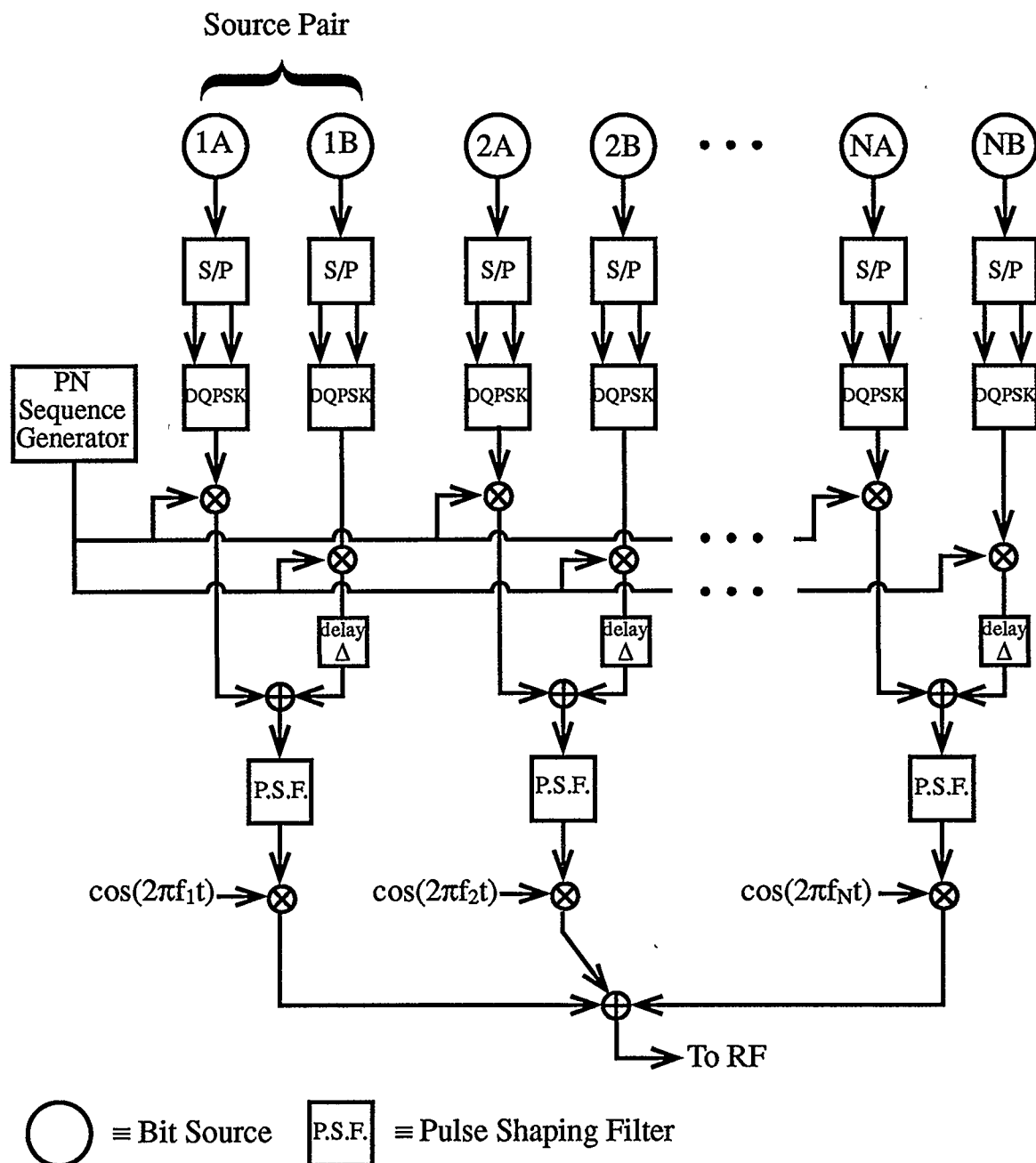


Figure 7.2 Transmitter block diagram for variable high data rate CFTDMA system.

7.1.1 Bit sources

Several parallel low rate bit sources are shown in Fig. 7.2. The bit sources are divided into N source pairs with each bit source operating at the same base rate of R_b bits/sec. The overall system rate is $2NR_b$ bits/sec.

7.1.2 DQPSK Modulation

Differential Quadrature Phase Shift Keying (DQPSK) is used to modulate the data from each source. QPSK allows for an efficient use of the channel by transmitting different information on the orthogonal inphase and quadrature phase components of the carrier [18]. Differential encoding is applied to eliminate the need for phase synchronization at the receiver [32].

DQPSK encodes two data bits at a time; thus, the serial source data is converted to parallel data. The two parallel input bits to the DQPSK encoder are mapped using Gray encoding to a QPSK signal phase constellation as outlined in [33]. The resulting angle, $\Delta\phi$, is used as a phase shift to determine the absolute phase for PSK encoding on the current symbol interval based on the angle of the previous symbol interval as follows:

$$\phi_i = \phi_{i-1} + \Delta\phi. \quad (7.1)$$

The encoding process results in a serial stream of complex symbols.

7.1.3 Symbol Timing

The time required to transmit a symbol is crucial to performance in a multipath channel, as discussed in Chapter 2. In order for ISI to be

negligible, the time to transmit a single symbol must be much greater than the multipath spread. The system has increased the bit duration by using several parallel low rate sources instead of one high rate source. In addition, the QPSK encoding results in a symbol with a length twice that of the bit length, providing further improvement. Another method to further reduce the effects of ISI is to insert a guard time, T_m , between symbol slots where T_m is to be greater than τ_{rms} . This can also be achieved by reducing the duty cycle. A system similar to this is shown in Fig. 7.3, where the gap is chosen to be larger than τ_{DS} for illustration purposes.

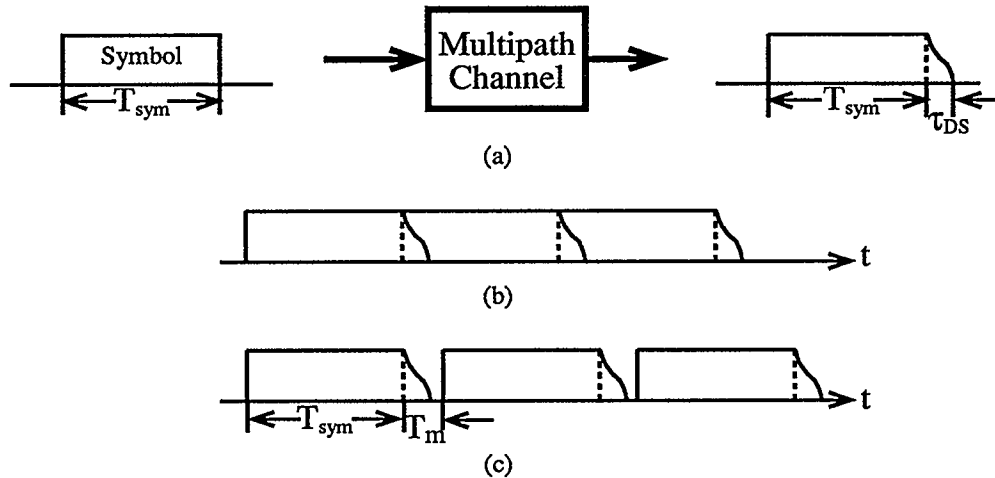


Figure 7.3 Intersymbol interference due to multipath channel. (a) Dispersion of single symbol transmitted over a multipath channel. (b) ISI due to multipath spread. (c) Illustration of method to combat ISI by leaving dead time between symbols.

The insertion of a time gap greater than the rms delay spread between symbols ensures that the ISI of a data symbol is negligible although the chips are still subject to ISI due to the small chip period. The time gap between symbols was implemented by limiting T_m to an integer multiple of the chip time. The term T_{mc} denotes the quantity T_m in chips. An extension of T_{mc} zeros was then added to the PN code used to spread the data. Thus

the PN sequence consists of continuous repetitions of the M chip PN code followed by T_{mc} zeros and hence has a period of

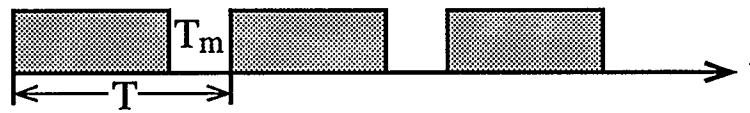
$$P = M + T_{mc}. \quad (7.2)$$

The inclusion of a time gap between symbols results in a reduction of the data rate or an increase in the system bandwidth, depending on implementation.

Case I:



Case II:



Case III:

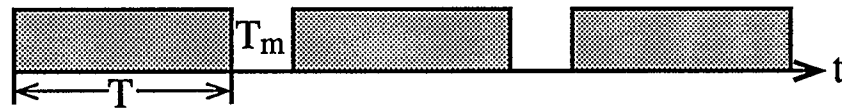


Figure 7.4 *Insertion of a time gap between symbols.*

To analyze the effect on bandwidth and data rate due to the inclusion of a time gap between symbols, the three scenarios shown in Fig. 7.4 are considered. The first case is for the system with no spacing between symbols. The spread bandwidth per source is

$$W_s = \frac{2M}{T}$$

and the system rate is

$$R_T = \frac{2N}{T}.$$

The second case is where the symbol duration is shortened due to the insertion of a time gap and is equivalent to a reduction in the duty cycle. The spread bandwidth is increased in this scenario to

$$W_s = \frac{2(M + T_{mc})}{T}$$

whereas the system rate remains the same. The third case is where the time gap is added to the end of the current symbol interval. The spread bandwidth is unaffected by this method but the system rate is reduced to

$$R_T = \frac{2N}{T + T_m}.$$

Case I was implemented for gaussian channel simulations. Case II was implemented for multipath channel simulations so that the performance for a constant rate could be determined independent of the guard time. Case III was not implemented due to the dependence of the system rate on the guard time.

7.1.4 Spreading Process

One PN code is used to spread all $2N$ sources' data in this block of the CFTDMA system. The PN code used to spread the data in this system is a m-sequence code. The code length M and the code time offset Δ control the amount of interference between source A and source B data.

7.1.4.1 Selection of PN Code Length, M , and Time Offset, Δ

CTDMA is achieved within a source pair by spreading the B sources' data with a time offset version of the m-sequence used for spreading the A

sources' data. The length of the PN code, M , and the code time offset, Δ , should be chosen to minimize interference between the A and B sources. Frequency diversity should also be taken into account when selecting the code length.

The ideal autocorrelation of a m-sequence was shown in Fig. 3.5 to be 2-valued, with normalized values of 1 and $-\frac{1}{M}$ corresponding to zero time shift and all other time shifts, respectively. Thus the autocorrelation of a m-sequence and its time shifted version is $-\frac{1}{M}$. This would seem to indicate that, for a CFTDMA system operating in a gaussian channel, $T_{mc} = 0$, the cross-correlation within a source pair would be $-\frac{1}{M}$. This is not so, as more than one symbol from the interfering stream overlaps the desired symbol, as shown in Fig. 7.5(a). As the two interfering symbols may not have the same symbol value, a variety of cross-correlation values result depending on the magnitude of time offset Δ . Each time offset Δ has 2^3 possible cross-correlation values as the three overlapping symbols may each take on values of ± 1 with equal probability. The plots in Fig. 7.5(b) show the results of taking the average of the magnitude of these cross-correlations, $E\{|R_{AB}(\tau)|\}$, for all possible Δ for three different lengths of a m-sequence. The value of $E\{|R_{AB}(\tau)|\}$ is not shown for $\Delta=M$ as it will clearly be unity. The average level of interference is seen to decrease for longer m-sequences. The plots of Fig. 7.5(b) can be used to select an optimum Δ for the system; however, it is important to note that the plots of Fig 7.5(b) are dependent on the m-sequence being used. The m-sequence selected for a particular order m is dependent on the selection of feedback taps of the linear feedback shift register used to generate the sequence.

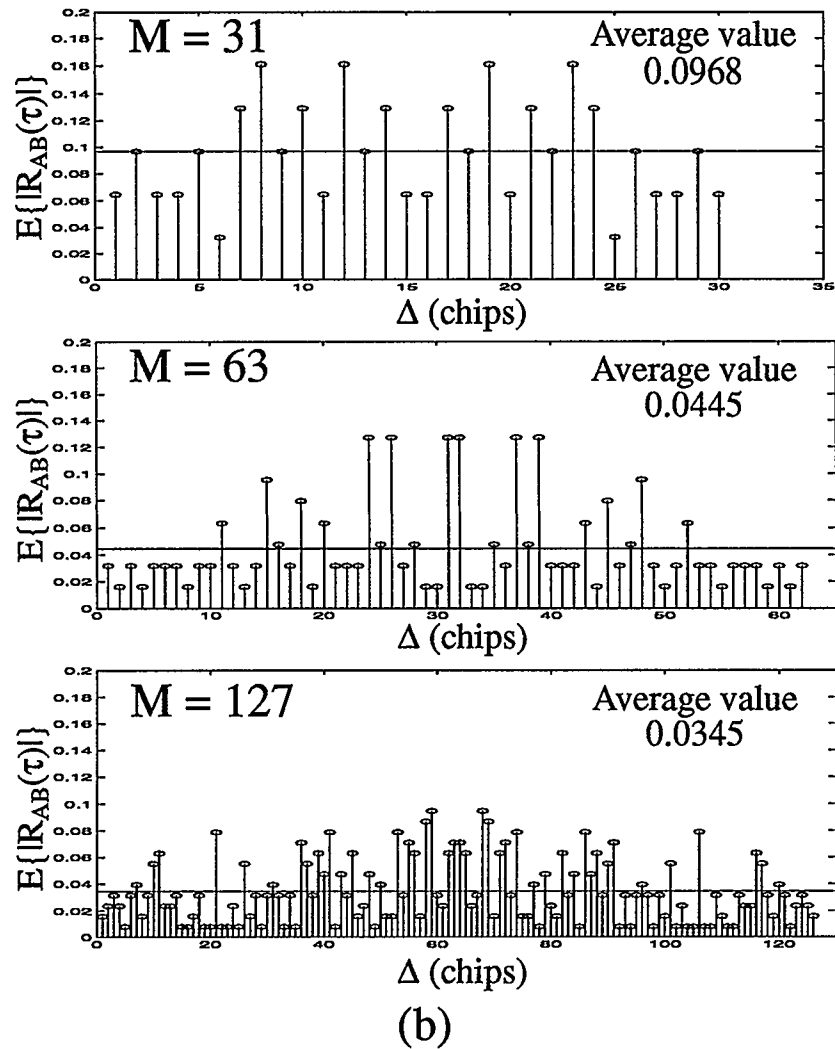
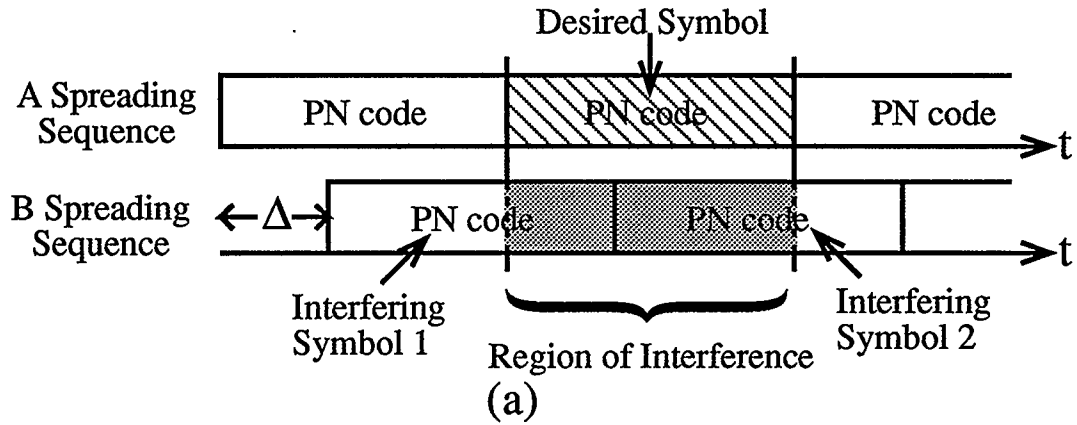


Figure 7.5 (a) Source of interference between $N_t = 2$ CTDMA system streams in a gaussian channel. (b) Level of interference between $N_t = 2$ CTDMA system streams in a gaussian channel for various m -sequence lengths.

Based on the results of Fig. 7.5(b), the CFTDMA experiences some interference between source A and source B data within a source pair. This interference is fairly small, enabling data spread by the PN-sequence and a time-offset version of the PN-sequence to be transmitted simultaneously in time as long as the time offset Δ is selected to be mT_c where T_c is the chip period and $1 \leq m < M$ where $m \in \text{integer}$.

In a multipath channel, further restrictions are placed on Δ due to delay spread. The time offset Δ should be greater than the channel rms delay spread so a potentially strong NLOS ray of multipath with delay equal to Δ does not align A data with the LOS path of B data. If this were to happen very poor performance would result. The time gap, T_m , between symbols is also selected to be greater than the channel rms delay spread, thus it can be assumed $T_m = \Delta$ without any performance degradation.

The timing diagram for the source pair taking the time offset Δ and the time gap T_m into account would appear as in Fig. 7.6.

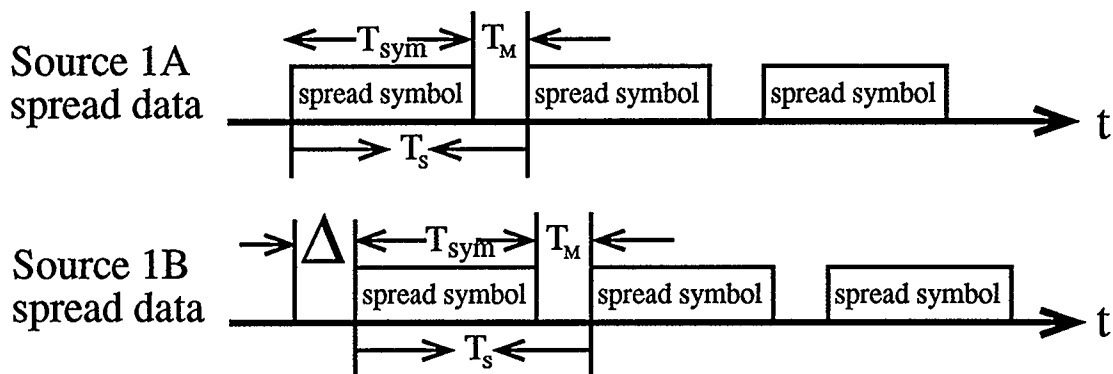
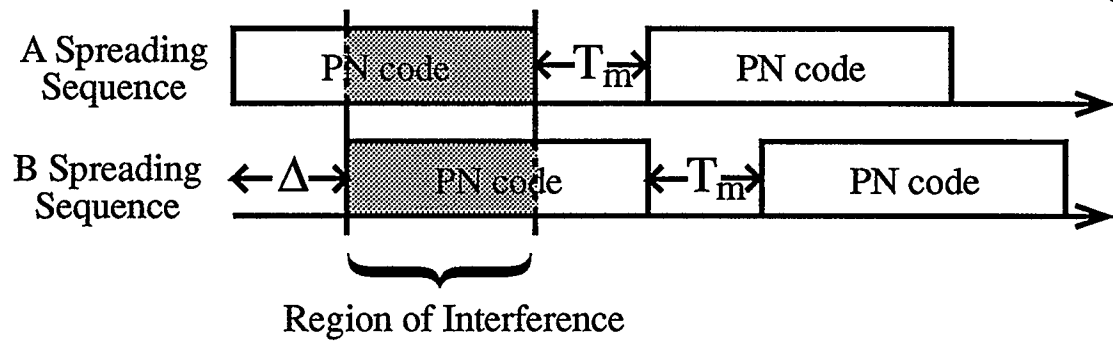
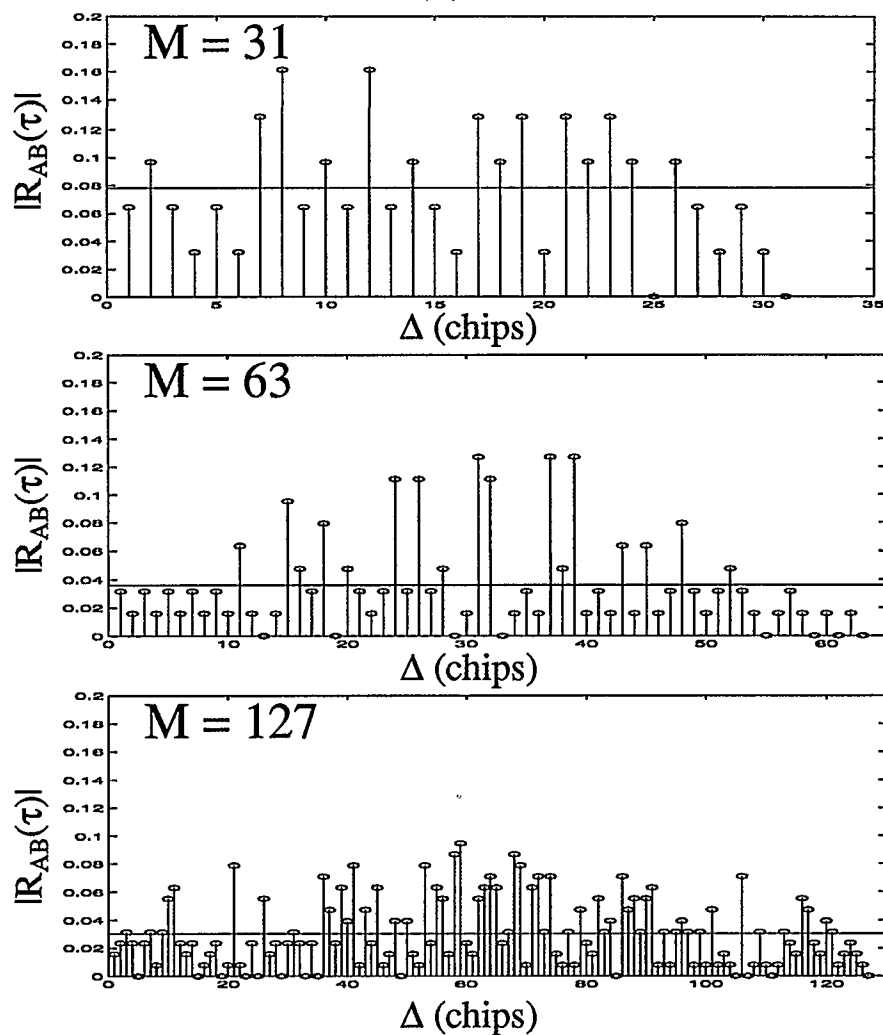


Figure 7.6 The timing diagram for a source pair.

The interference between the A and B streams of data is different from that illustrated in Fig. 7.5 for a multipath channel due to the insertion of T_m .



(a)



(b)

Figure 7.7 a) Region of interference between $N_t=2$ CTDMA streams in a multipath channel. (b) Level of interference between $N_t=2$ CTDMA streams in a multipath channel for various m -sequence lengths where $T_m=\Delta$.

Fig. 7.7(a) displays the portions of the two sequences that will interfere with one another. The level of this interference is shown in Fig. 7.7(b) for three different m-sequences. The amount of interference is seen to vary greatly depending on the choice of Δ , but decreases overall for longer m-sequences.

Spread spectrum may also provide frequency diversity for a frequency selective channel, as was discussed in Chapter 4. Frequency diversity is provided if the spread IF source bandwidth denoted W_s is greater than the coherence bandwidth, B_c , of the channel. The spread bandwidth for a single source can be written as

$$W_s = PB_s \quad (7.3)$$

where B_s is the IF bandwidth for a single source and is the same for all $2N$ sources. Sources within a source pair occupy the same frequency band at IF thus the IF bandwidth per source pair is also B_s . B_s is equal to the source bit rate when using quadrature modulation. Due to spectrum band limitation the spread bandwidth for a source is actually limited to $\frac{(1+\beta)}{2} W_s$ where β is a parameter of the filter used to achieve band limitation. The parameter β lies between 0 and 1, thus the filter results in a reduction of bandwidth. Band limitation of the spread spectrum will be discussed further in Section 7.1.5. The limiting bandwidth to ensure frequency diversity is found using equation (2.6) to be

$$B > \frac{1}{\min(\tau_{DS})}. \quad (7.4)$$

The typical delay spread in an indoor multipath channel was found to range from 20ns to 100ns in Chapter 2. As τ_{rms} will invariably be less than τ_{DS} , 20 ns can be used to determine the lower limit for the bandwidth which

is

$$B > 50 \text{ MHz.} \quad (7.5)$$

Therefore, a limitation can be imposed upon the spreading code length as follows:

$$M > \frac{100 \text{ MHz}}{(1 + \beta)B_s} - T_{mc}. \quad (7.6)$$

The choice of M is shown to depend greatly on the source bit rate in 7.6 in addition to the amount of interference that can be tolerated between the CTDMA multiplexed sources.

7.1.5 Spectrum Limiting

Signal bandwidth is often limited to avoid adjacent channel interference (ACI) which occurs when signals occupying adjacent frequency bands overlap. The discussion of CFDMA in Section 3.5.1 assumed that the narrowband data spectra were nonoverlapping when shifted to their corresponding IF bands prior to spreading. Thus despreading at the receiver resulted in a series of nonoverlapping narrowband spectra that can be isolated using filtering techniques. The discussion of despreading circuits in Chapter 6 presented a method of offsetting the adjacent source pairs by multiples of the symbol frequency thus allowing interference due to adjacent source pairs to be eliminated through integration over the symbol interval. This method is to be implemented. Band limitation of the narrowband data spectra prior to spreading is not necessary using this method; however, the system does still require the limitation of the overall system bandwidth prior to transmission. The bandwidth limitation will be achieved by pulse shaping the chips.

7.1.5.1 Pulse Shaping

Pulse shaping can be used to band-limit the data spectrum and subsequently limit ACI and ISI [18]. Pulse shaping refers to the process whereby the data value to be transmitted is modulated onto a pulse shape. The resulting pulses are offset in time and superimposed, resulting in a steady stream of pulses. The bandwidth of the resulting stream of pulses is dependent on the particular pulse shape used; a rectangular pulse has infinite bandwidth whereas a raised cosine pulse has variable finite bandwidth.

The raised cosine pulse or nyquist pulse is enlisted in this system as it obeys the nyquist principle [18]. The data is passed through a raised cosine filter in order to attain the desired pulse shape. The nyquist pulse is shown in Fig. 7.8 for several different rolloff factors where T is the symbol interval.

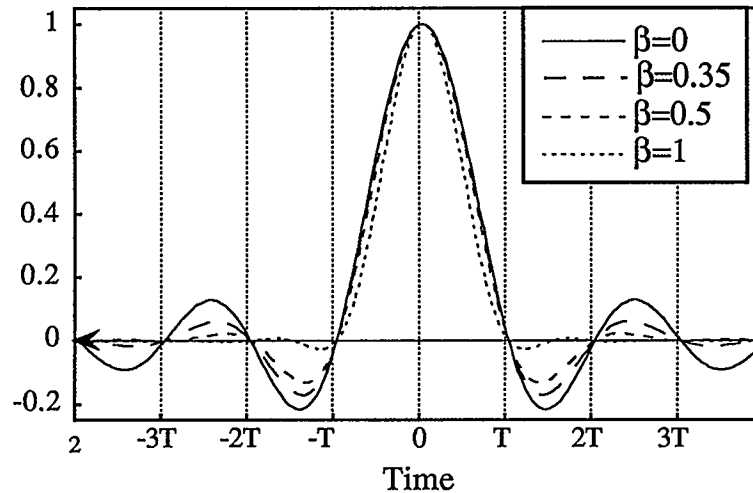


Figure 7.8 Time domain response of a nyquist pulse.

The nyquist pulse of Fig. 7.8 is zero for all integer multiples of T except for the one corresponding to the centre lobe. Pulses time-shifted by integer

values of T can then be transmitted without affecting the other symbols' values at the ideal sampling time, as illustrated in Fig. 7.9.

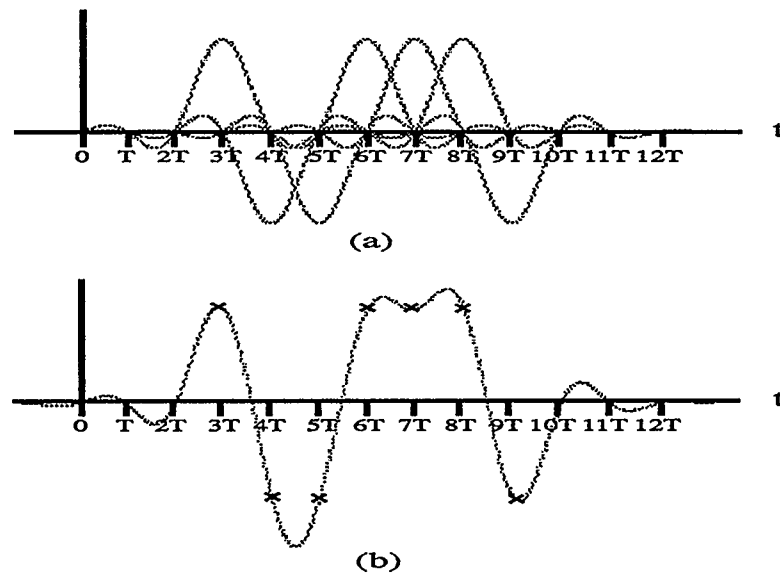


Figure 7.9 Consecutive nyquist pulses. (a) Overlay of time offset nyquist pulses. (b) Superposition of time shifted nyquist pulses showing ideal sampling time to recover information.

Fig. 7.10 shows the frequency response of a raised-cosine pulse for several rolloff factors.

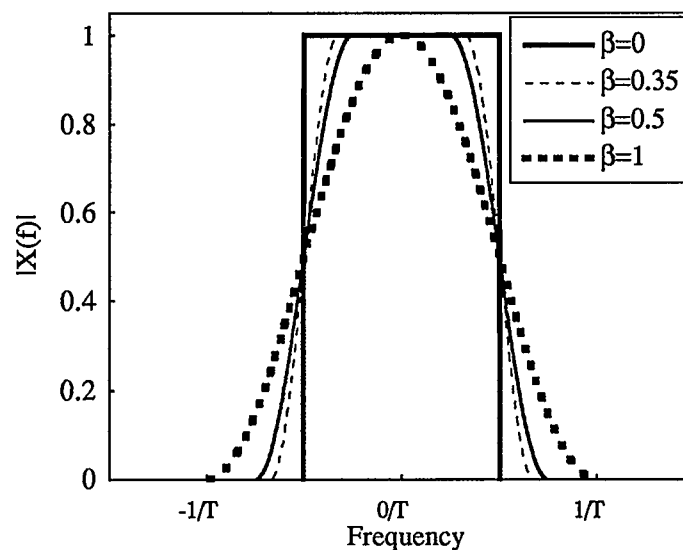


Figure 7.10 Frequency response of a nyquist pulse.

It is common practice to use a square-root raised-cosine filter, also known as a square-root nyquist (SRN) filter, at the transmitter in combination with an identical SRN filter at the receiver [34], [35]; hence, a nyquist pulse is attained after the data has passed through both filters. This method is used due to the optimum receiver in an AWGN environment being a filter matched to the signal pulse shape [12], [18], [34].

The square-root nyquist pulse is given in [14] by the waveform

$$\begin{aligned} p(t) = & (1 - \beta) \text{sinc}((1 - \beta)t / T) \\ & + \beta \cos(\pi t / T - \frac{\pi}{4}) \text{sinc}(\beta t / T - \frac{1}{4}) \\ & + \beta \cos(\pi t / T + \frac{\pi}{4}) \text{sinc}(\beta t / T + \frac{1}{4}) \end{aligned} \quad (7.7)$$

where β is the rolloff factor of the filter. The frequency response of a square-root nyquist pulse is given in [24] as

$$P(f) = \begin{cases} T & 0 \leq |f| \leq (1 - \beta) / 2T \\ T \cos \left[\frac{\pi T \left(|f| - \frac{(1 - \beta)}{2T} \right)}{2\beta} \right] & (1 - \beta) / 2T \leq |f| \leq (1 + \beta) / 2T. \\ 0 & |f| \geq (1 + \beta) / 2T \end{cases} \quad (7.8)$$

From equation 7.8 it can be seen that the SRN filter acts as a lowpass filter with a baseband bandwidth of $(1 + \beta) / 2T$.

The system bandwidth is limited prior to transmission through nyquist pulse shaping of the chips. In order to adhere to the optimum receiver in the AWGN environment two SRN filters, one in the transmitter and one in the receiver, should be utilized. The effect of the SRN filter at the transmitter is

to make the spread spectrum finite. As the chips are being pulse shaped, $T = T_c$ and the baseband bandwidth of SRN filter written in terms of the chip period is

$$B_{\text{SRN}} = \frac{(1+\beta)}{2T_c}. \quad (7.9)$$

The filtering of the spread spectrum is illustrated in Fig. 7.11.

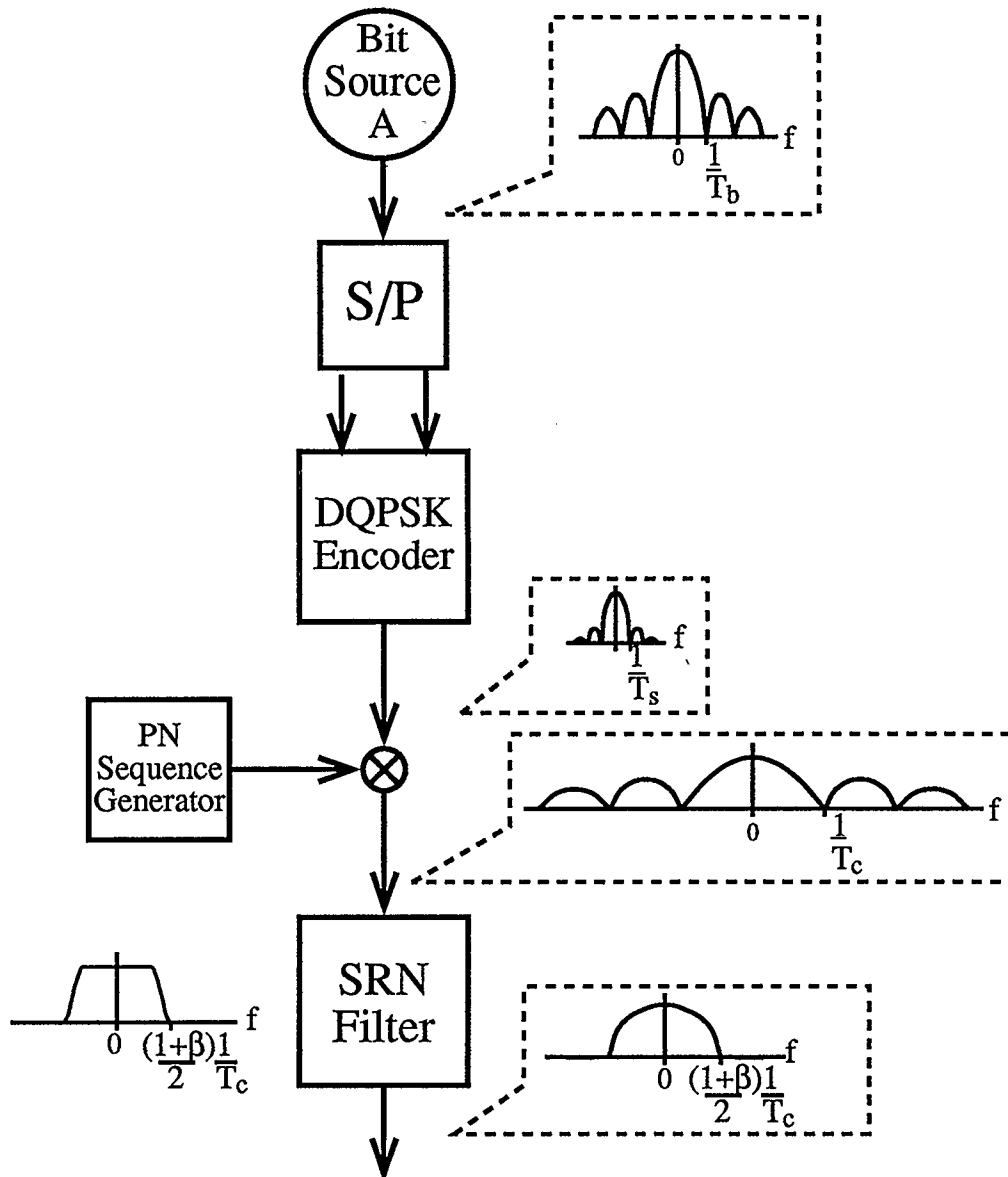


Figure 7.11 Frequency spectra at various points of the transmitter rails.

A direct result of this band limitation is a reduction of the source pair bandwidth from the null to null bandwidth of $W_s = 2/T_c$ to the finite IF bandwidth $\frac{(1+\beta)}{2} W_s$. This affects the choice of PN code length, M , as shown by equation (7.6).

Only one SRN filter is needed per source pair as the spread data from rail A and rail B can be combined prior to pulse shaping due to linearity.

7.1.6 Frequency Upshifting

Frequency upshifting is used to separate the source pair data in the frequency domain. The wideband spectra from each source pair is offset in the frequency domain from the previous source pair spectra by the frequency f_B . The offset frequency f_B is not simply the symbol rate as was discussed in Chapter 6 due to the method of insertion of the guard time T_m between symbols to combat multipath spread. The frequency f_B can be determined as

$$f_B = \frac{1}{T_{\text{sym}}} = \frac{R_c}{M}. \quad (7.10)$$

This ensures that an integer number of periods of a cosine wave lie within the symbol duration, T_{sym} , not the symbol interval, T_s , shown in Fig. 7.6. The chip rate is found as follows

$$R_c = \frac{1}{T_c} = \frac{M + T_{mc}}{T_s} \quad (7.11)$$

where T_{mc} is the delay between symbols normalized to the chip time. The spectra will overlap strongly at these IF's as shown in Fig. 7.12 since the spread bandwidth, $\frac{(1+\beta)}{2} W_s$, is greater than f_B .

The initial upshift frequency f_o should be at least half the spread bandwidth of one source pair, that is

$$f_o = \frac{(1+\beta)}{2} \frac{W_s}{2}. \quad (7.12)$$

The reasons for this will become clear in the discussion of the receiver in Chapter 8.

The combined spread source pair spectra will be collapsed by despreading at the receiver into a series of partially overlapping narrowband spectra. The data from different source pairs can be isolated at the receiver through downshifting to baseband and integration over the symbol duration.

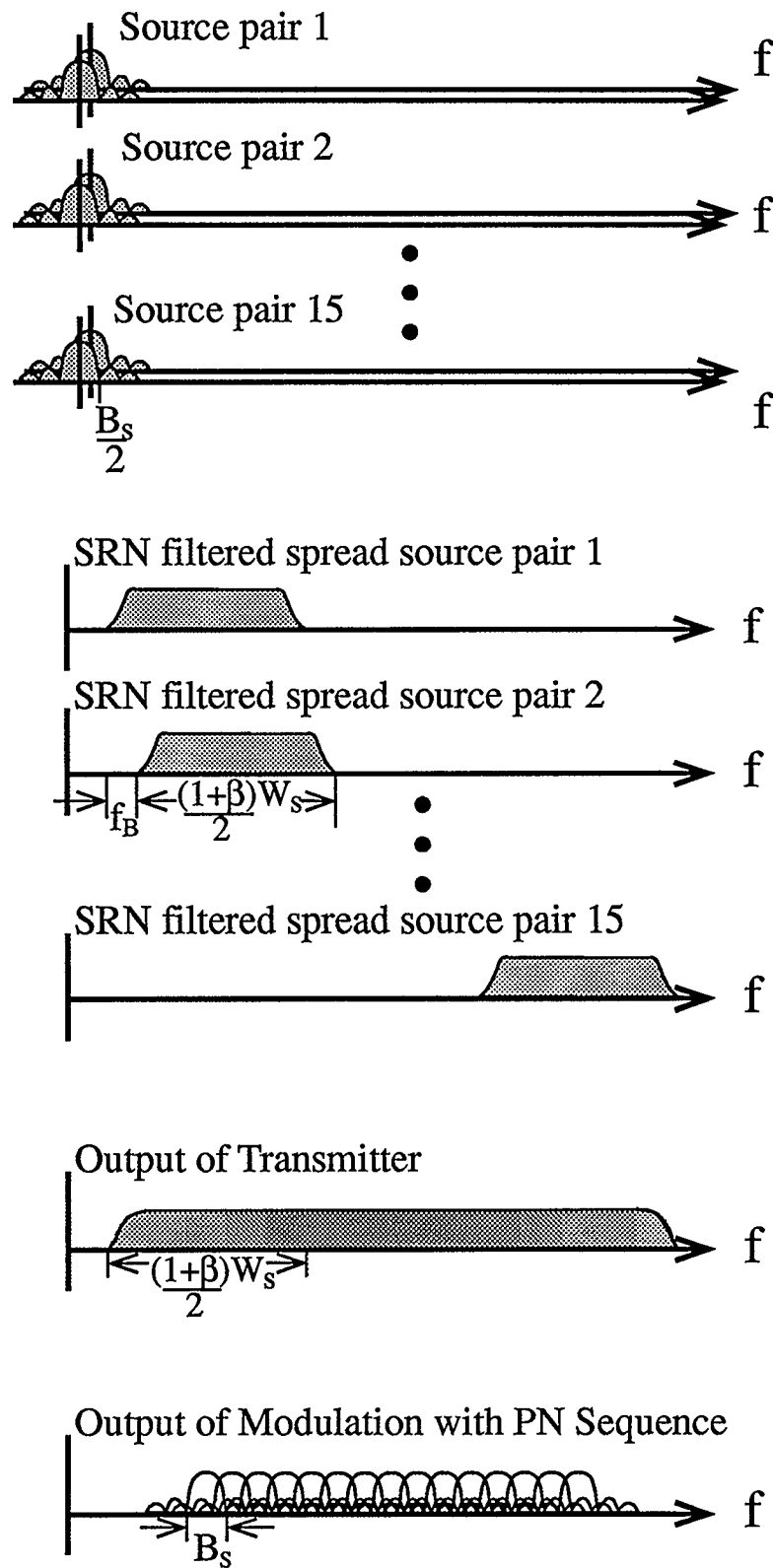


Figure 7.12 Example of CFDMA combining for setup with 15 source pairs.

7.2 Determination of CFTDMA Bandwidth

The CFTDMA system bandwidth is dependent on a number of parameters. From Fig. 7.12 it can be seen that the total IF bandwidth required by the system is

$$B_T = \frac{(1+\beta)}{2} W_s + (N-1)f_B \quad (7.13)$$

where W_s is the spread data bandwidth and f_B is the amount of frequency offset between source pairs. Substitution of equations (7.3) and (7.10) into equation (7.13) results in the total IF bandwidth being rewritten as

$$B_T = \left(1 + \beta + \frac{N-1}{M}\right) \left(\frac{M + T_{mc}}{2}\right) R_b. \quad (7.14)$$

Equation (7.14) shows the system bandwidth to be dependent on the number of source pairs, N ; the nyquist filter rolloff, β ; the PN code length, M ; the chip separation between symbols, T_{mc} ; and the source bit rate, R_b .

Consider a system with 20 sources operating at a rate of 5 Mbits/sec. The low rate sources are divided into 10 source pairs. A m-sequence code with length $M=127$ is used to spread the data with a guard time of 10 chips between the symbols. A SRN filter with a rolloff factor of 0.35 is used to band limit the data spectrum. The bandwidth of the resulting CFTDMA system using (7.14) would be 486.65 MHz.

$$\begin{aligned} B_T &= \left(1 + 0.35 + \frac{10-1}{127}\right) \left(\frac{127+10}{2}\right) 5 \cdot 10^6 \\ &= 486.65 \text{ MHz} \end{aligned}$$

Chapter 8

Receiver

Chapter Overview

This chapter discusses a receiver that recovers the entire transmitted signal and a receiver to recover portions of the transmitted signal. Prior to data recovery the receiver must demodulate the received signal. In order to correctly demodulate the signal the receiver must attain synchronization of the reference despreading sequence and the received code signal, lock onto the carrier frequency, and attain symbol synchronization. The receiver assumes perfect symbol and carrier synchronization. Chip synchronization is easily dealt with due to the use of a MF to despread.

8.1 Chip Synchronization

The CFTDMA receiver has apriori knowledge of the PN sequence and the time offset Δ used at the transmitter; however, the code phase of the received signal is unknown. Chip synchronization refers to the alignment of a locally generated code sequence at the receiver with the code sequence present in the received signal. Chip synchronization is important in systems that despread the received data using a correlator. In a system using a filter matched to the PN code to be despread there is no need for chip synchronization, as explained in Chapter 6. The implementation chosen for the CFTDMA system was based upon the use of a matched filter (MF) to despread.

8.2 Data Demodulation

The receiver implementation is greatly simplified by using a MF to despread the data. If the receiver were to use a correlator to despread, the data for each source pair would be downshifted to baseband, modulated with a chip synchronized reference code, sampled at the ideal chip time, integrated over the symbol interval, and sampled at the symbol rate to determine the received symbol's value as shown in Fig. 8.1. This can be implemented using a MF despreader by replacing the modulator, chip sampler and integrate and dump filter with a filter matched to the coefficients of the reference PN code. As each sample at the output of the MF represents the correlation of the received signal with a different time shift of the PN code, the source pair B data is recovered by sampling Δ seconds after sampling for the source pair A data. Thus a single MF can be

used to despread both streams of data within a single source pair. In addition chip synchronization circuits are no longer necessary.

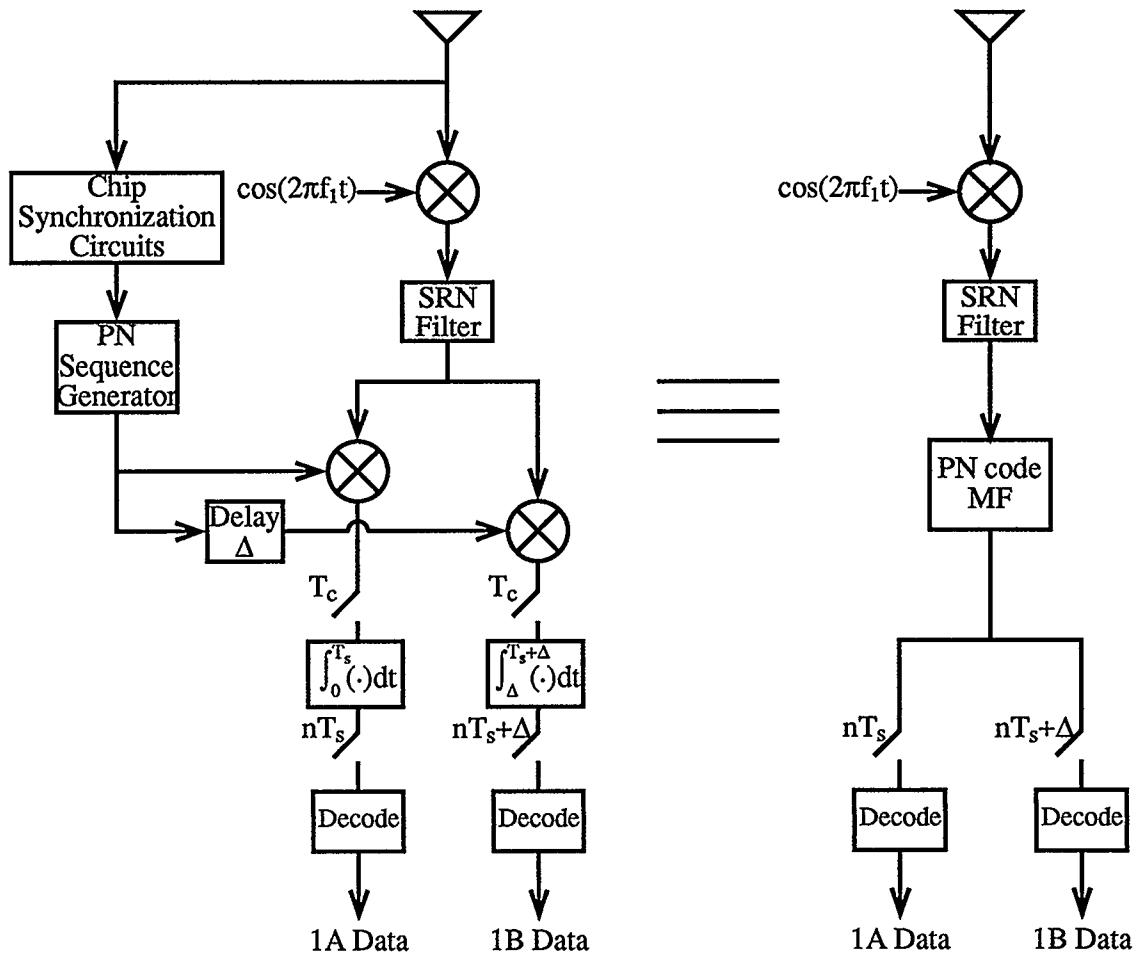


Figure 8.1 *Simplicity of receiver implementation for a single source pair using a MF for despreading versus a correlator.*

The block diagram for a CFTDMA receiver that recovers the entire transmitted signal is shown in Fig. 8.2. A receiver that is interested only in a portion of the transmitted signal will comprise only a subsection of the blocks in Fig. 8.2. Frequency downshifting is used to isolate data from a particular source pair at the receiver, whereas despreading is used to isolate a stream of data within a source pair. The details of these two processes are explained in the subsequent sections.

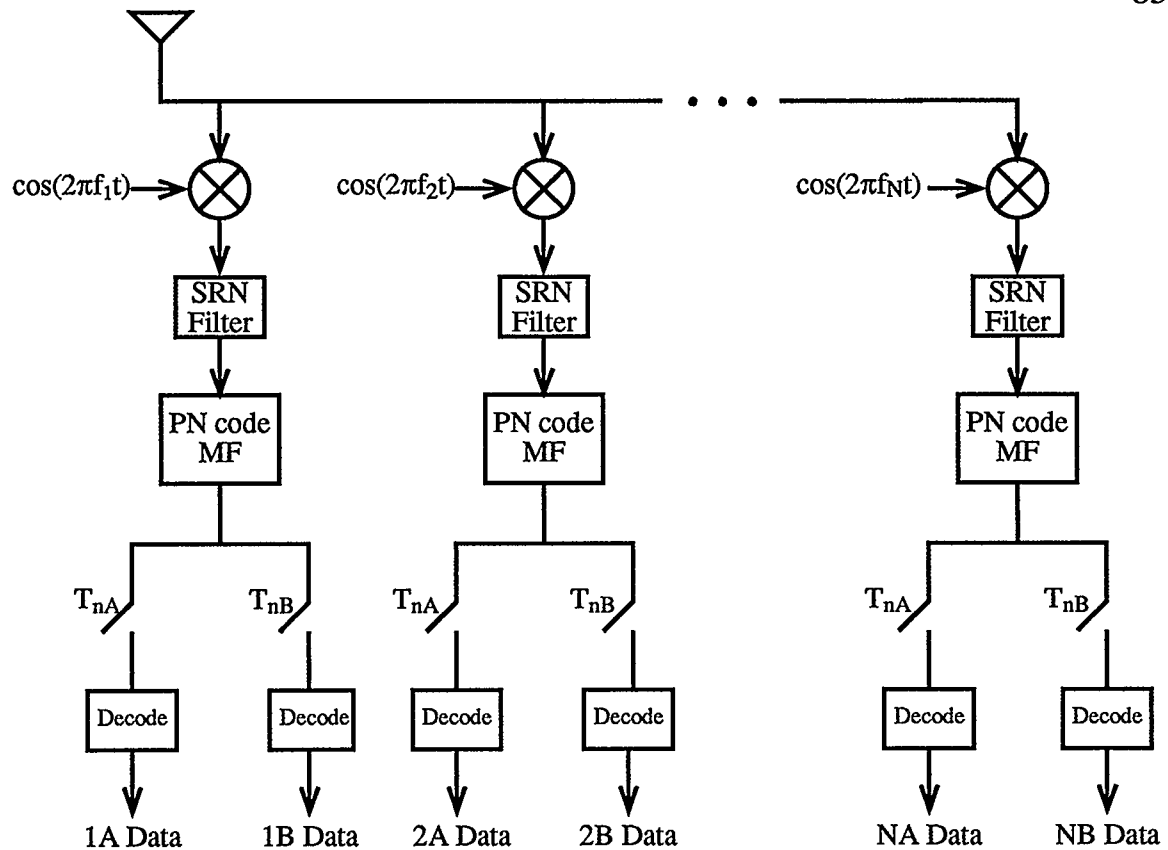


Figure 8.2 Block diagram of a CFTDMA receiver to recover the entire transmitted signal.

8.2.1 Frequency Downshifting

The transmitter used CFDMA to multiplex the data from the N source pairs. To demodulate the received data for a particular source pair, the received signal is downshifted by an intermediate frequency matching that used at the transmitter. The desired source pair's signal is now at baseband while the adjacent source pairs occur at integer multiples of f_B .

The downshifted signal is then passed through a wideband SRN filter identical to the one at the transmitter resulting in a nyquist pulse for the

chips. In addition to pulse shaping, the SRN filter is used to remove the double frequency components introduced by downshifting. The double frequency components are filtered out by the SRN filter only if the initial upshift frequency used at the transmitter, f_o , was chosen correctly. The spread spectra for one source pair centered at $2f_o$ must lie outside the SRN baseband bandwidth thus

$$f_o \geq B_{\text{SRN}} \quad (8.1)$$

in order for the double frequency components to be filtered out properly. Insertion of equation (7.9) into equation (8.1) results in an initial frequency of

$$f_o \geq \frac{1}{2} \left[\frac{(1+\beta)}{2} W_s \right]. \quad (8.2)$$

This was adhered to at the transmitter as seen by equation (7.12). Equation (8.1) ensures that all double frequencies introduced by downshifting are removed independent of which source pair is to be recovered.

8.2.2 Despreading

The data within a source pair is multiplexed using CTDMA and is thus recovered via the despreading process. If the receiver were to employ a correlator for despreading the data, two would be required per source pair: one synchronized to the PN-sequence $c(t)$ and a second synchronized to $c(t-\Delta)$. This is easily achieved via a single MF for each source pair.

The filter is matched to the spreading code and thus will have M taps spaced by T_c . The output of the MF exhibits correlation peaks for the source A symbols and for the source B symbols. These peaks are offset in time by

Δ as shown in Fig. 8.3 for a Gaussian channel. A multipath channel would exhibit multiple correlation peaks for the symbols corresponding to the different multipaths. The detection of both A and B data by the matched filter is due to the two sources using the same PN sequence for spreading except for a time offset Δ .

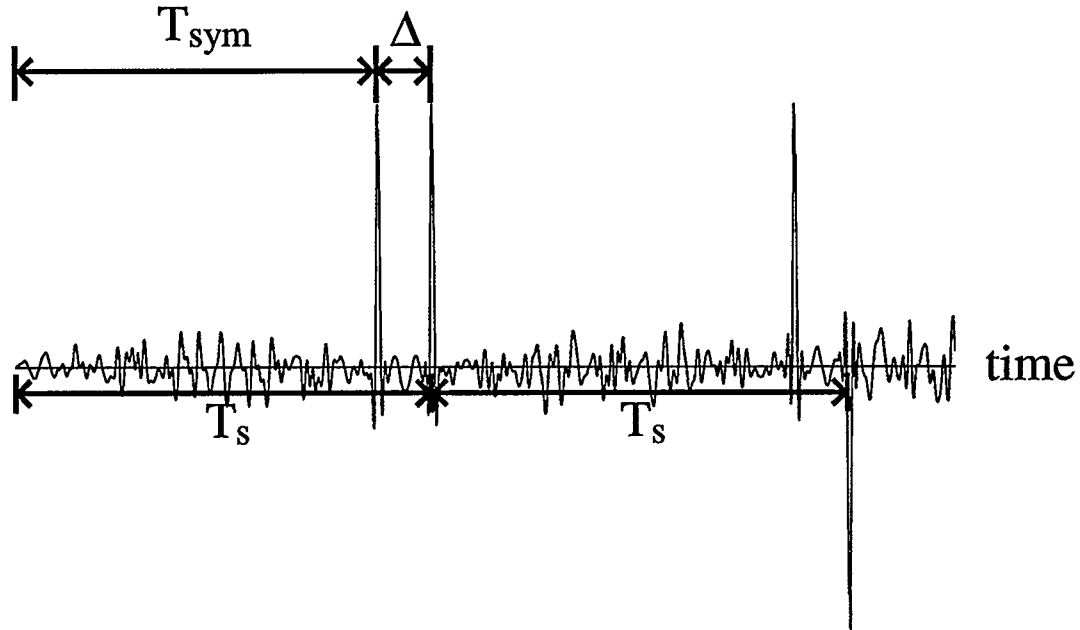


Figure 8.3 Output of the MF despreader for the CFTDMA system where $\Delta = T_m$ in a Gaussian channel.

The output of the MF is sampled twice per symbol period, T_s , corresponding to the correlation spikes shown in Fig. 8.3. Samples taken at T_{nA} and T_{nB} result in stream A and stream B symbol data, respectively, where the sampling times are defined as follows:

$$\begin{aligned} T_{nA} &= (n-1)T_s + T_{sym} \quad n \in \text{int} \\ T_{nB} &= T_{nA} + \Delta \end{aligned}$$

Perfect symbol synchronization is assumed in the data recovery process although changes in the multipath channel may cause the signal timing to drift. Applying logic similar to that used in the chip tracking

circuit of Chapter 4, timing drift can be easily corrected with the MF implementation. The output of the matched filter can be sampled on either side of ideal sampling time, resulting in early and late correlation values. The sampling clock can be adjusted depending on which of three correlation values has the largest magnitude [25].

As the MF has M taps at a spacing of T_c , the data has effectively been integrated over $[0, MT_c]$ for each symbol. The quantity MT_c is equal to $1/f_B$, using equation (7.10), thus an integer multiple of periods of the interfering sine waves lie in the integration interval, resulting in the removal of interference due to the remaining source pairs.

8.3 Data Recovery

The two streams of sampled data are passed through DQPSK decoders to recover the source A and source B bit values. The DQPSK decoder removes any phase ambiguity introduced by the channel; thus no phase synchronization circuits are needed at the receiver [36].

Chapter 9

Simulation Results and Analysis

Chapter Overview

Simulations were run using MATLAB® software based on the system implementation outlined in the preceding chapters. Two types of channels were modeled: a Gaussian channel, and a static two-ray channel where the magnitude of the second ray was varied. The Gaussian channel is simulated as means of ensuring that the simulation system implementation is correct. The results were analyzed, leading to some modifications of the system implementation. The two-ray channel is simulated to determine performance in a multipath channel. The channel noise was modeled as additive white Gaussian noise (AWGN) for both simulations.

9.1 Desired System Performance

Wireless data communications imposes greater restrictions on tolerable bit error rates (BER) than wireless voice communications. BER's on the order of 10^{-2} can be tolerated for packetized voice whereas BER's on the order of 10^{-5} and less are required for packetized data transmissions in addition to zero tolerance for packet loss [2].

The proposed system was desired to transmit at rates in excess of 150 Mbits/sec to provide a level of performance comparable to wired data systems. The success of the proposed system will depend on the rates that can be achieved while adhering to the above limitations on BER. The overall system rate is dependent on the number of source pairs and the source rate of the individual low rate sources to be multiplexed.

The source rate of the individual sources is limited by the multipath spread. As discussed in Section 7.1.3, the symbol duration must be much greater than the multipath spread in order for ISI to be negligible. Typically, the criteria is

$$T_{\text{sym}} \geq 10\tau_{\text{rms}}. \quad (9.1)$$

If a typical rms delay spread for an indoor channel is 50 ns then T_{sym} should be chosen to be greater than 500 ns according to (9.1). This limits the maximum bit rate for the low rate sources. Looking at Fig. 7.6, the symbol period is given by

$$T_s = T_{\text{sym}} + \frac{T_{\text{sym}}}{M} T_{\text{mc}}. \quad (9.2)$$

The bit rate for the low rate sources is given by

$$R_b = \frac{2}{T_s} \quad (9.3)$$

and the overall rate for the system is given by

$$R_T = 2NR_b. \quad (9.4)$$

The CFTDMA system with a 100% duty cycle, thus $T_{mc} = 0$, can be used to determine the lower limit on the number of source pairs required to achieve a system rate of 150 Mbits/sec. The bit rate for the individual sources for this case is found to be 4 Mbits/sec by using equations (9.2) and (9.3). In order to achieve a 150 Mbits/sec system, more than 18 source pairs are required. The minimum acceptable system performance is a BER of 10^{-5} for more than 18 source pairs.

The source bit rates will decrease as the duty cycle is decreased, leading to an increase in the number of required source pairs. The system rate will need to be recalculated taking the specific system parameters into account.

9.2 Simulation Parameters

A number of system parameters were varied to determine the system performance: the time offset, Δ ; the number of source pairs, N ; and the duty cycle. A chip oversampling rate of 5 samples/chip was used. A SRN filter order of 31 with 5 filter taps per side lobe was selected so that a good pulse shape was attained for the chips, while maintaining a low number of tap weights. A rolloff factor of 0.35 was chosen arbitrarily for the SRN filters.

A 7th order m-sequence was used thus the PN code length, M , is 127 chips. This length was selected as Chapter 7 showed that the amount of interference between A and B sources decreases for longer m-sequences. A longer m-sequence could be used, but would require substantially more bandwidth.

9.3 Performance in a Gaussian Channel

Only one transmission path is present in a Gaussian channel. Therefore, there is no symbol smearing and T_m is set to 0. In [16] the CFDMA receiver isolated bandlimited narrowband source data via filtering so that the only source of interference in a Gaussian channel was AWGN. If this method was used for the CFTDMA system the only predicted sources of interference would be AWGN and the other stream of data within a source pair. Thus, in a Gaussian channel, performance should be dependent on the level of interference between the two streams of data for a particular Δ , as given in Fig. 7.5(b). Performance in a Gaussian channel should also be independent of the number of source pairs. It is to be determined if the proposed method of removing inter-source pair interference via integration of harmonics achieves this level of performance.

9.3.1 Performance Dependence on Code Time Offset, Δ

The relative performance results for the CFTDMA system with 10 source pairs for different values of Δ will be used to determine if the cross-correlation values of Fig. 7.5(b) can be used to predict system

performance. The time offsets of $\Delta = 19$ and $\Delta = 20$ were chosen as they have identical cross-correlation values. The time offset $\Delta = 21$ chips was chosen as it has a higher cross-correlation value. Based on these correlation values, system performances for $\Delta = 19$ and 20 chips were predicted to be similar while a degradation in performance was predicted for $\Delta = 21$ chips. The simulation results are shown in Fig. 9.1.

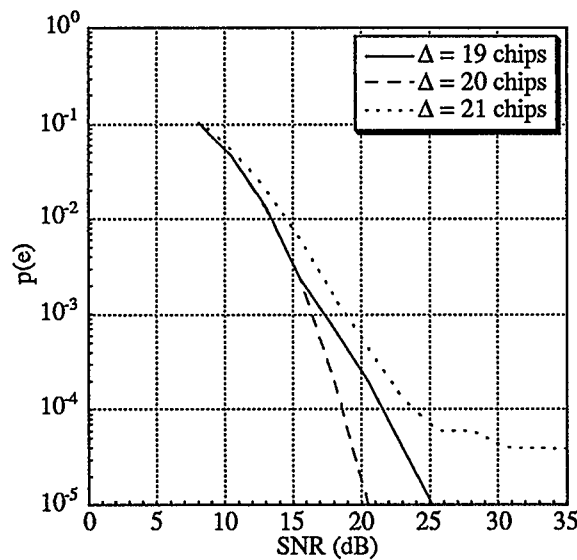


Figure 9.1 BER Performance in a Gaussian channel for CFTDMA system with $T_m=0$, 10 source pairs, and variable Δ .

The performance for $\Delta = 21$ chips is shown in Fig. 9.1 to be worse than $\Delta = 19$ and $\Delta = 20$ chips as was predicted. The performance exhibited by the system for $\Delta = 21$ chips is unacceptable as an error floor is introduced at a BER greater than 10^{-5} . The performance for $\Delta = 19$ chips and $\Delta = 20$ chips is much better than $\Delta = 21$ chips as the performance curves do not exhibit error floors at BER's greater than 10^{-5} . However it must be noted that the results are only for 10 source pairs and for a Gaussian channel. The performance for $\Delta = 19$ chips and $\Delta = 20$ chips is identical up to 16 dB. The

predicted system performance is not confirmed for all SNR as the time offset of $\Delta = 19$ chips is shown to exhibit a higher BER than $\Delta = 20$ chips for a SNR greater than 16 dB. The performance of the system with $\Delta = 20$ chips exhibits a 4.5 dB improvement over $\Delta = 19$ chips at a BER of 10^{-5} . These results indicate the system performance is not related entirely to the cross-correlation values of Fig. 7.5(b). The results imply that there is a source of interference other than the opposing stream of data within the source pair being demodulated. The adjacent source pairs may be providing some source of interference, this will be investigated in the next section.

9.3.2 Performance Dependence on Number of Source Pairs, N

In order to determine if the CFTDMA system performance is independent of the number of source pairs, the offset Δ should be held constant and the number of source pairs varied. This independence should occur regardless of the choice for Δ thus $\Delta = 19$ chips was chosen arbitrarily. The results for $\Delta = 19$ chips for various numbers of source pairs are shown in Fig. 9.2.

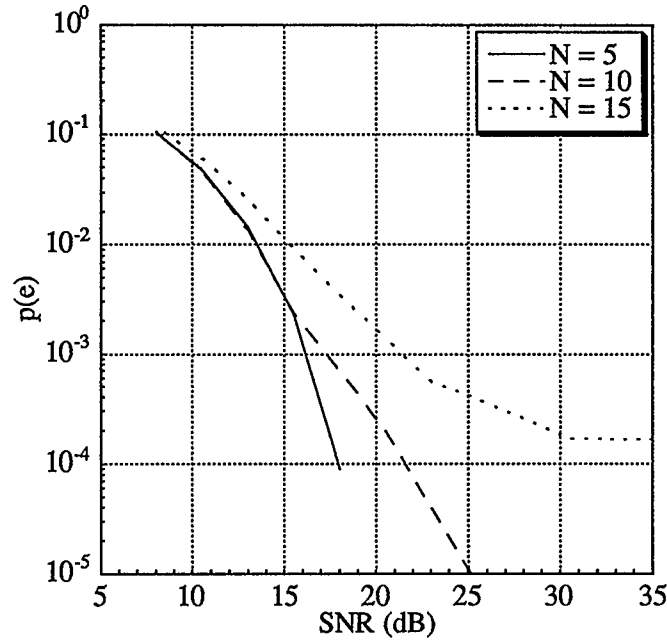


Figure 9.2 *BER performance in a Gaussian channel with $\Delta = 19$ chips, $T_m = 0$, and variable number of source pairs.*

Fig. 9.2 shows that the system performance degrades as the number of source pairs is increased, indicating that the adjacent source pairs are acting as a source of interference. The performance for 5 and 10 source pairs is identical for SNR less than 16 dB. The degradation of system performance becomes unacceptable at 15 source pairs as an error floor is exhibited at approximately 10^{-4} . The system is unable to achieve the high system rates desired according to Section 9.1 without additional measures like coding, even for transmission over a Gaussian channel.

The predicted ideal performance for a system which bandlimits the narrowband spectra prior to spreading at the transmitter and isolates source pair data via narrowband lowpass filtering at the receiver is a dependence on Δ and an independence of N . The removal of inter-source pair interference

via the use of harmonics does not attain this level of performance. The adjacent source pairs are acting as a source of interference. This interference may be due to an error in the pulse shaping leading to nonideal nyquist pulses for the chips. This would cause symbol values to influence their adjacent symbols affecting the integration process. As the integration process is the key to the success of the removal of inter-source pair interference via the use of harmonics this may lead to significant errors.

9.4 System Errors Due to SRN Pulse Shaping

The reason for system performance dependence on the number of source pairs and independence of Δ in a Gaussian channel must be determined. Upon inspection of the CFTDMA system, a possible source of error may be the method of pulse shaping the chips. As the method of inter-source pair interference cancellation due to harmonics is dependent on the adjacent source pairs' data integrating to zero, the loss of any portion of an adjacent source pair spectrum may affect this integration process. Examination of the demodulation process at the receiver revealed that the second SRN filter at the receiver does filter out a portion of the adjacent source pair's data, as shown in Fig. 9.3.

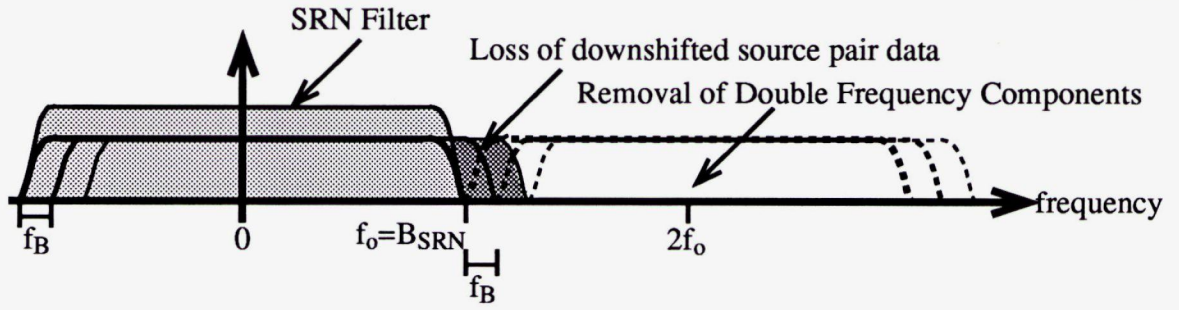


Figure 9.3 Loss of data due to SRN filtering at the receiver for 3 source pair CFTDMA system when recovering source pair 1 data.

A SRN filter was used at the transmitter to bandlimit the spectrum for each source pair thus the bandwidth of the spread spectra for a source pair is equal to the bandwidth of the SRN filter. The spectra of the adjacent source pairs are shifted in frequency relative to the desired source pair spectrum by an integer multiple of the frequency offset f_B . The part of the spectra shifted out of the SRN filter bandwidth is lost. The greater the number of source pairs, the greater the loss. The ratio of lost spectrum for source pair k when recovering data from source pair n , L_{nk} , is given by

$$L_{nk} = \frac{|n - k|f_B}{B_{SRN}}. \quad (9.5)$$

Equation (9.5) shows the loss of data to be more significant for source pairs located at greater frequency separations from the desired source pair. Substitution of equation (7.9) and (7.10) into equation (9.5) results in

$$L_{nk} = \frac{2|n - k|}{(1 + \beta)M}. \quad (9.6)$$

which shows the loss to be inversely proportional to the spreading code length M . Thus the loss of data becomes more substantial for a CFTDMA system using a spreading code of smaller order. This is due to the frequency offset between source pair spectra, f_B , becoming more significant in

comparison to the SRN filter bandwidth.

Examination of the simplest case of CFTDMA, i.e. N_t set to one in Fig. 5.6, which is equivalent to a CFDMA system, is done in Appendix 1 to determine the effect of this loss of data. Appendix 1 shows that the loss of data due to SRN filtering at the receiver does affect the removal of interfering data. The second SRN filter will only result in perfect nyquist chip pulses for the desired source's data. The adjacent sources' data will not have an ideal nyquist pulse shape for the chips and thus will provide interference at the ideal chip time, affecting the outcome of the integration process.

The SRN filter at the receiver must be identical to that used at the transmitter in order to attain a nyquist pulse. Thus the SRN filter at the receiver cannot be extended to cover all the lower spectra or it would no longer match the filter used at the transmitter. An alternative pulse shaping method must be employed.

9.5 Alternate Method of Pulse Shaping

Pulse shaping is necessary to band limit the CFTDMA signal spectrum; thus, an alternate method of pulse shaping the chips is required. A possible method to eliminate the loss of data through SRN filtering at the receiver is to use a raised-cosine filter at the transmitter to obtain the nyquist pulse shape and a low pass filter (LPF) at the receiver to remove the double frequency components. Although the receiver is no longer the "optimum receiver" for a Gaussian channel as discussed in Chapter 7, performance

should improve. The raised-cosine filter will have the same bandwidth as the SRN filter; thus

$$B_{\text{RCF}} = \frac{(1+\beta)}{2} \frac{W_s}{2}. \quad (9.7)$$

A wideband LPF will be required at the receiver to filter out the double frequency components after downshifting. In order for similar distortion not to result due to the loss of data, there can be no frequency overlap of the double frequency components of the source pair spectra with the downshifted source pair spectra. This frequency overlap can be prevented by selection of the initial upshift intermediate frequency. Consider the demodulation of source pair 1 data. The maximum frequency of the downshifted spectra, $f_{\ell\text{max}}$, must be less than the minimum frequency of the double frequency components, $f_{\text{u min}}$, thus

$$f_{\ell\text{max}} \leq f_{\text{u min}}. \quad (9.8)$$

Solving for these frequencies,

$$f_{\ell\text{max}} = \frac{(1+\beta)}{2} \frac{W_s}{2} + (N-1)f_B \quad (9.9)$$

and

$$f_{\text{u min}} = 2f_o - \frac{(1+\beta)}{2} \frac{W_s}{2}. \quad (9.10)$$

Substitution of (9.9) and (9.10) into (9.8) and solving for f_o gives the initial frequency

$$f_o \geq B_{\text{RCF}} + \frac{(N-1)f_B}{2} \quad (9.11)$$

which is seen to be greater than previously specified in Chapter 8. The bandwidth of the LPF must be large enough that none of the downshifted spectra for the source pairs is lost, while small enough such that the double frequency components are eliminated; thus

$$f_{\ell\max} \leq B_{\text{LPF}} \leq f_{\text{u}\min}. \quad (9.12)$$

Fig. 9.4 shows the frequency spectra for a $N_f = 3$ CFTDMA system. The lower limit on f_o assumes an ideal LPF with a sharp cutoff. For practical purposes a f_o greater than the lower limit should be selected so that a guard band is left between the downshifted spectra and the double frequency spectra as shown in Fig. 9.4.

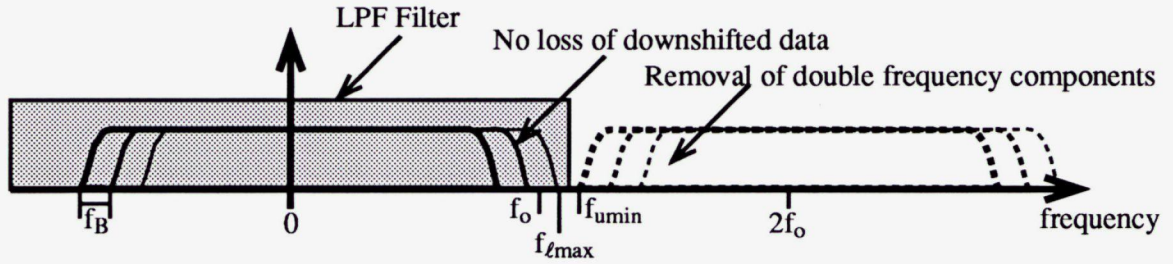


Figure 9.4 Removal of double frequency components through the use of a LPF after frequency downshifting to recover source pair 1 data for a 3 source pair CFTDMA system.

Appendix 2 investigates a CFDMA system analytically to determine if pulse shaping via a raised-cosine filter introduces any errors to the system. The analysis shows that the method does not introduce errors to a CFDMA system. Thus performance is predicted to improve for a CFTDMA system using a raised-cosine filter at the transmitter and a LPF at the receiver.

9.5.1 Performance Dependence on Code Time Offset, Δ

The simulations that produced the results shown in Fig. 9.1 were rerun using the raised-cosine filter pulse shaping method. The initial upshift frequency used was $f_o = B_{\text{RCF}} + (N - 1)f_B$. To obtain the same pulse shape as achieved by two cascaded 31 tap SRN filters, a 61 tap raised-cosine filter

is used. A 63 tap LPF with bandwidth of $B_{\text{LPF}} = B_{\text{RCF}} + (N - 1)f_B$ is used. Thus a guard band of $B_G = (N - 1)f_B$ was left between the upper and lower frequency bands resulting from downshifting. The new simulation results are plotted on the same graph as the cascaded SRN filter results in Fig. 9.5.

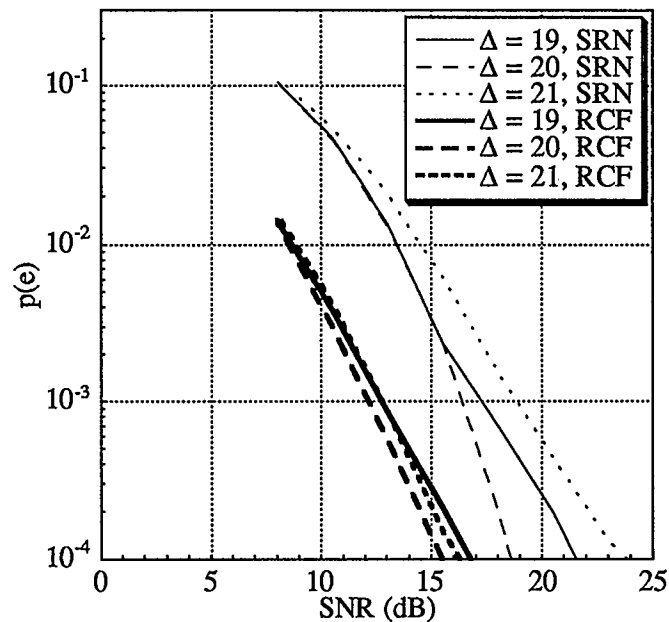


Figure 9.5 Comparison of performance results using 2 cascaded SRN filters to pulse shape versus one single raised-cosine filter (RCF) for a 10 source pair CFTDMA system.

The performance improvement using a raised-cosine filter for pulse shaping is significant. The amount of improvement varies for the different Δ ranging from 3 dB to 8 dB at a BER of 10^{-4} . As predicted by the analysis of Appendix 1 and 2, the raised-cosine filter method out performs the SRN filter method.

The raised-cosine filter system exhibits less dependence on the choice

of Δ , as shown by differences in the SNR of less than 1 dB at a BER of 10^{-4} for the three different values of Δ . The performance for the three different values of Δ for the SRN method differed by up to 2.5 dB at a BER of 10^{-4} .

9.5.2 Performance Dependence on Number of Source Pairs, N

The parameter Δ was held constant and the number of source pairs varied to determine if the change of filtering techniques removed the system dependence on the number of source pairs. The results are plotted in Fig. 9.6, Fig. 9.7, and Fig. 9.8 for Δ equal to 19, 20, and 21 chips, respectively.

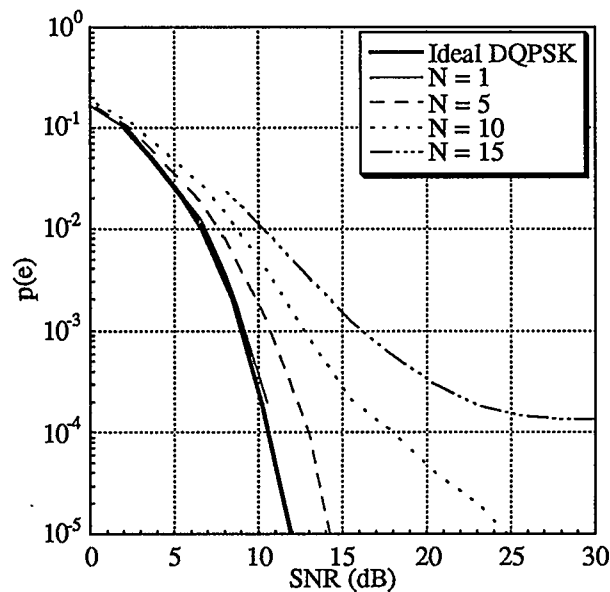


Figure 9.6 Performance in a Gaussian channel using a RCF for band limitation for a variable number of source pairs where $\Delta = 19$ chips.

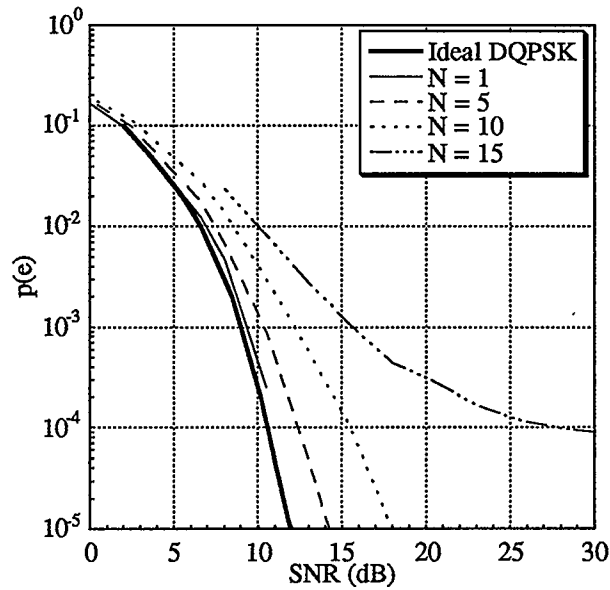


Figure 9.7 Performance in a Gaussian channel using a RCF for band limitation for a variable number of source pairs where $\Delta = 20$ chips.

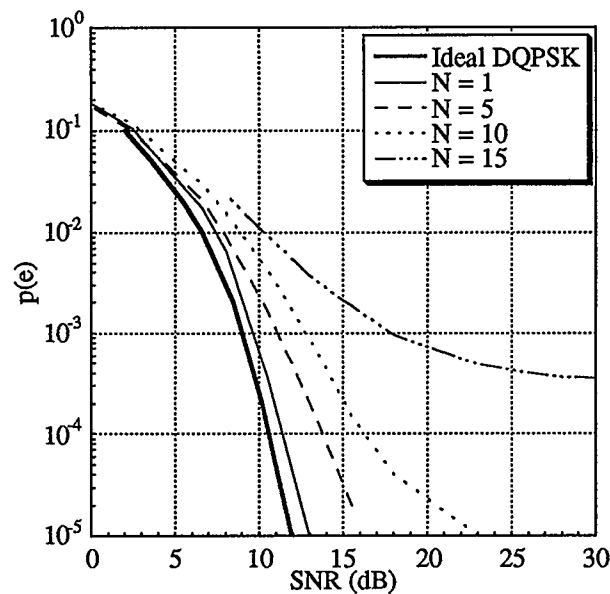


Figure 9.8 Performance in a Gaussian channel using a RCF for band limitation for a variable number of source pairs where $\Delta = 21$ chips.

The performance for an ideal single source DQPSK system in a Gaussian channel is shown for comparison. The single source pair system was expected to behave similar to the ideal DQPSK case except for a slight degradation due to the low cross-correlation values existing between the source A and source B data. This is observed to be true in Fig. 9.6, Fig. 9.7, and Fig. 9.8. As predicted by the cross-correlation values of Fig. 7.7(b), $\Delta = 21$ chips performs slightly worse than $\Delta = 19$ chips and $\Delta = 20$ chips.

The results in Fig. 9.6, Fig. 9.7, and Fig. 9.8 show that the system performance is dependent on Δ for high SNR. The $\Delta = 19$, 20 and 21 chips systems require a minimum SNR of 25 dB, 18 dB and 23 dB, respectively, to achieve a BER of 10^{-5} for a 10 source pair system. The relative performance of the CFTDMA system for a particular Δ is difficult to determine for more than one source pair.

The results of Fig. 9.6, Fig. 9.7, and Fig. 9.8 show that the system performance is still dependent on the number of source pairs. A degradation of performance is observed as the number of source pairs is increased. The use of harmonics to limit ACI is still not performing as expected but the degradation is not as severe as when the system was using SRN filters for pulse shaping. The performance results of Fig. 9.6, Fig. 9.7, and Fig. 9.8 show that an error floor appears at approximately 10^{-4} for 15 source pairs. Thus the system will not be able to achieve a bit rate of 150 Mbits/sec without additional measures like coding. The performance curves for all three Δ show the performance to be acceptable for 10 source pairs or less in a Gaussian channel. Thus lower rate systems may be achieved using this

method. The reason for the great dependence on the number of source pairs must be investigated so a means of increasing the number of sources can be found.

9.6 Analysis of System Dependence on Number of Source Pairs

Analysis was done in Appendix 3 and 4 to determine the reason for the degradation of performance with an increase in the number of source pairs. The analysis looked at the demodulation of 1A data for a CFTDMA system with a direct connection between the transmitter and receiver in order to isolate errors introduced by the system. The demodulated signal for data stream A of the 1st source pair can be written as

$$r_{1A}(t) = D_{1A}(t) + \sum_{\ell=2}^N I_{\ell A}^A(t) + \sum_{\ell=1}^N I_{\ell B}^A(t) \quad (9.13)$$

where $D_{1A}(t)$ denotes the desired part of the signal; $I_{\ell A}^A(t)$, the interference due to the ℓ^{th} source pair's A data when demodulating stream A data; and $I_{\ell B}^A(t)$, the interference due to the ℓ^{th} source pair's B data when demodulating stream A data. The various parts of equation (9.13) will be resolved for $T_m = 0$ and $T_m = \Delta$ for one symbol.

9.6.1 CFTDMA System with $T_m = 0$

Appendix 3 resolves the various parts of equation (9.13) for the demodulation of a single 1A symbol for a N source pair CFTDMA system with $T_m = 0$. There are two interfering B symbols per one A symbol for the scenario where $T_m = 0$ as shown in Fig. 7.5(a).

The desired portion of the signal for the i^{th} demodulated symbol is found to be

$$D_{1A}^i = \frac{1}{2} d_{1A}^i M \quad (9.14)$$

where d_{1A}^i is the desired A symbol value. The interference due to the remaining $N-1$ source pairs' A data on the i^{th} symbol interval was found in Appendix 3 to be

$$\sum_{\ell=2}^N I_{\ell A}^{iA} = 0. \quad (9.15)$$

Thus the data from A sources in the adjacent source pairs have no effect on the desired source pair's source A data. This is due to the integration of the harmonics to zero. The proposed method of Chapter 6 for removal of ACI through integration of harmonics successfully removes the interference due to adjacent source pairs' A data. However, the adjacent source pairs' B data is still a source of interference as shown in Appendix 3 by

$$\begin{aligned} I_{\ell B}^{iA} = & \frac{1}{2} d_{\ell B}^{i-1} \sum_{k=0}^{\Delta-1} c_k c_{M-\Delta+k} \cos(2\pi(\ell-1)\frac{k+\frac{1}{2}}{M}) \\ & + \frac{1}{2} d_{\ell B}^i \sum_{k=\Delta}^{M-1} c_k c_{k-\Delta} \cos(2\pi(\ell-1)\frac{k+\frac{1}{2}}{M}). \end{aligned} \quad (9.16)$$

where $d_{\ell B}^{i-1}$ and $d_{\ell B}^i$ are the two consecutive interfering B symbols. Evaluation of $I_{\ell B}^{iA}$ for a particular Δ will result in quantity that on average will have the same magnitude as the values given in Fig. 7.5(b) for the corresponding Δ . The summations in equation (9.16) do not go to zero as the term inside the summation does not exhibit even symmetry. A signal that is symmetric about its midpoint in the specified domain demonstrates even symmetry. Interference due to the B sources would be tolerable if it adhered to the low cross-correlation values of Fig. 7.5(b), for example for $\Delta = 19$ chips each additional source pair would introduce approximately 1%

of error. Investigation of equation (9.16) shows that these cross-correlation values are not valid for the other source pairs due to the presence of a cosine term, hence an independence of system performance from the correlation values of Fig. 7.5(b). The values for $I_{\ell B}^{iA}$ normalized to the magnitude of the desired term are given for various ℓ in Table A.3.1 for the case where $\Delta = 19$ chips, $M = 127$ chips and $T_m = 0$. Table A.3.1 shows that the interference due to the other source pairs' B data can be quite large, for example source pair 4 can cause up to 12% of error to source pair 1. The adjacent source pair's source A data will effect the recovery of the desired source pair's source B data in the same way. The end result being that each additional source pair provides additional interference in a Gaussian channel.

9.6.2 CFTDMA System with $T_m = \Delta$

A similar analysis is done in Appendix 4 for a N source pair CFTDMA system with $T_m = \Delta$. The demodulation of a single 1A symbol for the system with $T_m = \Delta$ in Appendix 4 results in different signals for the various parts of (9.13). The desired portion of the signal remains the same for the i^{th} demodulated symbol and is given by

$$D_{1A}^i = \frac{1}{2} d_{1A}^i M. \quad (9.17)$$

As in the case of $T_m = 0$, the interference due to the remaining N-1 source pairs' A data is

$$\sum_{\ell=2}^N I_{\ell A}^{iA} = 0 \quad (9.18)$$

due to the integration of the harmonics to zero. Thus the data from A sources in the adjacent source pairs has no effect on the desired source pair's source A data. The B data was found to be a large source of interference. A

system with $T_m = \Delta$ has only one interfering B symbol per A symbol as shown in Fig. 7.7(a). The interference due to the source pairs' B data is given in Appendix 4 by

$$I_{\ell B}^{iA} = \frac{1}{2} d_{\ell B}^i \sum_{k=\Delta}^{M-1} c_k c_{k-\Delta} \cos\left(2\pi(\ell-1)\frac{k+\frac{1}{2}}{M}\right) \quad (9.19)$$

where $d_{\ell B}^i$ is the interfering B symbol. Evaluation of $I_{\ell B}^{iA}$ for a particular Δ will result in quantity that on average will have the same magnitude as the values given in Fig. 7.7(b) for the corresponding Δ . The cross-correlation values of Fig. 7.7(b) are not valid for $I_{\ell B}^{iA}$ for $\ell \neq 1$. The values for $I_{\ell B}^{iA}$ normalized to the magnitude of the desired term are given for various ℓ in Table A.4.1 for the case where $\Delta = 19$ chips, $M = 127$ chips, and $T_{mc} = 19$ chips. Table A.4.1 shows that the B data from the other source pairs is a large source of interference for a CFTDMA system with $\Delta = T_{mc}$.

9.6.3 Analysis Results

Poor performance for both $T_m = 0$ and $T_m = \Delta$ occurs due to the B stream of the interfering source pairs not integrating to zero over the symbol interval. Thus each additional source pair introduces interference. The amount of interference can vary greatly depending on the choice of Δ and requires complex analysis to predict.

A method of reducing this interference is to set both Δ and T_{mc} equal to the PN code length M to result in a 50% duty cycle, as in Fig. 9.9. Source A and source B symbols will no longer overlap for this case, thus the interference in (9.19) and (9.21) reduces to zero; however, this results in a substantial increase in bandwidth. Using equation (7.14) the bandwidth for

the CFTDMA system is given by

$$B_T = \left(1 + \beta + \frac{N-1}{M}\right) \left(\frac{M + T_{mc}}{2}\right) R_b.$$

Thus increasing T_{mc} to 127 chips from say 20 chips increases the bandwidth by the factor $254/147$ which is almost double the bandwidth.

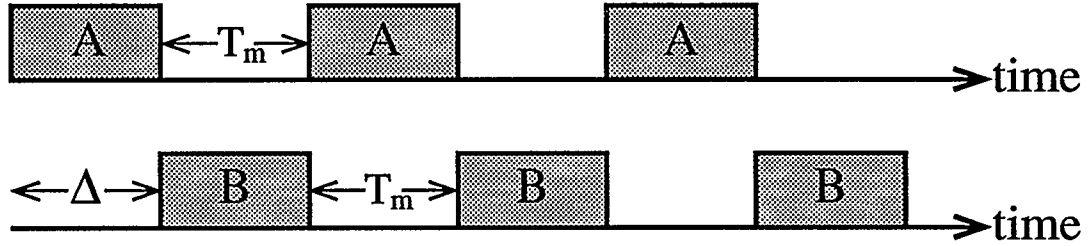


Figure 9.9 *Symbol timing for CFTDMA system with $\Delta = T_m = M$.*

Examination of the CFTDMA system with $\Delta = T_{mc} = M$ reveals that due to periodicity of the PN sequence, the system implementation of the $2N$ source CFTDMA system is equivalent to a N source CFDMA system with 100% duty cycle and source bit rates half that used for the CFTDMA system. Therefore the CFTDMA systems can also be implemented using CFDMA.

The system performance of the CFTDMA system with $\Delta = T_{mc} = M$ was determined for a variable number of source pairs to see if the system performance is independent of the number of source pairs. The results of Fig. 9.10 show that there still is a degradation of system performance with an increase in the number of source pairs but it is an acceptable degradation. This degradation is most likely due to nonideal filtering.

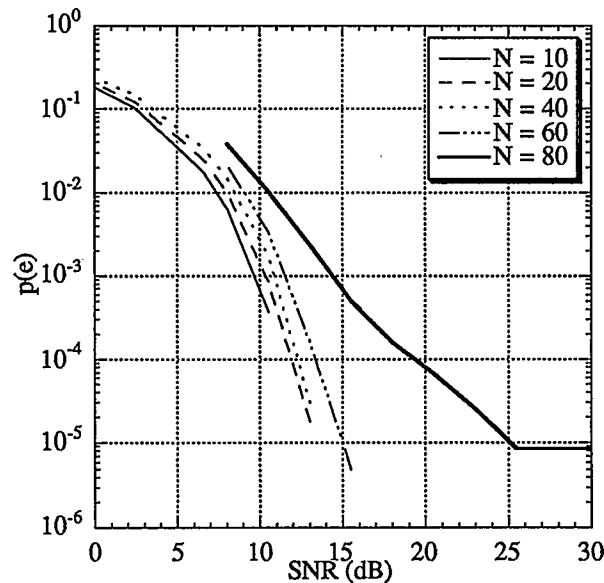


Figure 9.10 *Performance in a Gaussian channel for a CFTDMA system with $\Delta = T_{mc} = M$.*

The performance in Fig. 9.10 is deceiving since there is a large reduction in the source bit rates due to a significant decrease in the duty cycle. Using equations (9.2) and (9.3) the maximum source bit rate is 2 Mbits/sec. Thus to attain 150 Mbits/sec using this system requires more than 37 source pairs. Fig. 9.10 shows that a BER of 10^{-5} is possible for a SNR greater than 15 dB with 60 source pairs. Thus a system rate of 150 Mbits/sec can be achieved over a single path channel.

9.7 Performance in a Two-Ray Channel

The CFTDMA system performance for $\Delta = T_{mc} < M$ over a single ray channel degraded rapidly as the number of source pairs is increased. System performance was improved by using a single raised-cosine filter for pulse shaping rather than two SRN filters. System performance was further

improved by setting the system parameters to $\Delta = T_{mc} = M$ so that the A and B symbols do not overlap in the time domain. The performance of the CFTDMA system with $\Delta = T_{mc} = M$ and raised-cosine filter pulse shaping was evaluated over a two-ray static channel.

The worst case scenario for a two-ray channel is when the rays are equal in magnitude. The performance for this case is shown in Fig. 9.11 for a ray separation of 10 chips. This ray separation was chosen arbitrarily.

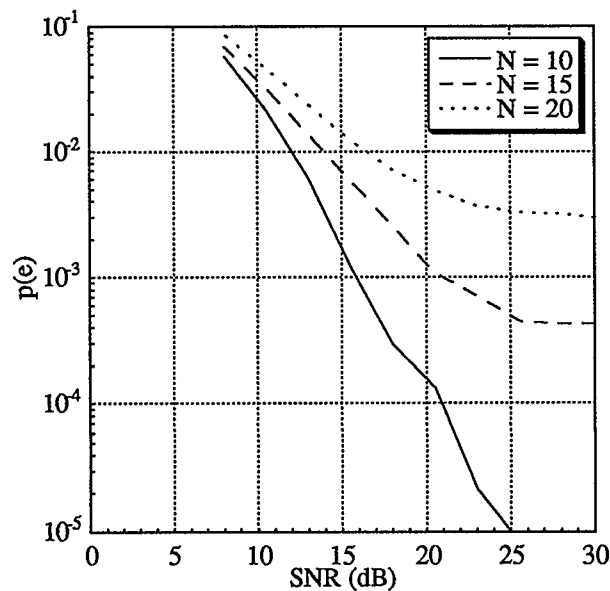


Figure 9.11 Performance over a 2 equal ray channel for CFTDMA system with $\Delta = T_{mc} = M$.

Fig. 9.11 shows that the CFTDMA system with 10 source pairs may be used in an equal 2-ray channel without any additional measures for SNR greater than 25 dB. This will provide a system with a maximum bit rate of 40 Mbits/sec. The system performance with greater than 10 source pairs shows poor performance, exhibiting error floors at .0004 and .003 for 15 and 20 source pairs, respectively.

Fig. 9.12 and Fig. 9.13 show the results when the second ray is of smaller magnitude than the first ray. The ray separation is also 10 chips.

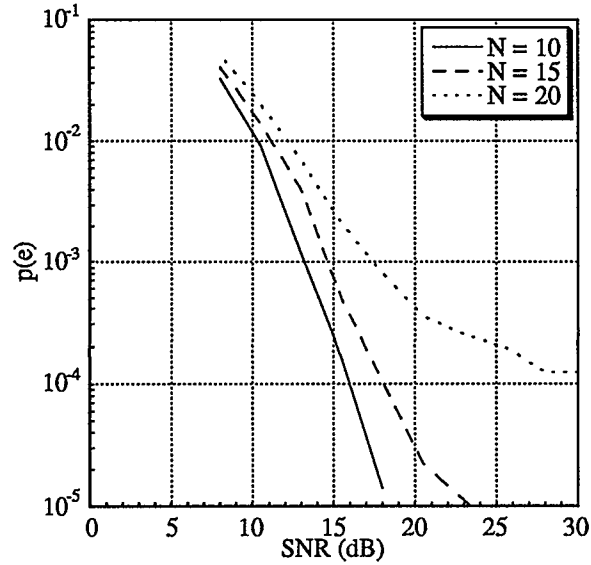


Figure 9.12 Performance over a 2 ray channel where the magnitude of the second ray is 75% of the magnitude of the first ray for a CFTDMA system with $\Delta = T_{mc} = M$.

Fig. 9.12 shows that, if the magnitude of the second ray is less than 75% of the first ray, that no additional measures are needed for up to 15 source pairs if the SNR is greater than 23.5 dB. This allows for a system rate of up to 60 Mbits/sec.

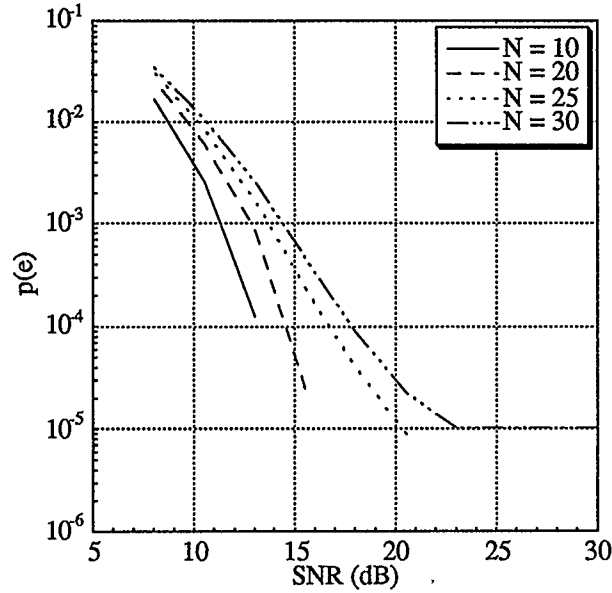


Figure 9.13 Performance over a 2 ray channel where the magnitude of the second ray is 50% of the magnitude of the first ray for a CFTDMA system with $\Delta = T_{mc} = M$.

Fig. 9.13 shows that up to 25 source pairs can be used without additional measures for SNR greater than 20 dB. This results in system that can achieve rates up to 100 Mbits/sec.

The performance of the system for a 2 ray channel is shown to improve as the magnitude of the second ray decreases and the number of source pairs is reduced. The degradation in performance with an increase in the number of source pairs can be explained by considering the signal due to the second ray as another two streams of data, say stream C and stream D, as shown in Fig. 9.14. The data streams C and D will serve as interference to the A and B streams due to the first ray. This interference is similar to how the B stream was shown to affect the A stream for $\Delta < M$ in a Gaussian channel. Note that the A sources will be the source of interference when

demodulating the desired source A data and the B sources will be the source of interference when demodulating the desired source B data. In the Gaussian channel with $\Delta < M$, it was the opposing stream of data that acted as the source of interference.

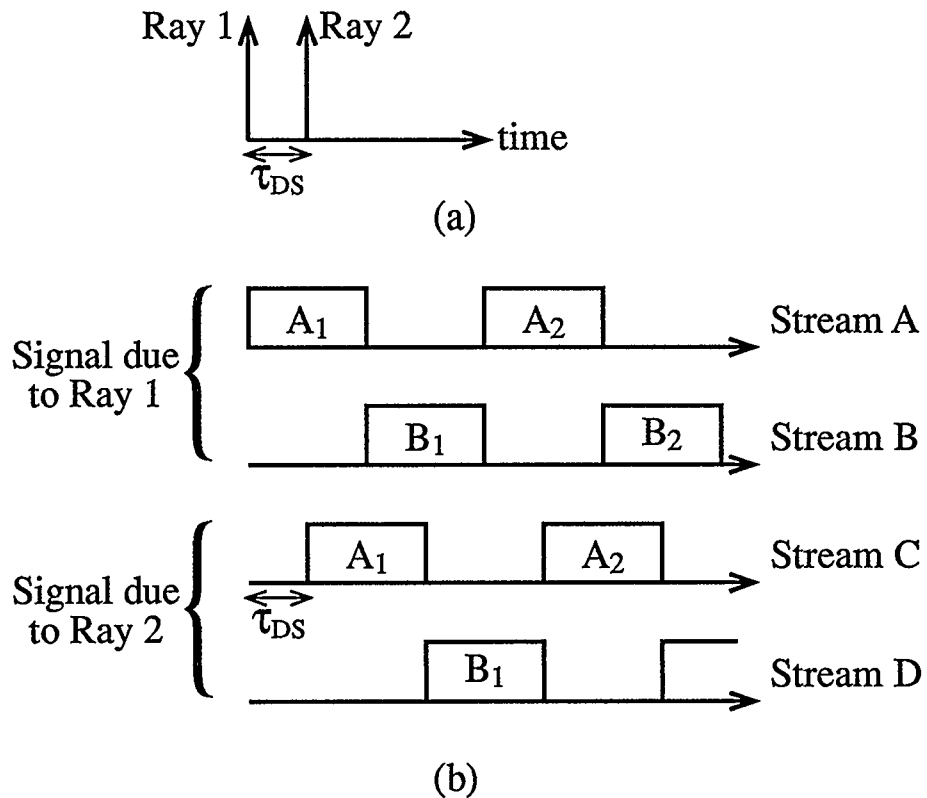


Figure 9.14 (a) Two equal ray channel impulse response.
 (b) Two ray channel creates delayed versions of the stream A and stream B data.

The ray separation will affect the system performance in a two ray channel just as Δ affected the system performance in a Gaussian channel for $\Delta < M$, resulting in an unpredictable dependence on the ray separation. As in the Gaussian channel scenario with $\Delta < M$, each additional source pair will provide interference to the system as was shown in Fig. 9.11. This interference is reduced as the magnitude of the second ray is decreased.

9.8 Performance in a Four-Ray Channel

The indoor multipath channel will exhibit more than two paths from the transmitter to the receiver thus the interference will be greater as the number of interfering rays is increased. The multipath channel is assumed to follow a Ricean distribution where there is a strong line of sight (LOS) path in addition to several low level scattered paths [20]. The system performance in a two ray channel, with the second ray being of smaller magnitude than the first ray, seems to indicate that relatively good performance could be achieved for lower rates than originally desired. Fig. 9.15 shows the performance of a 20 source pair (80 Mbits/sec) CFTDMA system in a 4 ray channel with a strong LOS. Denoting the rays by $(\alpha_k, \theta_k, \tau_k)$ the 4 rays are given by $(1, 0^\circ, 0)$, $(0.5, 0^\circ, 10T_c)$, $(0.25, 45^\circ, 15T_c)$, and $(0.25, -29.64^\circ, 20T_c)$.

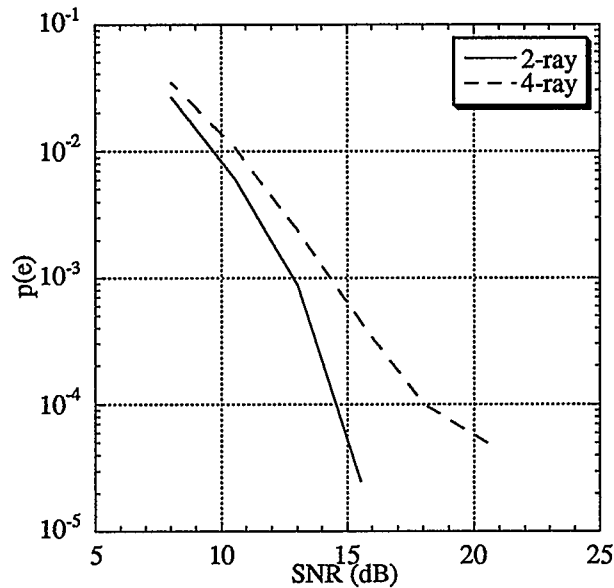


Figure 9.15 CFTDMA system performance in a 2 ray and 4 ray channel for 20 source pairs where magnitude of LOS is greater than or equal to twice the NLOS rays.

The performance results of Fig. 9.13 for 20 source pairs has also been plotted to show the amount of degradation introduced by the additional multipaths. There is a 4 dB degradation at a BER of 10^{-4} . The system performance in a channel with more than two rays need to be investigated further. As the system performance in a two ray channel is quite good if the second ray is less than 50% of the magnitude of the first ray, the statistical properties of an indoor channel should be investigated to determine how often the low level multipaths exceed 50% of the magnitude of the LOS ray.

9.9 Summary

This chapter analyzed the CFTDMA system performance using a MF despreader. The basis of the MF despreader method was the ability to eliminate adjacent source pair signals via integration of harmonics. It has been shown that in a Gaussian channel the interfering data from the adjacent source pairs is only eliminated by integration for the sources corresponding to the data stream being demodulated. For example, A sources provide no interference when demodulating the data from an A source, whereas the B sources provide large sources of interference. The interference due to adjacent source pairs can be virtually eliminated in a Gaussian channel by setting $\Delta = T_m = M$; however, this was not successful in a two ray channel. In the two ray channel simulations both the A and the B sources for adjacent source pairs will serve as interference thus each source pair contributes interference limiting the number of source pairs that can be used. The system rate is dependent on the number of source pairs and hence is limited.

The use of harmonics to cancel inter-source pair interference in a multipath channel for a CFTDMA system has been shown to be inadequate in achieving the desired rate of 150 Mbits/sec for a BER of 10^{-5} . However the CFTDMA shows promise in achieving rates on the order of 80 Mbits/sec for multipath channels with a strong LOS.

The goal of this thesis was to determine the CFTDMA system performance without the complexities of equalization, coding, and diversity. Because the system did not achieve the specified bit rate of 150 Mbits/sec for a maximum BER of 10^{-5} these methods of channel protection should be considered.

Chapter 10

Conclusions

Chapter Overview

This research project has investigated conditions under which adequate performance of a transmitter/receiver pair for a high variable rate CFTDMA system can be achieved without the complexities of coding, equalization, and diversity techniques. The CFTDMA system combines CTDMA and CFDMA to allow multiple low rate sources to operate simultaneously. The system resulted in a series of source pairs whereby CTDMA is used to multiplex the two sources within a source pair and CFDMA is used to multiplex the source pairs. The CFTDMA system employs direct-sequence spread spectrum (DS-SS) and thus requires code synchronization. A method of despreading via a matched filter (MF) was proposed in an attempt to avoid the complexities of code synchronization required by DS-SS.

10.1 System Overview

Data from a number of low rate sources were multiplexed using CFTDMA to achieve a high rate system. CFDMA multiplexes data by offsetting the narrowband data from a number of sources to adjacent nonoverlapping frequency bands. The narrowband data for each source is then spread using direct-sequence spread spectrum where only one code is employed for all the sources. CTDMA multiplexes data by offsetting two direct-sequence spread spectrum signals in time prior to transmission. The two methods are combined by dividing the low rate sources into two equal groups. Both groups were multiplexed using CFDMA and an identical code. The two resulting CFDMA waveforms were offset in time to achieve CFTDMA. The CFTDMA system can be considered as a series of source pairs whereby CTDMA is used to multiplex the two sources within a source pair and CFDMA is used to multiplex the source pairs. The two sources of data multiplexed within a source pair are referred to as source A and source B. The data from these two sources for all source pairs will be referred to as stream A and stream B. The processing of source pair data at the transmitter and receiver results in a modular design. The modular design facilitates the variable system rate requirement.

CTDMA and CFDMA both employ direct-sequence spread spectrum (DS-SS). Due to the complex code synchronization required by DS-SS systems, the design tried to incorporate the use of a matched filter at the receiver for despreading. Code synchronization is inherent when a filter matched to the code is used to despread the signal.

The elimination of inter-source interference through narrow band filtering by CFDMA led to difficulties in the MF implementation for the CFTDMA system. The proposed solution was to frequency offset source pairs so that an integer multiple of periods of the interfering sine wave lies in the integration interval when the desired source's signal is at baseband. Analysis was carried out to predict the theoretical system performance under various conditions.

10.2 Simulation Results

The system was expected to achieve data rates in excess of 150 Mbits/sec with a maximum tolerable BER of 10^{-5} .

Performance in a Gaussian channel was shown to vary with the choice of time offset, Δ , between the A and B streams of data. The relative performance of the CFTDMA system for different Δ was shown to be difficult to predict. The signals due to the CFTDMA sources corresponding to the same stream being recovered were integrating to zero as desired; however the interference due to the CFTDMA sources due to the other stream were not removed by integration. This caused error floors at BER's greater than 10^{-5} to be exhibited in the performance curves for 15 source pair systems. This level of performance was deemed inadequate as a limiting rate of 4 Mbits/sec was placed on the low rate sources based on the amount of time dispersion expected in a multipath channel. Thus the system was unable to achieve a system rate of even 120 Mbits/sec in a Gaussian channel.

Performance was greatly improved in the Gaussian channel by setting the time offset Δ equal to the spreading code length and the symbol duty cycle to 0.5 at the cost of almost doubling the system bandwidth. This large increase in bandwidth may not be an issue in the 30 GHz band. In excess of 60 source pairs were possible with these changes in the system parameters. Due to the large decrease in duty cycle the low rate sources were limited to 2 Mbits/sec by a multipath channel. The system with 50% duty cycle and $\Delta = M$ achieved data rates in excess of 240 Mbits/sec in a Gaussian channel.

In a two ray channel system the receiver locked onto the strongest ray, or line of sight (LOS) path. The signals arriving at the receiver via the LOS were integrating to zero as desired. The signals arriving at the receiver due to the second ray were not integrating to zero. This led to a significant degradation of performance with an increase in the number of source pairs. Performance was gauged by looking at a static two ray channel with variable magnitude of the second ray. The CFTDMA system could support up to 10 source pairs resulting in a system rate of 40 Mbits/sec when the two rays were equal in magnitude. The magnitude of the second ray was decreased to 75% of the first ray. The number of source pairs increased to 15 source resulting in a CFTDMA system rate of 60 Mbits/sec. The magnitude of the second ray was further decreased to 50% of the first ray. The number of source pairs increased to 25 resulting in a system rate of 100 Mbits/sec.

Performance was shown to be limited by the chosen implementation of the CFTDMA system. The MF despreader did not remove the interference due to adjacent source pairs as expected. Thus the desired rate

of 150 Mbits/sec was not achieved in a two ray channel. However, the results in a two ray channel did show promise for lower rate systems in a Ricean channel where a strong LOS is present as performance improved as the magnitude of the second ray decreased.

A typical indoor channel would have more than two multipaths thus a further degradation of system performance is expected. A simple simulation for a four ray channel was run where the 3 interfering rays had a magnitude of 50% or less than that of the LOS ray. The performance was shown to degrade by 3.5 dB at a BER of 10^{-4} for a 20 source pair system. Further analysis of the indoor multipath channel at high frequencies must be done in future work.

10.3 Recommendations for Future Work

The chosen implementation of the CFTDMA system used the fact that the integration of an integer multiple of a period of a cosine wave is zero. As half a period of a cosine wave also integrates to zero, the frequency offset between sources used in this system can be halved. Although bandwidth is not of concern in the proposed 30 GHz band this will lead to a reduction in bandwidth for the system. The amount of bandwidth reduction increases as the spreading code length is decreased. Future work should look at the reduction of the PN code length M and the frequency offset f_B . Two such CFTDMA systems with a smaller number of source pairs may be placed on adjacent disjoint frequency bands to achieve a higher rate system. This may allow for an increase in the system rates without introducing any

coding, equalization or diversity to the system.

The analysis of the system in a two ray channel showed that interference due to the second ray of multipath led to a dependency on the number of source pairs in the system. Channel protections techniques such as coding and equalization should be investigated to determine a method for the possible reduction of the dependency on the number of source pairs.

If a virtual independence of the system on the number of source pairs is desired for the CFTDMA system without the use of coding or equalization then the system performance should be investigated using band limitation of the narrowband spectra prior to spreading. The interference due to adjacent sources would be removed by a narrowband filter at the receiver after modulation of the received signal by a reference code and prior to integration over the symbol duration. A MF despreader can not be accommodated by such a system so further investigation into code acquisition and tracking is required.

References

- [1] W.C.Y. Lee, "Mobile Communications", McGraw-Hill Book Company, 1982.
- [2] K. Pahlavan, A.H. Levesque, "Wireless Data Communications", Proc. IEEE, vol. 82, no. 9, pp. 1398-1430, Sept. 1994.
- [3] G.A. Halls, "HIPERLAN: the high performance radio local area network standard", Electronics & Communication Engineering Journal, Dec. 1994.
- [4] K. Pahlavan, T.H. Probert, M.E. Chase, "Trends in Local Wireless Networks", IEEE Comm. Mag., vol. 33, no. 3, pp. 88-95, March 1995.
- [5] J. Padgett, C.G. Günther, T. Hattori, "Overview of Wireless Personal Communication", IEEE Comm. Mag., vol. 33, no. 1, pp. 28-41, Jan. 95.
- [6] W. Hollemans, A. Verschoor, "Performance study of WaveLAN and Altair Radio-LANs", Proc. Wireless '94, vol. 3, pp. 831-837, July 1994.
- [7] A. Plattner, N. Prediger, W. Herzig, "Indoor and Outdoor Propagation Measurements at 5 and 60 GHz for Radio LAN Applications", IEEE MTT-S International Microwave Symposium Digest, vol. 2, pp. 853-856, June 1993.

- [8] G. Kalivas, M. El-Tanany, S. Mahmoud, "The Design of a Radio Link for Indoor Wireless Communications at 29 GHz", Proc. 3rd International Conf. on Universal Personal Communications, pp. 6-10, Sept. 1994.
- [9] S. Todd, M. El-Tanany, G. Kalivas, S. Mahmoud, "Indoor Radio Path Loss Comparison Between the 1.7 GHz and 37 GHz Bands", Proc. 2nd International Conf. on Universal Personal Communications, vol. 2, pp. 621-625, Oct. 1993.
- [10] G. Kalivas, M. El-Tanany, S. Mahmoud, "Channel Characterization for Indoor Wireless Communications at 21.6 GHz and 37.2 GHz", Proc. 2nd International Conf. on Universal Personal Communications, vol. 2, pp. 626-630, Oct. 1993.
- [11] M. Chase, K. Pahlavan, "Performance of DS-CDMA Over Measured Indoor Radio Channels Using Random Orthogonal Codes", IEEE Trans. on Comm., vol. 42, no. 4, pp. 617-621, Nov. 1993.
- [12] G.L. Turin, "Introduction to Spread-Spectrum Antimultipath Techniques and Their Application to Urban Digital Radio", Proc. IEEE, vol. 68, no. 3, pp. 328-353, March 1980.
- [13] M.J. Stehouwer, "Effects of Imperfect Synchronization on a Direct Sequence Spread Spectrum Communication System", Proc. Personal, Indoor, and Mobile Radio Communications Conf., pp. 462-466, Sept. 1994.

- [14] F.J. Hagmanns, V. Hespelt, "On the Detection of Bandlimited Direct-Sequence Spread-Spectrum Signals Transmitted via Fading Multipath Channels", IEEE J. on Selected Areas in Comm., vol. 12, no. 5, pp. 891-899, June 1994.
- [15] D.M. Krinsky, A.H. Haddad, C. Lee, "An Adaptive Direct-Sequence Spread-Spectrum Receiver for Burst Type Interference", IEEE J. on Selected Areas in Comm., vol. 13, no. 1, pp. 59-69, Jan. 1995.
- [16] C. Günther, J. Ruprecht, J. Habermann, R. Rüegg, P. Jung, "Code Frequency Division Multiple Access: A Downlink Multiplexing in Support of Effective Multi-User Equalization", Proc. 2nd International Conf. on Universal Personal Communications, vol. 1, pp. 39-43, Oct. 1993.
- [17] J. Ruprecht, F.D. Neeser, M. Hufschmid, "Code Time Division Multiple Access: An Indoor Cellular System", Proc. 42nd VTS Conf., vol. 2, pp. 736-739, May 1992.
- [18] J.G. Proakis, "Digital Communications", New York, McGraw-Hill, 1989.
- [19] J.E. Salt, S. Kumar, D. Dodds, "Spread Spectrum for Indoor Wireless Communication", Tutorial provided jointly by National Wireless and TRILabs, 1992.
- [20] H. Hashemi, "The Indoor Radio Propagation Channel", Proc. of the IEEE, vol. 81, no. 7, pp. 943-962, July 1993.

- [21] J. Lee, T. Kim, K. Whang, "Performance of $\pi/4$ -shift DQPSK Direct-Sequence Spread-Spectrum Multiple-Access with Diversity Combining over Frequency-Selective Rician Fading Channels", Proc. 43rd IEEE Vehicular Technology Conf., pp. 827-830, May 1993.
- [22] R.M. Gagliardi, "Satellite Communications", Van Nostrand Reinhold, 1991.
- [23] A.W. Lam, S. Tantaratana, "Theory and Applications of Spread-Spectrum Systems", IEEE/EAB Self-Study Course, May 1994.
- [24] E. Patton, "Hardware Implementation of the Digital Rake Transceiver", University of Calgary Masters Thesis, Aug. 1993.
- [25] R.E. Ziemer, R.L. Peterson, "Digital Communications and Spread Systems", New York, Macmillan Publishing Co., 1985.
- [26] A. Polydoros, C.L. Weber, "A Unified Approach to Serial Search Spread-Spectrum Code Acquisition-Part I: General Theory", IEEE Trans. on Comm., vol. 32, no. 5, pp. 542-549, May 1984.
- [27] G.J.R. Povey, P.M. Grant, "Simplified matched filter receiver designs for spread spectrum communications applications", Electronics & Communications Engineering Journal, pp. 59-64, April 1993.
- [28] S. Haykin, "Adaptive Filter Theory", Englewood Cliffs, New Jersey, Prentice-Hall, 1991.

- [29] P.M. Grant, "The Potential Application of Analogue Matched and Adaptive Filters in Spread-Spectrum Communications", *The Radio and Electronic Engineer*, vol. 52, no. 5, pp. 246-258, May 1982.
- [30] J.C. Haarsten, "A Differential-Delay SAW Correlator for Combined DSSS Despreading and DPSK Demodulation", *IEEE Trans. on Comm.*, vol. 41, no. 9, pp. 1278-1280, Sept. 1993.
- [31] H. Nakase, T. Kasai, Y. Nakamura, K. Masu, K. Tsubouchi, "One Chip Demodulator Using RF Front-End SAW Correlator for 2.4 GHz Asynchronous Spread Spectrum Modem", *Proc. Personal, Indoor, and Mobile Radio Communications Conf.*, pp. 374-378, Sept. 1994.
- [32] S. Haykin, "An Introduction of Analog and Digital Communications", New York, John Wiley & Sons, 1989.
- [33] R. Umstattd, "Assay Quadrature Modulators for PCS Applications", *Microwaves & RF*, pp. 90-102, Aug. 1993.
- [34] R. De Gaudenzi, M. Luise, R. Viola, "A Digital Chip Timing Recovery Loop for Band-Limited Direct-Sequence Spread-Spectrum Signals", *IEEE Trans. on Comm.*, vol. 41, no. 11, pp. 1760-1768, Nov. 1993.
- [35] S. Chennakeshu, G.J. Saulnier, "Differential Detection of $\pi/4$ -shifted-DQPSK for Digital Cellular Radio", *Proc. 41st IEEE Vehicular Technology Conf.*, pp. 186-191, May 1991.

- [36] H. Aghvami, "Digital modulation techniques for mobile and personal communication systems", *Electronics & Communication Engineering Journal*, pp. 126 132, June 1993.

Appendix 1

Analysis of Pulse Shaping via matching SRN Filters in the Transmitter and Receiver for a CFDMA System

An N source CFDMA transmitter and receiver is analyzed in order to determine the errors introduced by pulse shaping via matching SRN filters at the transmitter and receiver. The system is shown in Fig. A.1.1. To isolate errors due to filtering, a direct connection has been assumed between the transmitter and the receiver.

The symbols adjacent to the desired symbol may influence the symbol data at the ideal sampling times due to improper filtering. Thus the analysis looks at the desired symbol and its two surrounding symbols as shown in Fig. A.1.2.

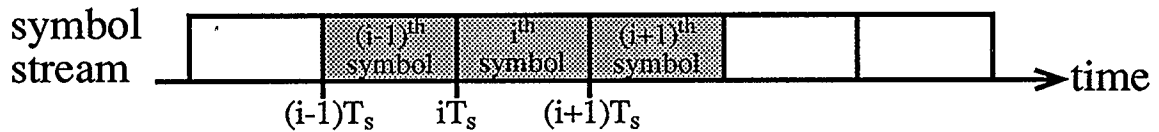


Figure A.1.2 *Symbol stream for one source.*

For one source the signal consisting only of the three necessary symbols can be written as

$$d_n(t) = d_n^{i-1} p^{i-1}(t) + d_n^i p^i(t) + d_n^{i+1} p^{i+1}(t) \quad (\text{A.1.1})$$

where d_n^i refers to the i^{th} symbol value for source n and $p^i(t)$ is the pulse for the i^{th} symbol. Rectangular pulses are used for the symbols thus $p^i(t)$ is given by

$$p^i(t) = u(t - iT_s) - u(t - (i+1)T_s) \quad (\text{A.1.2})$$

where $u(t)$ is the unit step function.

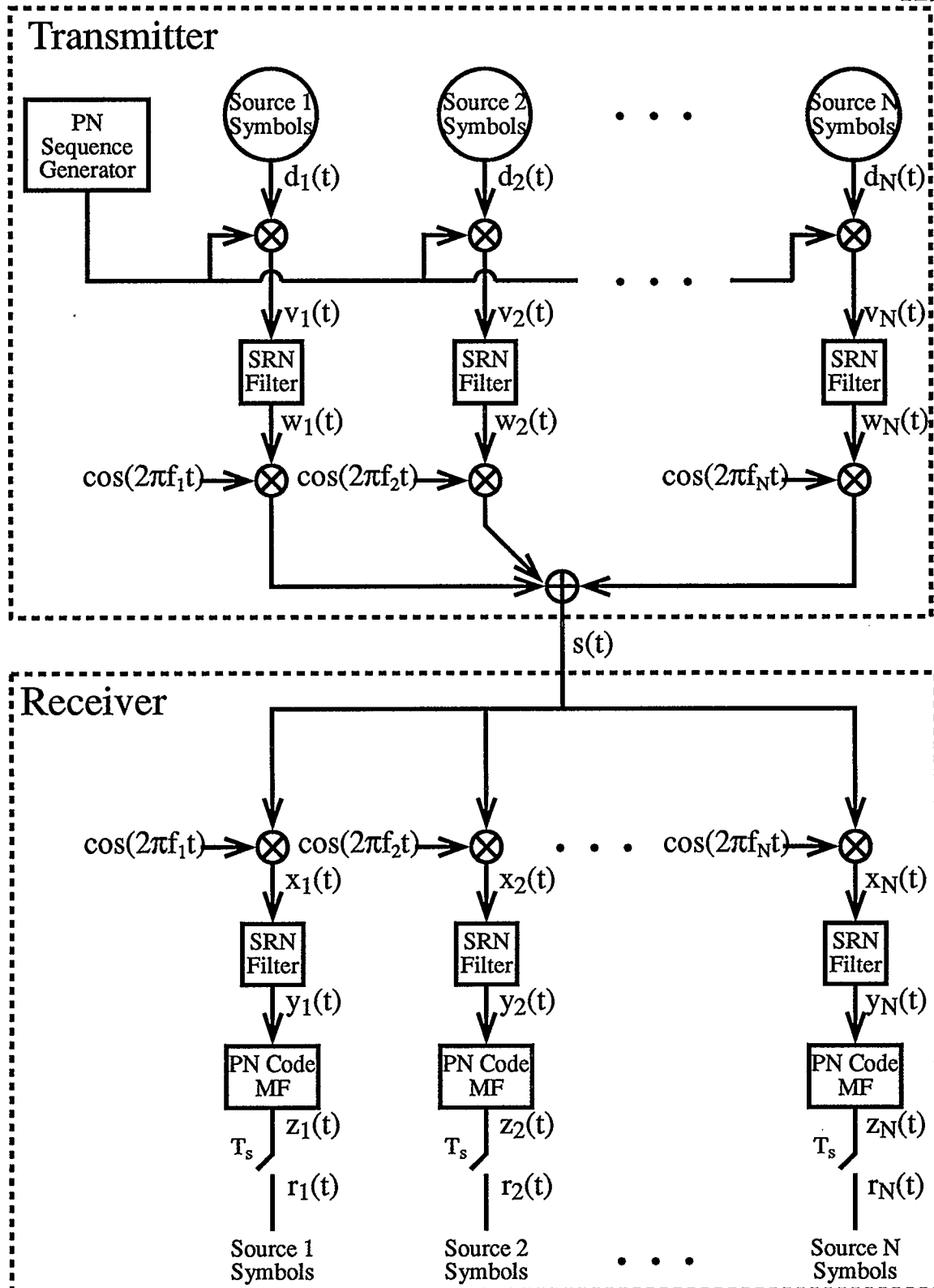


Figure A.1.1 CFDMA system employing matching SRN filters for pulse shaping with a direct connection between transmitter and receiver.

The CFDMA system is analyzed using the signal denotations of Fig. A.1.1.

The encoded symbols for each source are spread resulting in

$$v_n(t) = c(t)d_n(t) \quad (\text{A.1.3})$$

where $c(t)$ is the periodic PN code sequence. The spread data is then pulse shaped with a square-root nyquist filter to get

$$w_n(t) = g(t)*[c(t)d_n(t)] \quad (\text{A.1.4})$$

where $g(t)$ is the impulse response of a square-root nyquist filter with bandwidth

$$B_{\text{SRN}} = \frac{(1+\beta)}{2} \frac{M}{T_s}. \quad (\text{A.1.5})$$

The pulse shaped data from the N different sources are then upshifted to different intermediate frequencies and combined to obtain the composite at the output of the transmitter as follows:

$$\begin{aligned} s(t) = & \cos(2\pi f_1 t)g(t)*[c(t)d_1(t)] \\ & + \cos(2\pi f_2 t)g(t)*[c(t)d_2(t)] \\ & \vdots \\ & + \cos(2\pi f_N t)g(t)*[c(t)d_N(t)] \end{aligned} \quad (\text{A.1.6})$$

where

$$f_1 = f_o = \frac{(1+\beta)}{2} \frac{M}{T_s}, \quad (\text{A.1.7})$$

$$f_n = f_1 + (n-1)f_B \quad (\text{A.1.8})$$

and

$$f_B = \frac{1}{T_s}. \quad (\text{A.1.9})$$

Because a direct connection has been assumed $s(t)$ arrives at the receiver unaltered. Looking specifically at the demodulation of source 1 data, the incoming signal $s(t)$ is downshifted by f_1 in order to shift the source 1 data to baseband. The downshifted signal is given by

$$\begin{aligned}
x_1(t) = & \frac{1}{2}g(t)*[c(t)d_1(t)] \\
& + \frac{1}{2}\cos(2\pi(f_2 - f_1)t)g(t)*[c(t)d_2(t)] \\
& \vdots \\
& + \frac{1}{2}\cos(2\pi(f_N - f_1)t)g(t)*[c(t)d_N(t)] \\
& + \frac{1}{2}\cos(2\pi(2f_1)t)g(t)*[c(t)d_1(t)] \\
& + \frac{1}{2}\cos(2\pi(f_2 + f_1)t)g(t)*[c(t)d_2(t)] \\
& \vdots \\
& + \frac{1}{2}\cos(2\pi(f_N + f_1)t)g(t)*[c(t)d_N(t)].
\end{aligned} \tag{A.1.10}$$

The downshifted signal is passed through the second SRN filter resulting in

$$y_1(t) = g(t)* \begin{bmatrix} \frac{1}{2}g(t)*[c(t)d_1(t)] \\ + \frac{1}{2}\cos(2\pi(f_2 - f_1)t)g(t)*[c(t)d_2(t)] \\ \vdots \\ + \frac{1}{2}\cos(2\pi(f_N - f_1)t)g(t)*[c(t)d_N(t)] \\ + \frac{1}{2}\cos(2\pi(2f_1)t)g(t)*[c(t)d_1(t)] \\ + \frac{1}{2}\cos(2\pi(f_2 + f_1)t)g(t)*[c(t)d_2(t)] \\ \vdots \\ + \frac{1}{2}\cos(2\pi(f_N + f_1)t)g(t)*[c(t)d_N(t)] \end{bmatrix}. \tag{A.1.11}$$

The spectra of the double frequency components are filtered out by the SRN filter as they lie entirely outside of the bandwidth of the SRN filter simplifying (A.1.11) to

$$y_1(t) = g(t)* \begin{bmatrix} \frac{1}{2}g(t)*[c(t)d_1(t)] \\ + \frac{1}{2}\cos(2\pi(f_2 - f_1)t)g(t)*[c(t)d_2(t)] \\ \vdots \\ + \frac{1}{2}\cos(2\pi(f_N - f_1)t)g(t)*[c(t)d_N(t)] \end{bmatrix}. \tag{A.1.12}$$

Because the baseband spectrum lies entirely within the bandwidth of the square-root nyquist filter, the two SRN impulse responses can be combined to form a raised-cosine impulse response. The other terms can not be simplified in this manner as part of their spectra lies outside the bandwidth of the second SRN filter.

$$\begin{aligned}
y_1(t) = & \frac{1}{2} g_r(t) * [c(t) d_1(t)] \\
& + \frac{1}{2} g(t) * [\cos(2\pi(f_2 - f_1)t) [g(t) * [c(t) d_2(t)]]] \\
& \vdots \\
& + \frac{1}{2} g(t) * [\cos(2\pi(f_N - f_1)t) [g(t) * [c(t) d_N(t)]]]
\end{aligned} \tag{A.1.13}$$

where

$$g_r(t) = g(t) * g(t) \tag{A.1.14}$$

is the impulse response of a raised cosine filter with bandwidth equal to

$$B_{\text{RCF}} = \frac{(1 + \beta)}{2} \frac{M}{T_s}. \tag{A.1.15}$$

Correlation of the SRN filtered output with a synchronized code sequence $c(t)$ can be used to determine the output of the PN code MF at the ideal sampling time as in Fig. A.1.3.

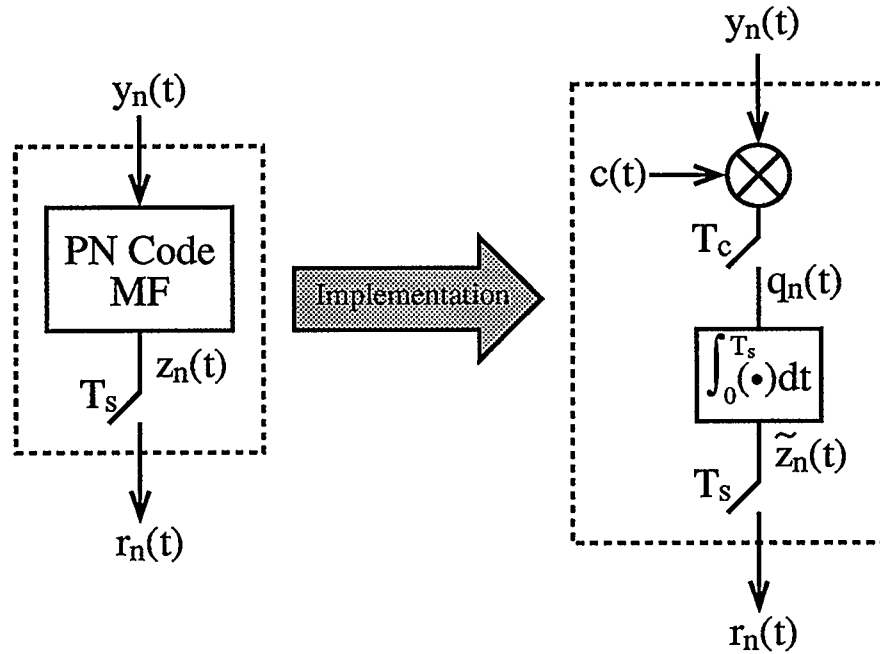


Figure A.1.3 Use of correlation to determine the MF output at the ideal sampling time.

The output of the MF, $z_n(t)$, and the correlator, $\tilde{z}_n(t)$, are only equal at the symbol period.

$$\begin{cases} z_n(t) = \tilde{z}_n(t) & t = kT_s \quad k \in \text{int} \\ z_n(t) \neq \tilde{z}_n(t) & \text{otherwise} \end{cases}$$

Using correlation, the signal $y_1(t)$ is modulated by the reference code and sampled at the ideal chip time on the desired symbol interval:

$$q_1(t) = c(t) \begin{bmatrix} \frac{1}{2} g_r(t) * [c(t)d_1(t)] \\ + \frac{1}{2} g(t) * [\cos(2\pi f_{21}t) [g(t) * c(t)d_2(t)]] \\ \vdots \\ + \frac{1}{2} g(t) * [\cos(2\pi f_{N1}t) [g(t) * c(t)d_N(t)]] \end{bmatrix} \sum_{k=0}^{3M-1} \delta(t - (i-1)T_s - kT_c) \quad \dots(\text{A.1.16})$$

where

$$f_{\ell 1} = f_{\ell} - f_1 = (\ell - 1)f_B. \quad (\text{A.1.17})$$

A perfect nyquist pulse exists for each chip in the baseband term, thus the two symbols adjacent to the desired symbol do not affect the desired symbol at the ideal chip sampling times. If the desired component is sampled at the ideal chip time, the resulting signal is an impulse train as the two $c(t)$ terms can be combined resulting in a constant value of 1 over the symbol interval. The other terms can not be simplified in this manner as perfect nyquist chip pulses do not exist for these terms.

$$q_1(t) = \frac{1}{2} [g_r(t) * d_1(t)] \sum_{k=0}^{3M-1} \delta(t - (i-1)T_s - kT_c) \\ + c(t) \begin{bmatrix} \frac{1}{2} g(t) * [\cos(2\pi f_{21}t) [g(t) * [c(t)d_2(t)]] \\ \vdots \\ + \frac{1}{2} g(t) * [\cos(2\pi f_{N1}t) [g(t) * [c(t)d_N(t)]] \end{bmatrix} \sum_{k=0}^{3M-1} \delta(t - (i-1)T_s - kT_c) \quad \dots(\text{A.1.18})$$

Expansion of the term $d_1(t)$ in equation (A.1.18) results in

$$\begin{aligned}
q_1(t) = & \frac{1}{2} \begin{bmatrix} d_1^{i-1} \sum_{k=0}^{M-1} \delta(t - (i-1)T_s - kT_c) \\ + d_1^i \sum_{k=0}^{M-1} \delta(t - iT_s - kT_c) \\ + d_1^{i+1} \sum_{k=0}^{M-1} \delta(t - (i+1)T_s - kT_c) \end{bmatrix} \\
& + c(t) \begin{bmatrix} \frac{1}{2} g(t) * [\cos(2\pi f_{21}t) [g(t) * [c(t)d_2(t)]] \\ \vdots \\ + \frac{1}{2} g(t) * [\cos(2\pi f_{N1}t) [g(t) * [c(t)d_N(t)]] \end{bmatrix} \sum_{k=0}^{3M-1} \delta(t - (i-1)T_s - kT_c)
\end{aligned}
\quad \dots(A.1.19)$$

To complete the correlation process the $q_1(t)$ is integrated over the desired symbol duration and sampled at $(i+1)T_s$ resulting in

$$\begin{aligned}
\tilde{z}((i+1)T_s) = & \frac{1}{2} d_1^{i-1} \sum_{k=0}^{M-1} \int_{iT_s}^{(i+1)T_s} \delta(t - (i-1)T_s - kT_c) dt \\
& + \frac{1}{2} d_1^i \sum_{k=0}^{M-1} \int_{iT_s}^{(i+1)T_s} \delta(t - iT_s - kT_c) dt \\
& + \frac{1}{2} d_1^{i+1} \sum_{k=0}^{M-1} \int_{iT_s}^{(i+1)T_s} \delta(t - (i+1)T_s - kT_c) dt \\
& + \frac{1}{2} \int_{iT_s}^{(i+1)T_s} c(t) \begin{bmatrix} g(t) * [\cos(2\pi f_{21}t) [g(t) * [c(t)d_2(t)]] \\ \vdots \\ + g(t) * [\cos(2\pi f_{N1}t) [g(t) * [c(t)d_N(t)]] \end{bmatrix} \sum_{k=0}^{3M-1} \delta(t - (i-1)T_s - kT_c) dt
\end{aligned}
\quad \dots(A.1.20)$$

The adjacent symbols at baseband, therefore those originating from the same source, can be seen to provide no interference as the first and third term of equation (A.1.20) clearly integrate to zero. The desired recovered symbol for source 1 can be written as

$$\begin{aligned}
r_1^i(t) = & \frac{1}{2} d_1^i M \\
& + \frac{1}{2} \int_{iT_s}^{(i+1)T_s} c(t) \begin{bmatrix} g(t) * [\cos(2\pi f_{21}t) [g(t) * [c(t)d_2(t)]] \\ \vdots \\ + g(t) * [\cos(2\pi f_{N1}t) [g(t) * [c(t)d_N(t)]] \end{bmatrix} \sum_{k=0}^{M-1} \delta(t - iT_s - kT_c) dt
\end{aligned}
\quad \dots(A.1.21)$$

The integral terms due to the other sources do not integrate perfectly zero. This is due to imperfect raised-cosine pulses for the chips for these sources. The symbols adjacent to the desired symbol interval for these sources affect the integration for this same reason.

Ideally the source 1 demodulated symbol value for the i^{th} symbol should be

$$r_1^i = \frac{1}{2} d_1^i M \quad (\text{A.1.22})$$

where in fact it is given by

$$r_1^i = \frac{1}{2} d_1^i M + \frac{1}{2} M \sum_{j=2}^N \left[d_j^i x_{|j-1|} + y_{|j-1|} (d_j^{i-1} + d_j^{i+1}) \right] \quad (\text{A.1.23})$$

where the terms $x_{|j-1|}$ and $y_{|j-1|}$ denote the error introduced by non ideal pulses.

In general terms the demodulated data for each source is found to be:

$$r_s^i = \frac{1}{2} d_s^i M + \frac{1}{2} M \sum_{\substack{j=1 \\ j \neq s}}^N \left[d_j^i x_{|j-s|} + y_{|j-s|} (d_j^{i-1} + d_j^{i+1}) \right]. \quad (\text{A.1.24})$$

where s refers to the source being recovered, in the case above $s = 1$, and x_n and y_n are found in the following tables. The quantity x_n is due to nonideal pulse shaping on the desired symbol interval while the quantity y_n is due to nonideal pulse shaping on the adjacent symbol intervals. The values in the following table were found using analytical means for a chip oversampling factor of 5, SRN filter rolloff of 0.35, and SRN filter order of 31. It is seen that for smaller PN code lengths the integration error due to nonideal pulses becomes more significant.

Table A.1.1 Error values introduced by SRN pulse shaping.

n	M = 31		M = 63		M = 127	
	x_n	y_n	x_n	y_n	x_n	y_n
1	1.613e-3	5.933e-5	3.637e-4	-1.302e-5	1.086e-4	4.559e-6
2	9.980e-5	8.372e-5	1.106e-4	2.734e-5	2.622e-4	6.111e-6
3	5.483e-3	1.422e-4	-2.230e-3	9.293e-5	3.993e-4	8.683e-6
4	1.341e-2	2.587e-3	5.293e-4	1.814e-4	5.630e-4	1.225e-5
5	6.982e-4	4.618e-3	2.644e-3	2.895e-4	-4.233e-4	1.679e-5
6	1.194e-2	7.798e-3	-6.470e-3	4.137e-4	1.438e-3	2.226e-5
7	2.021e-2	1.236e-3	1.042e-2	5.498e-4	-2.167e-3	2.862e-5
8	-1.350e-2	1.844e-3	9.489e-3	6.937e-4	4.398e-4	3.583e-5
9	-1.774e-2	2.601e-3	1.103e-3	8.413e-4	-1.530e-3	4.383e-5
10	-1.692e-2	3.491e-3	9.647e-3	9.889e-4	1.989e-3	5.256e-5
11	6.919e-3	4.476e-3	-1.727e-3	1.133e-3	3.799e-3	6.198e-5
12	-3.938e-2	5.504e-3	1.495e-2	1.272e-3	-1.267e-3	7.203e-5
13	8.296e-2	6.509e-3	6.099e-3	1.404e-3	-2.633e-3	8.267e-5
14	-2.269e-2	7.417e-3	1.716e-2	1.528e-3	7.137e-3	9.394e-5
15	-1.346e-1	8.156e-3	-2.272e-2	1.645e-3	7.732e-3	1.055e-4
16	-9.523e-2	8.661e-3	4.113e-3	1.756e-3	-2.774e-3	1.176e-4
17	3.847e-3	8.884e-3	2.236e-2	1.862e-3	5.855e-5	1.302e-4
18	6.004e-2	8.800e-3	3.264e-2	1.967e-3	5.149e-3	1.432e-4
19	-2.419e-2	8.409e-3	-4.214e-2	2.072e-3	-7.968e-4	1.567e-4

Appendix 2

Analysis of Pulse Shaping via a RCF for a CFDMA System

An N source CFDMA transmitter and receiver is analyzed in order to determine the errors introduced by pulse shaping via a RCF filter at the transmitter. The system is shown in Fig. A.2.1. To isolate errors due to filtering, a direct connection has been assumed between the transmitter and receiver.

The symbols adjacent to the desired symbol may influence the desired symbol values at the ideal sampling times due to improper filtering. Thus the analysis looks at the desired symbol and its two surrounding symbols as shown in the Fig. A.2.2.

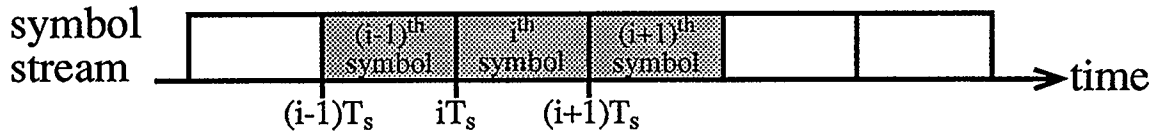


Figure A.2.2 *Symbol stream for one source.*

For one source the signal consisting only of the three necessary symbols can be written as

$$d_n(t) = d_n^{i-1} p^{i-1}(t) + d_n^i p^i(t) + d_n^{i+1} p^{i+1}(t) \quad (\text{A.2.1})$$

where d_n^i refers to the i^{th} symbol value for source n and $p^i(t)$ is the pulse for the i^{th} symbol. Rectangular pulses are used for the symbols thus $p^i(t)$ is given by

$$p^i(t) = u(t - iT_s) - u(t - (i+1)T_s). \quad (\text{A.2.2})$$

where $u(t)$ is the unit step function.

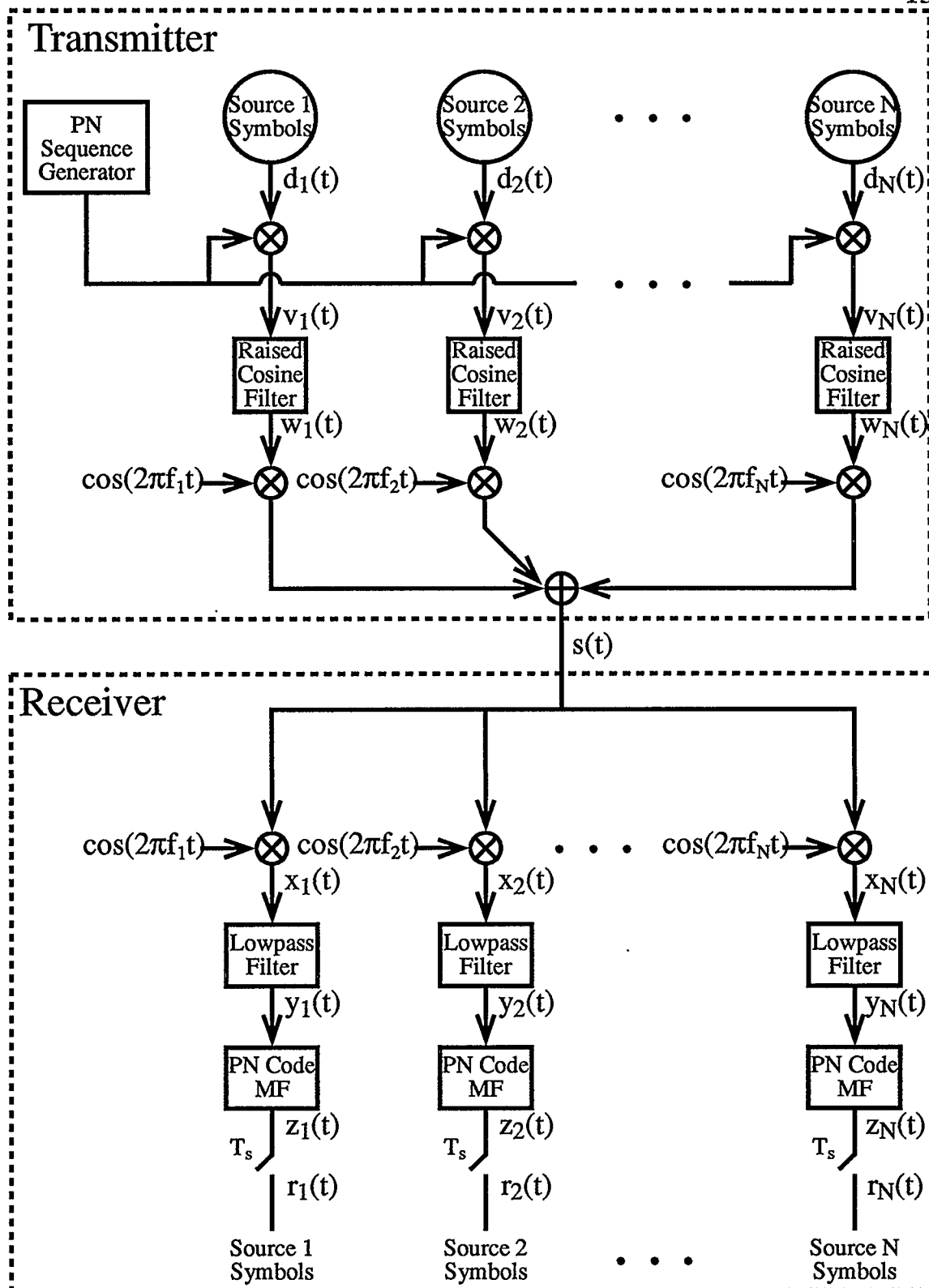


Figure A.2.1 CFDMA system employing raised-cosine filters for pulse shaping.

The CFDMA system is analyzed using the signal denotations of Fig. A.2.1. The encoded symbols for each source are spread resulting in

$$v_n(t) = c(t)d_n(t) \quad (\text{A.2.3})$$

where $c(t)$ is the periodic PN code sequence. The spread data is then pulse shaped with a raised-cosine filter to get

$$w_n(t) = g_r(t) * [c(t)d_n(t)] \quad (\text{A.2.4})$$

where $g_r(t)$ is the impulse response of a raised-cosine filter with bandwidth

$$B_{\text{RCF}} = \frac{(1+\beta)}{2} \frac{M}{T_s}. \quad (\text{A.2.5})$$

The pulse shaped data from the N different sources are then upshifted to different intermediate frequencies and combined to obtain the composite at the output of the transmitter as follows:

$$\begin{aligned} s(t) = & \cos(2\pi f_1 t) g_r(t) * [c(t)d_1(t)] \\ & + \cos(2\pi f_2 t) g_r(t) * [c(t)d_2(t)] \\ & \vdots \\ & + \cos(2\pi f_N t) g_r(t) * [c(t)d_N(t)] \end{aligned} \quad (\text{A.2.6})$$

where

$$f_1 = f_o = \frac{(1+\beta)}{2} \frac{M}{T_s} + (N-1)f_B, \quad (\text{A.2.7})$$

$$f_n = f_1 + (n-1)f_B \quad (\text{A.2.8})$$

and

$$f_B = \frac{1}{T_s}. \quad (\text{A.2.9})$$

Because a direct connection has been assumed $s(t)$ arrives at the receiver unaltered. Looking specifically at the demodulation of source 1 data, the incoming signal $s(t)$ is downshifted by f_1 in order to shift the source 1 data to baseband. The downshifted signal is given by

$$\begin{aligned}
x_1(t) = & \frac{1}{2} g(t) * [c(t)d_1(t)] \\
& + \frac{1}{2} \cos(2\pi(f_2 - f_1)t) g_r(t) * [c(t)d_2(t)] \\
& \vdots \\
& + \frac{1}{2} \cos(2\pi(f_N - f_1)t) g_r(t) * [c(t)d_N(t)] \\
& + \frac{1}{2} \cos(2\pi(2f_1)t) g_r(t) * [c(t)d_1(t)] \\
& + \frac{1}{2} \cos(2\pi(f_2 + f_1)t) g_r(t) * [c(t)d_2(t)] \\
& \vdots \\
& + \frac{1}{2} \cos(2\pi(f_N + f_1)t) g_r(t) * [c(t)d_N(t)].
\end{aligned} \tag{A.2.10}$$

The downshifted data is then passed through a LPF filter, $h(t)$, with bandwidth:

$$B_{\text{lpf}} = \frac{(1 + \beta) M}{2 T_s} + (N - 1)f_B \tag{A.2.11}$$

The spectra of all the double frequency terms lie entirely outside the bandwidth of the LPF while all the lower frequency spectra lie entirely within the bandwidth of the LPF. Thus the signal is greatly simplified resulting in

$$\begin{aligned}
x_1(t) = & \frac{1}{2} g(t) * [c(t)d_1(t)] \\
& + \frac{1}{2} \cos(2\pi(f_2 - f_1)t) g_r(t) * [c(t)d_2(t)] \\
& \vdots \\
& + \frac{1}{2} \cos(2\pi(f_N - f_1)t) g_r(t) * [c(t)d_N(t)].
\end{aligned} \tag{A.2.12}$$

Correlation of the LPF output with a synchronized code sequence $c(t)$ can be used to determine the output of the PN code MF at the ideal sampling time as in Fig. A.2.3.

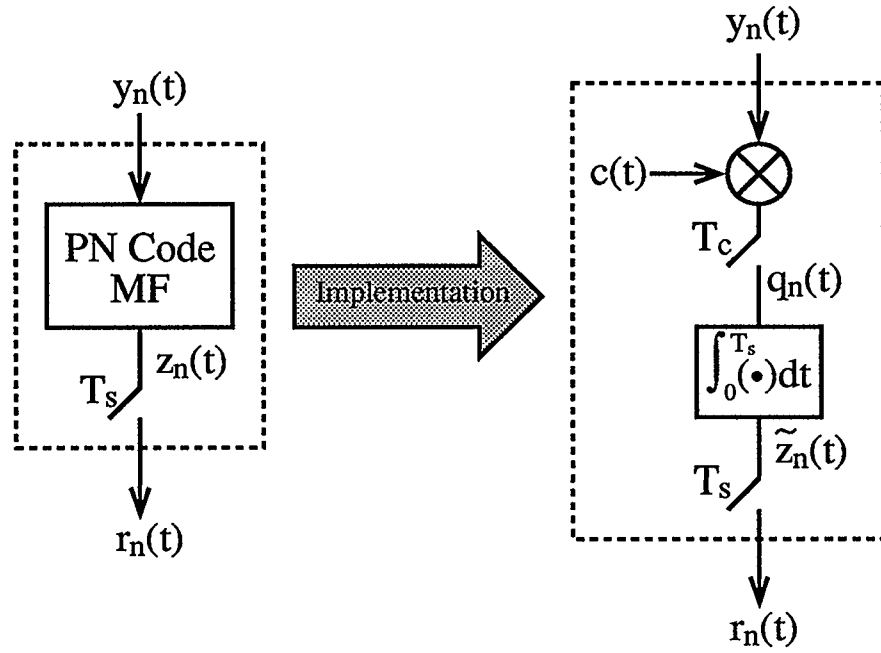


Figure A.2.3 Use of correlation to determine the MF output at the ideal sampling time.

Using correlation, the signal $y_1(t)$ is modulated by the reference code and sampled at the ideal chip time on the desired symbol interval:

$$q_1(t) = c(t) \begin{bmatrix} \frac{1}{2} g_r(t) * [c(t) d_1(t)] \\ + \frac{1}{2} \cos(2\pi f_{21} t) [g_r(t) * c(t) d_2(t)] \\ \vdots \\ + \frac{1}{2} \cos(2\pi f_{N1} t) [g_r(t) * c(t) d_N(t)] \end{bmatrix} \sum_{k=0}^{3M-1} \delta(t - (i-1)T_s - (k + \frac{1}{2})T_c) \quad \dots(A.2.13)$$

where

$$f_{\ell 1} = f_{\ell} - f_1 = (\ell - 1)f_B. \quad (A.2.14)$$

The two $c(t)$ terms can be combined to give a constant value at the ideal chip sampling time resulting in

$$\begin{aligned}
q_1(t) = & \frac{1}{2} [g_r(t) * d_1(t)] \sum_{k=0}^{3M-1} \delta(t - (i-1)T_s - (k + \frac{1}{2})T_c) \\
& + \frac{1}{2} [\cos(2\pi f_{21}t) [g_r(t) * d_2(t)]] \sum_{k=0}^{3M-1} \delta(t - (i-1)T_s - (k + \frac{1}{2})T_c) \quad (A.2.15) \\
& \vdots \\
& + \frac{1}{2} [\cos(2\pi f_{N1}t) [g(t) * d_N(t)]] \sum_{k=0}^{3M-1} \delta(t - (i-1)T_s - (k + \frac{1}{2})T_c).
\end{aligned}$$

If the output of the raised-cosine filter with impulse response $g_r(t)$ is sampled at the ideal chip time, the resulting signal is an impulse train thus further simplification of $q_1(t)$ is achieved.

$$\begin{aligned}
q_1(t) = & \frac{1}{2} d_1(t) \sum_{k=0}^{3M-1} \delta(t - (i-1)T_s - (k + \frac{1}{2})T_c) \\
& + \frac{1}{2} [\cos(2\pi f_{21}t) d_2(t)] \sum_{k=0}^{3M-1} \delta(t - (i-1)T_s - (k + \frac{1}{2})T_c) \quad (A.2.16) \\
& \vdots \\
& + \frac{1}{2} [\cos(2\pi f_{N1}t) d_N(t)] \sum_{k=0}^{3M-1} \delta(t - (i-1)T_s - (k + \frac{1}{2})T_c)
\end{aligned}$$

To complete the correlation process the signal is integrated over the desired symbol duration and sampled at $(i+1)T_s$.

$$\begin{aligned}
\tilde{z}((i+1)T_s) = & \frac{1}{2} \int_{iT_s}^{(i+1)T_s} d_1(t) \sum_{k=0}^{3M-1} \delta(t - (i-1)T_s - (k + \frac{1}{2})T_c) dt \\
& + \frac{1}{2} \int_{iT_s}^{(i+1)T_s} [\cos(2\pi f_{21}t) d_2(t)] \sum_{k=0}^{3M-1} \delta(t - (i-1)T_s - (k + \frac{1}{2})T_c) dt \\
& \vdots \\
& + \frac{1}{2} \int_{iT_s}^{(i+1)T_s} [\cos(2\pi f_{N1}t) d_N(t)] \sum_{k=0}^{3M-1} \delta(t - (i-1)T_s - (k + \frac{1}{2})T_c) dt \\
& \dots (A.2.17)
\end{aligned}$$

Assuming the filter order is adequate, the filtering did not introduce any symbol smearing. Thus only the desired symbol affects the region of

integration. Expanding the $d_n(t)$ terms and simplifying results in

$$\begin{aligned}
 r_n((i+1)T_s) = & \frac{1}{2} d_1^i \int_{iT_s}^{(i+1)T_s} \sum_{k=0}^{M-1} \delta(t - (i-1)T_s - (k + \frac{1}{2})T_c) dt \\
 & + \frac{1}{2} d_2^i \int_{iT_s}^{(i+1)T_s} \cos(2\pi f_{21}t) \sum_{k=0}^{M-1} \delta(t - (i-1)T_s - (k + \frac{1}{2})T_c) dt \\
 & \vdots \\
 & + \frac{1}{2} d_N^i \int_{iT_s}^{(i+1)T_s} \cos(2\pi f_{N1}t) \sum_{k=0}^{M-1} \delta(t - (i-1)T_s - (k + \frac{1}{2})T_c) dt.
 \end{aligned}
 \tag{A.2.18}$$

Using the sifting property

$$\int_{t_A}^{t_B} f(t) \delta(t - t_o) dt = f(t_o) \quad t_A \leq t_o \leq t_B \tag{A.2.19}$$

equation (A.2.18) can be simplified further to get

$$\begin{aligned}
 r_n^i = & \frac{1}{2} d_1^i \sum_{k=0}^{M-1} 1 \\
 & + \frac{1}{2} d_2^i \sum_{k=0}^{M-1} \cos\left(2\pi f_{21}\left(iT_s - (k + \frac{1}{2})T_c\right)\right) \\
 & \vdots \\
 & + \frac{1}{2} d_N^i \sum_{k=0}^{M-1} \cos\left(2\pi f_{N1}\left(iT_s - (k + \frac{1}{2})T_c\right)\right).
 \end{aligned}
 \tag{A.2.20}$$

Solving for $f_{\ell 1}$ in (A.2.20) results in

$$\begin{aligned}
 r_n^i = & \frac{1}{2} d_1^i \sum_{k=0}^{M-1} 1 \\
 & + \frac{1}{2} d_2^i \sum_{k=0}^{M-1} \cos\left(2\pi(1)\left(i - \frac{k + \frac{1}{2}}{M}\right)\right) \\
 & \vdots \\
 & + \frac{1}{2} d_N^i \sum_{k=0}^{M-1} \cos\left(2\pi(N-1)\left(i - \frac{k + \frac{1}{2}}{M}\right)\right).
 \end{aligned}
 \tag{A.2.21}$$

The terms that occur at harmonic frequencies of the symbol rate will sum perfectly to zero over the symbol interval. This results in a recovered

symbol value of

$$r_1^i = \frac{1}{2} d_1^i M \quad (\text{A.2.22})$$

which is equal to the ideal recovered symbol value. Thus no errors are introduced by pulse shaping with a single raised cosine filter at the transmitter as long as the proper precautions are taken with the initial upshift frequency and the bandwidth of the LPF used at the receiver to remove double frequency components.

Appendix 3

Theoretical Analysis of a CFTDMA System with $T_m = 0$ Over a Direct Connection

Analysis of a $N_f = N$ CFTDMA system with $T_m = 0$ is done to isolate the reason for the degradation of system performance as the number of source pairs is increased. The analysis will consist of the demodulation of one source pair at the receiver for a direct connection, i.e. no channel is present. The system is shown in Fig. A.3.1.

The output of the MF at the ideal sampling time can be determined via correlation assuming perfect chip synchronization as shown in Fig. A.3.1. In order to isolate the source of error, the frequency upshifting is assumed to be perfectly reversed at the receiver except for the introduction of a factor of $\frac{1}{2}$.

The incoming signal will consist of data from N source pairs. Each source pair has an A stream of data and a B stream of data. The receiver will demodulate the data for one particular data stream for a given source pair. The stream of interest will be denoted L . \bar{L} will be used to denote the interfering stream of data. The demodulated signal for data stream L of the n^{th} source pair is written

$$r_{nL}(t) = D_{nL}(t) + \sum_{\substack{\ell=1 \\ \ell \neq n}}^N I_{\ell L}^L(t) + \sum_{\ell=1}^N I_{\ell \bar{L}}^L(t) \quad L \in [A, B] \quad (\text{A.3.1})$$

where $D_{nL}(t)$, denotes the desired part of the signal; $I_{\ell L}^L(t)$, the interference due to the ℓ^{th} source pair's L data when demodulating stream L ; and $I_{\ell \bar{L}}^L(t)$, the interference due to the ℓ^{th} source pair's \bar{L} data when demodulating stream L .

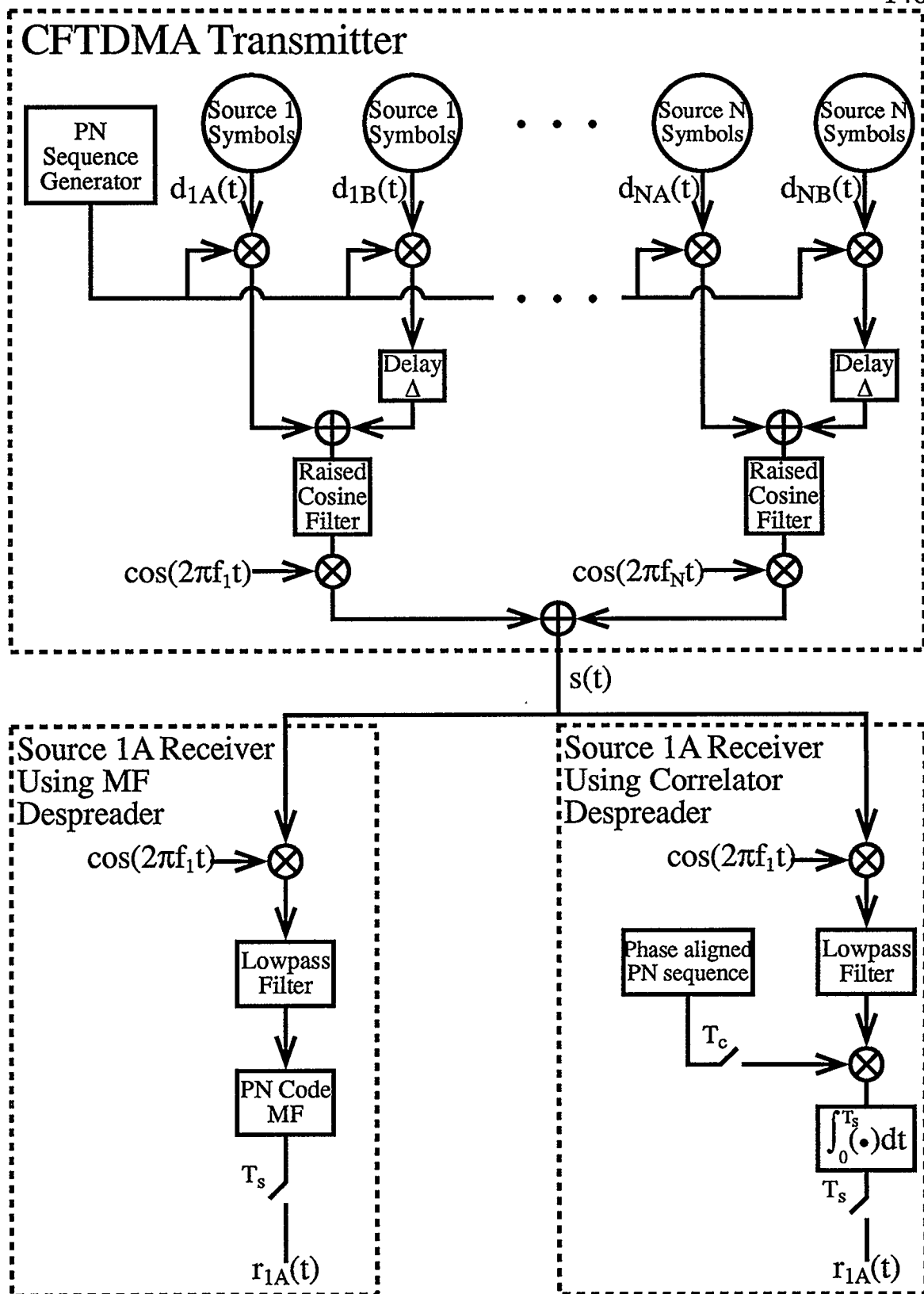


Figure A.3.1 CFTDMA system to be analyzed.

Looking specifically at the demodulation of 1A data, equation (A.3.1) can be written as

$$r_{1A}(t) = D_{1A}(t) + \sum_{\ell=2}^N I_{\ell A}^A(t) + \sum_{\ell=1}^N I_{\ell B}^A(t). \quad (\text{A.3.2})$$

For simplicity only one A symbol is considered, thus there are two interfering B symbols as shown in Fig. A.3.2.

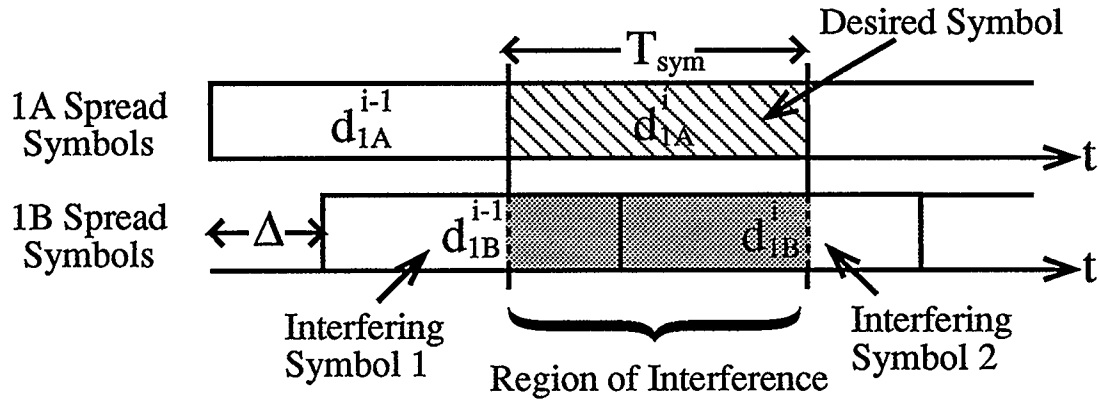


Figure A.3.2 Interference due to B data when demodulating A data for a $T_m=0$ CFTDMA system.

The receiver isolates the source pair 1 data by shifting it to baseband. Correlation with the reference code results in $r_{1A}(t)$ or $r_{1B}(t)$ depending on the phase of the reference code. Since it is the demodulation of the A stream data that is of interest, the code is synchronized to the A data to yield $r_{1A}(t)$.

Considering only the desired symbol interval as in Fig. A.3.1 and taking into consideration the factor of $\frac{1}{2}$ introduced by downshifting, equation (A.3.2) can be written as follows

$$r_{1A}^i(t) = \frac{1}{2} \int_0^{T_{\text{sym}}} c_T(t) \cos(2\pi(\ell-1)f_B t) \left[\begin{array}{l} d_{\ell B}^{i-1} c_T(t + (M-\Delta)T_c) \\ + d_{\ell A}^i c_T(t) \\ + d_{\ell B}^i c_T(t - \Delta T_c) \end{array} \right] dt. \quad (\text{A.3.3})$$

For simplicity it has been assumed in equation (A.3.3) that the symbol

interval is from 0 to T_{sym} . d_{1A}^i is the desired A symbol value; d_{1B}^{i-1} and d_{1B}^i are the two consecutive interfering B symbols; and $c_T(t)$ is one period of the PN sequence defined as follows

$$c_T(t) = \sum_{k=0}^{M-1} c_k \delta(t - (k + \frac{1}{2})T_c) \quad (\text{A.3.4})$$

where c_k are the M coefficients of the PN code. The downshifted signals for the adjacent source pairs, i.e. $\ell \neq 1$, are at intermediate frequencies that are integer multiples of f_B . Substitution of (A.3.4) into (A.3.3) results in

$$\begin{aligned} r_{1A}^i(t) = & \frac{1}{2} d_{1A}^i \int_0^{T_{\text{sym}}} \cos(2\pi(\ell-1)f_B t) \sum_{k=0}^{M-1} c_k^2 \delta(t - (k + \frac{1}{2})T_c) dt \\ & + \frac{1}{2} d_{1B}^{i-1} \int_0^{T_{\text{sym}}} \cos(2\pi(\ell-1)f_B t) \sum_{k=0}^{\Delta-1} c_k c_{M-\Delta+k} \delta(t - (k + \frac{1}{2})T_c) dt \\ & + \frac{1}{2} d_{1B}^i \int_0^{T_{\text{sym}}} \cos(2\pi(\ell-1)f_B t) \sum_{k=\Delta}^{M-1} c_k c_{k-\Delta} \delta(t - (k + \frac{1}{2})T_c) dt. \end{aligned} \quad (\text{A.3.5})$$

Using the fact that $c_k^2 = 1$ for all k and the sifting property of the delta dirac function, (A.3.5) can be written as

$$\begin{aligned} r_{1A}^i = & \frac{1}{2} d_{1A}^i \sum_{k=0}^{M-1} \cos(2\pi(\ell-1)f_B (k + \frac{1}{2})T_c) \\ & + \frac{1}{2} d_{1B}^{i-1} \sum_{k=0}^{\Delta-1} c_k c_{M-\Delta+k} \cos(2\pi(\ell-1)f_B (k + \frac{1}{2})T_c) \\ & + \frac{1}{2} d_{1B}^i \sum_{k=\Delta}^{M-1} c_k c_{k-\Delta} \cos(2\pi(\ell-1)f_B (k + \frac{1}{2})T_c). \end{aligned} \quad (\text{A.3.6})$$

Substituting in the values for T_{sym} and f_B into (A.3.6) results in

$$\begin{aligned} r_{1A}^i = & \frac{1}{2} d_{1A}^i \sum_{k=0}^{M-1} \cos\left(2\pi(\ell-1) \frac{k + \frac{1}{2}}{M}\right) \\ & + \frac{1}{2} d_{1B}^{i-1} \sum_{k=0}^{\Delta-1} c_k c_{M-\Delta+k} \cos\left(2\pi(\ell-1) \frac{k + \frac{1}{2}}{M}\right) \\ & + \frac{1}{2} d_{1B}^i \sum_{k=\Delta}^{M-1} c_k c_{k-\Delta} \cos\left(2\pi(\ell-1) \frac{k + \frac{1}{2}}{M}\right). \end{aligned} \quad (\text{A.3.7})$$

The first term of (A.3.7) goes to zero for all $\ell \neq 1$ as it is the summation of a evenly sampled cosine wave over an integer multiple of its period. The cosine term in the first term evaluates to 1 for $\ell = 1$. Equation (A.3.7) can be simplified to

$$\begin{aligned} r_{1A}^i = & \frac{1}{2} d_{1A}^i M + \frac{1}{2} d_{\ell B}^{i-1} \sum_{k=0}^{\Delta-1} c_k c_{M-\Delta+k} \cos\left(2\pi(\ell-1)\frac{k+\frac{1}{2}}{M}\right) \\ & + \frac{1}{2} d_{\ell B}^i \sum_{k=\Delta}^{M-1} c_k c_{k-\Delta} \cos\left(2\pi(\ell-1)\frac{k+\frac{1}{2}}{M}\right). \end{aligned} \quad (\text{A.3.8})$$

The first term in (A.3.8) represents the desired component of the demodulated signal thus

$$D_{1A}^i = \frac{1}{2} d_{1A}^i M. \quad (\text{A.3.9})$$

There is no interference due to other source pairs' A data in (A.3.8) resulting in

$$I_{\ell A}^{iA} = 0, \quad \ell \neq 1. \quad (\text{A.3.10})$$

The interference due to the B data can be written as

$$\begin{aligned} I_{\ell B}^{iA} = & \frac{1}{2} d_{\ell B}^{i-1} \sum_{k=0}^{\Delta-1} c_k c_{M-\Delta+k} \cos\left(2\pi(\ell-1)\frac{k+\frac{1}{2}}{M}\right) \\ & + \frac{1}{2} d_{\ell B}^i \sum_{k=\Delta}^{M-1} c_k c_{k-\Delta} \cos\left(2\pi(\ell-1)\frac{k+\frac{1}{2}}{M}\right). \end{aligned} \quad (\text{A.3.11})$$

The values for $I_{\ell B}^{iA}$ for a CFTDMA system with $M = 127$ and $\Delta = 19$ chips were determined analytically for a 10 source pair system. The values normalized to the magnitude of the desired term are shown in Table A.3.1. The normalized values of $I_{\ell B}^{iA}$ shown in Table A.3.1 indicate that the B data from the other source pairs can be a large source of interference.

Table A.3.1 Interference due to adjacent source pairs' B data when demodulating stream 1A data for $T_m = 0$.

$\Delta=19, M = 127, T_m = 0$				
	$\frac{I_{\ell B}^{iA}}{ D_{1A}^i } \text{ for } [d_{\ell B}^{i-1}, d_{\ell B}^i]$			
ℓ	[1,1]	[1,-1]	[-1,1]	[-1,-1]
1	-0.0079	-0.0079	0.0079	0.0079
2	-0.0530	0.0503	-0.0503	0.0530
3	0.0379	-0.0090	0.0090	-0.0379
4	-0.0629	0.1237	-0.1237	0.0629
5	0.0039	0.0691	-0.0691	-0.0039
6	0.0851	-0.0308	0.0308	-0.0851
7	0.0168	-0.0077	0.0077	-0.0168
8	-0.0828	0.0389	-0.0389	0.0828
9	-0.0606	-0.0204	0.0204	0.0606
10	-0.0309	-0.0557	0.0557	0.0309

Appendix 4

Theoretical Analysis of a CFTDMA System with $T_m = \Delta$ Over a Direct Connection

Analysis of a $N_f = N$ CFTDMA system with $T_m = \Delta$ is done to isolate the reason for the degradation of system performance as the number of source pairs is increased. The analysis will consist of the demodulation of one source pair at the receiver for a direct connection, i.e. no channel is present. The system is the same as that of Appendix 3 shown in Fig. A.3.1.

The output of the MF at the ideal sampling time can be determined via correlation assuming perfect chip synchronization as shown in Fig. A.3.1. In order to isolate the source of error, the frequency upshifting is assumed to be perfectly reversed at the receiver except for the introduction of a factor of $\frac{1}{2}$.

The incoming signal will consist of data from N source pairs. Each source pair has an A stream of data and a B stream of data. The receiver will demodulate the data for one particular data stream for a given source pair. The stream of interest will be denoted L . \bar{L} will be used to denote the interfering stream of data. The demodulated signal for data stream L of the n^{th} source pair is written

$$r_{nL}(t) = D_{nL}(t) + \sum_{\substack{\ell=1 \\ \ell \neq n}}^N I_{\ell L}^L(t) + \sum_{\ell=1}^N I_{\ell \bar{L}}^L(t) \quad L \in [A, B] \quad (\text{A.4.1})$$

where $D_{nL}(t)$, denotes the desired part of the signal; $I_{\ell L}^L(t)$, the interference due to the ℓ^{th} source pair's L data when demodulating stream L ; and $I_{\ell \bar{L}}^L(t)$, the interference due to the ℓ^{th} source pair's \bar{L} data when demodulating stream L .

Looking specifically at the demodulation of 1A data, equation (A.4.1) can be written as

$$r_{1A}(t) = D_{1A}(t) + \sum_{\ell=2}^N I_{\ell A}^A(t) + \sum_{\ell=1}^N I_{\ell B}^A(t). \quad (\text{A.4.2})$$

For simplicity only one A symbol is considered, thus there are two interfering B symbols as shown in A.4.1.

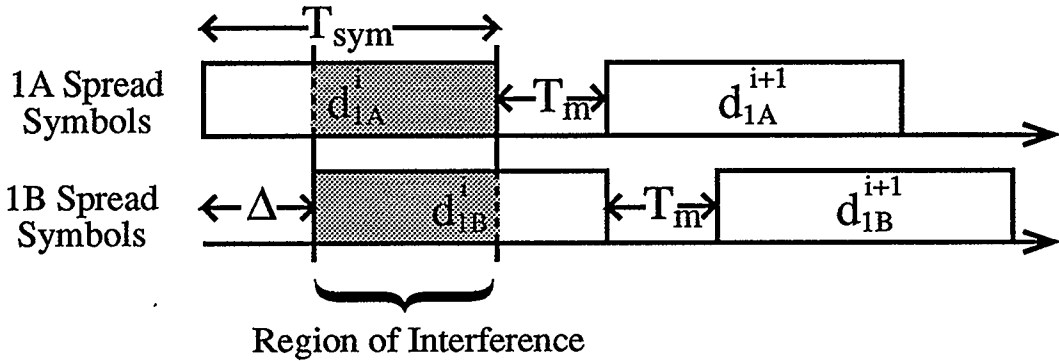


Figure A.4.1 *Interference due to B data when demodulating A data for a $T_m = \Delta$ CFTDMA system.*

The receiver isolates the source pair 1 data by shifting it to baseband. Correlation with the reference code results in $r_{1A}(t)$ or $r_{1B}(t)$ depending on the phase of the reference code. Since it is the demodulation of the A stream data that is of interest, the code is synchronized to the A data to yield $r_{1A}(t)$.

Considering only the desired symbol interval as in Fig. A.4.1 and taking into consideration the factor of $\frac{1}{2}$ introduced by downshifting, equation (A.4.2) can be written as follows

$$r_{1A}^i(t) = \frac{1}{2} \int_0^{T_{\text{sym}}} c_T(t) [d_{1A}^i c_T(t) + d_{1B}^i c_T(t - \Delta T_c)] dt. \quad (\text{A.4.3})$$

For simplicity it has been assumed in equation (A.4.3) that the symbol interval is from 0 to T_{sym} . d_{1A}^i is the desired A symbol value, d_{1B}^i is the

interfering B symbol value, and $c_T(t)$ is one period of the PN sequence defined as follows

$$c_T(t) = \sum_{k=0}^{M-1} c_k \delta(t - (k + \frac{1}{2})T_c) \quad (\text{A.4.4})$$

where c_k are the M coefficients of the PN code. The downshifted signals for the adjacent source pairs, i.e. $\ell \neq 1$, are at intermediate frequencies that are integer multiples of f_B . Substitution of (A.4.4) into (A.4.3) results in

$$\begin{aligned} r_{1A}^i(t) = & \frac{1}{2} d_{\ell A}^i \int_0^{T_{\text{sym}}} \cos(2\pi(\ell-1)f_B t) \sum_{k=0}^{M-1} c_k^2 \delta(t - (k + \frac{1}{2})T_c) dt \\ & + \frac{1}{2} d_{\ell B}^i \int_0^{T_{\text{sym}}} \cos(2\pi(\ell-1)f_B t) \sum_{k=\Delta}^{M-1} c_k c_{k-\Delta} \delta(t - (k + \frac{1}{2})T_c) dt. \end{aligned} \quad (\text{A.4.5})$$

Using the fact that $c_k^2 = 1$ for all k and the sifting property of the delta dirac function, (A.4.5) can be written as

$$\begin{aligned} r_{1A}^i = & \frac{1}{2} d_{\ell A}^i \sum_{k=0}^{M-1} \cos(2\pi(\ell-1)f_B (k + \frac{1}{2})T_c) \\ & + \frac{1}{2} d_{\ell B}^i \sum_{k=\Delta}^{M-1} c_k c_{k-\Delta} \cos(2\pi(\ell-1)f_B (k + \frac{1}{2})T_c). \end{aligned} \quad (\text{A.4.6})$$

Substituting in the values for T_{sym} and f_B into (A.4.6) results in

$$\begin{aligned} r_{1A}^i = & \frac{1}{2} d_{\ell A}^i \sum_{k=0}^{M-1} \cos\left(2\pi(\ell-1) \frac{k + \frac{1}{2}}{M}\right) \\ & + \frac{1}{2} d_{\ell B}^i \sum_{k=\Delta}^{M-1} c_k c_{k-\Delta} \cos\left(2\pi(\ell-1) \frac{k + \frac{1}{2}}{M}\right). \end{aligned} \quad (\text{A.4.7})$$

The first term of (A.4.7) goes to zero for all $\ell \neq 1$ as it is the summation of a evenly sampled cosine wave over an integer multiple of its period. The cosine term in the first term evaluates to 1 for $\ell = 1$. Equation (A.4.7) can be simplified to

$$r_{1A}^i = \frac{1}{2} d_{\ell A}^i M + \frac{1}{2} d_{\ell B}^i \sum_{k=\Delta}^{M-1} c_k c_{k-\Delta} \cos\left(2\pi(\ell-1) \frac{k + \frac{1}{2}}{M}\right). \quad (\text{A.4.8})$$

The first term in (A.4.8) represents the desired component of the demodulated signal thus

$$D_{1A}^i = \frac{1}{2} d_{1A}^i M. \quad (\text{A.4.9})$$

There is no interference due to other source pairs' A data in (A.4.8) resulting in

$$I_{\ell A}^{iA} = 0, \quad \ell \neq 1. \quad (\text{A.4.10})$$

The interference due to the source B data can be written as

$$I_{\ell B}^{iA} = \frac{1}{2} d_{\ell B}^i \sum_{k=\Delta}^{M-1} c_k c_{k-\Delta} \cos \left(2\pi(\ell-1) \frac{k + \frac{1}{2}}{M} \right). \quad (\text{A.4.11})$$

The values for $I_{\ell B}^{iA}$ for a CFTDMA system with $M=127$ and $\Delta = T_{mc} = 19$ chips were determined analytically for a 10 source pair system. The values normalized to the magnitude of the desired term are shown in Table A.4.1. The normalized values of $I_{\ell B}^{iA}$ shown in Table A.4.1 indicate that the B data from the other source pairs can be a large source of interference.

Table A.4.1 Interference due to adjacent source pairs' B data when demodulating stream 1A data for $T_m = \Delta$.

$\Delta=19, M=127, T_{mc}=19$		
	$\frac{I_{\ell B}^{iA}}{ D_{1A}^i }$ for $[d_{\ell B}^i]$	
ℓ	[1]	[-1]
1	0	0
2	-0.0516	0.0516
3	0.0235	-0.0235
4	-0.0933	0.0933
5	-0.0326	0.0326
6	0.0579	-0.0579
7	0.0123	-0.0123
8	-0.0609	0.0609
9	-0.0201	0.0201
10	0.0124	-0.0124